Structural and functional characterization of the gene products responsible for phototrophic iron oxidation by purple bacteria

Shining light on iron oxidation

Ivo H. Saraiva

Dissertation presented to obtain the Ph.D degree in Biochemistry

Instituto de Tecnologia Química e Biológica | Universidade Nova de Lisboa

Oeiras, December, 2012

INSTITUTO
DE TECNOLOGIA
QUÍMICA E BIOLÓGICA
/UNL

Knowledge Creation

From left to right: Professor Miguel Teixeira, Professor Carlos Geraldes, Dr. Marta Bruix, Ivo Saraiva, Professor Paula Tamagnini, Dr. Catarina Paquete and Dr. Ricardo Louro.

December 3rd 2012.

President of the Juri:

Professor Miguel Teixeira.

Main opponents:

Dr. Marta Bruix

Dr. Paula Tamagnini

Thesis committee:

Dr. Ricardo Louro

Professor Dianne Newman

Professor Carlos Geraldes

cover: surface of the FoxE homotrimer.

Acknowledgements

I would like to thank

Doctor Ricardo O. Louro for the friendship, supervision, the guidance, the advices, for all that he taught me and for accepting me in his lab, where I found a fun and relaxed work environment always prone to scientific debate.

Professor Dianne K. Newman for kindly receiving me in her home and in her lab, where I had the privilege of working with a team of scientific and human excellence, and where I found the perfect work environment that always made me feel at home. I thank in particular Itzel Ramos-Solis and Lars Dietrich for the support in the lab and Lina Bird for her collaboration on the study of PioC.

Professor Carlos Salgueiro with whom I enjoyed a successful collaboration and who has kindly provided necessary support in the study of PioC.

Doctor Catarina Paquete for the support and useful discussions on the kinetics of FoxE.

Doctor Carlos Frazão and Luís Pereira for the X-ray crystallography studies of FoxE.

Doctor Manolis Matzapetakis for the friendship and for support and key suggestions on structural studies of PioC.

Professor Miguel Teixeira for obtaining the EPR spectra of FoxE and for subsequent useful discussion on the data.

Professor Carlos Geraldes for accompanying my work during these years and for the continuous support.

My lab colleagues who´s merry nature always made it hard to do some actual work in the lab. I thank in particular Bruno Fonseca for the friendship and Eduardo Calçada for the friendship and for the contributions in the study of PioC.

Agradeço em especial à minha irmã e aos meus pais que iniciaram a formação necessária a escrever esta tese e agradeço à Mafalda que a concluiu. A eles dedico esta tese.

I was awarded a PhD fellowship (SFRH/BD/36582/2007) by Fundação para a Ciência e Tecnologia.

Abstract

Iron is an essential element in life. It is used in a variety of different processes in the energetic metabolism of different organisms. Among these bioenergetic processes is photoferrotrophy, characterized by the utilization of Fe(II) as the sole electron source for photosynthesis. The metabolic activity of photoferrotrophs is proposed to have had a relevant role in the formation of ancient geological structures consisting of Fe(III) minerals, such as the Banded Iron Formations.

Photoferrotrophy was only recently discovered (in the 1990s) and lacks a detailed molecular description. The objective of this work was to characterize photoferrotrophy at a molecular level, in order to understand how photoferrotrophs transfer electrons from Fe(II) to the photosynthetic reaction center, while avoiding Fe(III) precipitation inside cells.

The first target of this work was the bacterium *Rhodobacter ferrooxidans* SW2. In this organism, the three-gene *fox* operon was proposed to be responsible for Fe(II) oxidation. The first gene, *foxE*, encodes a diheme *c*-type cytochrome, which is predicted to oxidize Fe(II), performing the first step in photoferrotrophy. Using NMR, EPR and UV-visible spectroscopies, together with electrochemistry techniques, the reduction potentials of the hemes of FoxE were determined, providing a thermodynamic characterization. Stopped-flow experiments, monitored by UV-visible spectroscopy, allowed for the study of the kinetics of Fe(II) oxidation by FoxE. Finally, X-ray crystallography was used to determine the structure of this protein. All together, the data show that, *in vitro*, FoxE forms a homo-trimer in solution that is thermodynamically and kinetically capable of oxidizing Fe(II). This reaction is pH-dependent in a manner that correlates with Fe(III) solubility. This correlation may be involved in preventing Fe(III) precipitation within cells.

The second focus of this work was on the bacterium *Rhodopseudomonas palustris* TIE-1. In this organism, the three-gene *pio* operon was shown to be responsible for photoferrotrophy. The third gene of this operon, *pioC*, encodes a High Potential Iron-Sulfur Protein (HiPIP), predicted to transfer electrons to the cyclic photosynthesis apparatus. Cyclic voltammetry was used to determine the reduction potential of PioC. NMR and EPR spectroscopic characterizations were performed and NMR was used to determine the solution structure of this HiPIP. The reduction potential is in agreement with the predicted function of PioC, and the solution structure contains conserved features observed in all HiPIP structures determined so far.

The gathered data allowed for mechanisms of iron oxidation in the two selected bacteria to be proposed. These mechanisms involve a path from Fe(II) to the cyclic photosynthesis apparatus and strategies to avoid Fe(III) precipitation within cells.

Resumo

O ferro é um elemento essencial à vida. É usado de várias maneiras diferentes no metabolismo energético de diferentes organismos. A fotoferrotrofia é uma destas estratégias bioenergéticas e caracteriza-se pela utilização de Fe(II) como fonte exclusiva de electrões para a fotossíntese. Foi proposto que a actividade de organismos fotoferrotróficos teve um papel relevante na formação de estruturas geológicas constituídas por minerais de Fe(III), como as Formações de Ferro em Banda.

Tendo a fotoferrotrofia sido recentemente descoberta, na década de 1990, uma descrição molecular detalhada ainda não foi efectuada. O objectivo deste trabalho é obter esta descrição de modo a compreender como os organismos fotoferrotróficos transferem electrões do Fe(II) até ao centro reactivo fotossintético e, ao mesmo tempo, evitam a precipitação de Fe(III) nas células.

O primeiro alvo deste trabalho foi a bactéria *Rhodobacter ferrooxidans* SW2. Nesta bactéria o operão com três genes *fox* foi proposto ser responsável pela oxidação fotossintética de Fe(II). O primeiro gene, *foxE*, codifica um citocromo di-hémico tipo *c*, que se prevê oxidar Fe(II), sendo responsável pelo primeiro passo no metabolismo fotoferrotrófico. Conjugando espectroscopias de RMN, RPE e UV-visível com técnicas de electroquímica, os potenciais de redução dos hemos do FoxE foram determinados, para uma caracterização termodinâmica. A conjugação das técnicas de fluxo-interrompido e espectroscopia de UV-visível permitiu estudar a cinética de oxidação de Fe(II) pelo FoxE e cristalografia de raios-X foi usada na determinação da estrutura desta proteína. Os dados adquiridos indicam que, *in vitro*, o FoxE forma um homo-trímero em solução que é termodinâmica e cineticamente apto para oxidar Fe(II). Esta oxidação é controloada pelo pH de um modo que se correlaciona com a

solubilidade do Fe(III). Esta correlação pode ser relevante na prevenção da precipitação de Fe(III) nas células.

O segundo alvo deste trabalho foi a bactéria *Rhodopseudomonas palustris* TIE-1. Neste organismo, foi demonstrado que o operão com três genes *pio* é responsável pela fotoferrotrofia. O terceiro gene deste operão, *pioC*, codifica uma Proteína Ferro-Enxofre de Alto Potencial (HiPIP), que se prevê que transfere electrões para o sistema de fotossíntese cíclica. O método de Voltametria Cíclica foi usado para determinar o potential de redução do PioC. Foi feita uma caracterização espectrocópica por RMN e RPE e a estrutura do PioC em solução foi determinada por RMN. O potencial de redução está de acordo com a função prevista e a estrutura mantém todas as características conservadas nas estruturas de HiPIPs determinadas até agora.

Os dados obtidos levaram à proposta de mecanismos de oxidação de Fe(II) pelas bactérias estudadas. Estes envolvem uma cadeia de transferência electrónica entre o Fe(II) e o sistema de fotossíntese cíclica e estratégias para prevenir a precipitação de Fe(III) nas céluas.

Table of contents

List of figures

List of tables

1

Introduction

1 Introduction

Since life began on Earth, it has changed and shaped the planet's geochemistry. In every niche where thermodynamics is favorable and kinetics allows, evolution has given life strategies to thrive. The understanding of the geochemical evolution of the planet is tightly linked to the evolution of life and of its metabolic strategies. Evidence shows that major geochemical events, like the Great Oxidation Event (1) or the origin of Banded Iron Formations (BIF) (2), were triggered by specific microbial metabolisms. In order to answer the questions on how and when these events happened, it is necessary to know the biochemistry of the microorganisms associated with them. This is a goal that can only be achieved by studying the present microbial communities and their metabolic strategies that might answer these questions. Ultimately, the correlation of evolution of life and of the geochemistry of the planet should allow the association of particular geochemical events with the appearance of particular metabolic pathways, their respective genes and proteins, and allow understanding how specific metabolic strategies shape the environment (3).

Of the many strategies living organisms use to obtain energy, this thesis focuses on photoferrotrophy, *i.e.* the utilization of ferrous iron oxidation as an electron source for photosynthesis (4, 5). This photosynthetic iron oxidation is described by the following reaction:

$$4Fe^{2+} + CO_2 + 11H_2O + h\nu \rightarrow [CH_2O] + 4Fe(OH)_3 + 8H^+$$

This particular metabolic strategy is a good illustration of how life and Earth have co-evolved since the origin of Life on the planet. First, photoferrotrophy is an ancient form of photosynthesis that may be an important step in its evolution (6). Second, in some periods of Earth history, it is also the most

probable cause of BIFs, stratified geological structures that compose the largest iron ore deposits in the world (2). This work focuses on the biochemical and functional characterization of proteins involved in photoferrotrophy, namely the products of genes recently discovered to be involved in this metabolism in the Gram-negative bacteria *Rhodopseudomonas palustris* TIE-1 and *Rhodobacter ferrooxidans* SW2. The detailed biochemical characterization of this metabolism will help understand its role in the biogeochemistry of iron (Figure 1.1).

1.1 Iron redox cycle

Iron is the most abundant element on Earth and the fourth most abundant on the Earth's crust. It belongs to the fourth period and eighth group in the periodic table and has a [Ar] $3d^6$ $4s^2$ electron configuration. The most common oxidation states in the biosphere are +2 and +3 with electronic configurations d^6 (ferrous) and d^5 (ferric), respectively. Depending on environmental conditions (ligand field, pH, redox conditions) iron can be readily convertible between these two states.

The reduction potential of the Fe(II)/Fe(III) pair is conditioned by the complexing agents in solution. Non-complexed soluble ferric and ferrous iron ions only exist at low pH with a reduction potential of 770 mV. At circumneutral pH, iron forms complexes with other species in solution, which results in a decrease of the reduction potential to values between 100 mV and 400 mV, depending on the complexing agents. These can be phosphates, carbonates or organic acids present in the environment. The nature of these complexing agents also determines if iron is soluble or not at circumneutral pH. In general, ferrous iron is more soluble than ferric iron and, at this pH, iron frequently precipitates upon oxidation in the form of ferric (hydr)oxides.

With O_2 having a reduction potential of 870 mV at pH 7 and of 1.12 V at pH 2 the oxidation of iron by O_2 (autooxidation) is always thermodynamically favorable. The rate of this reaction is given by the following equation (7):

$$-\frac{d[Fe^{2+}]}{dt} = k\frac{[O_2][Fe^{2+}]}{[H^+]^2} = k[O_2][Fe^{2+}]10^{2pH} \quad \text{1-1}$$

According to this equation the rate of autooxidation decreases two orders of magnitude for each unit of pH decrease, indicating that this reaction is slow in acidic environments.

Given iron's availability and chemical properties, it is not surprising that Life, throughout evolution, has incorporated this metal in its many bioenergetic strategies. Microorganisms are able to use the forward and backward conversion between Fe(II) and Fe(III) in several different environmental conditions. This argues for the importance of microorganisms in the biogeochemical cycle of iron (8).

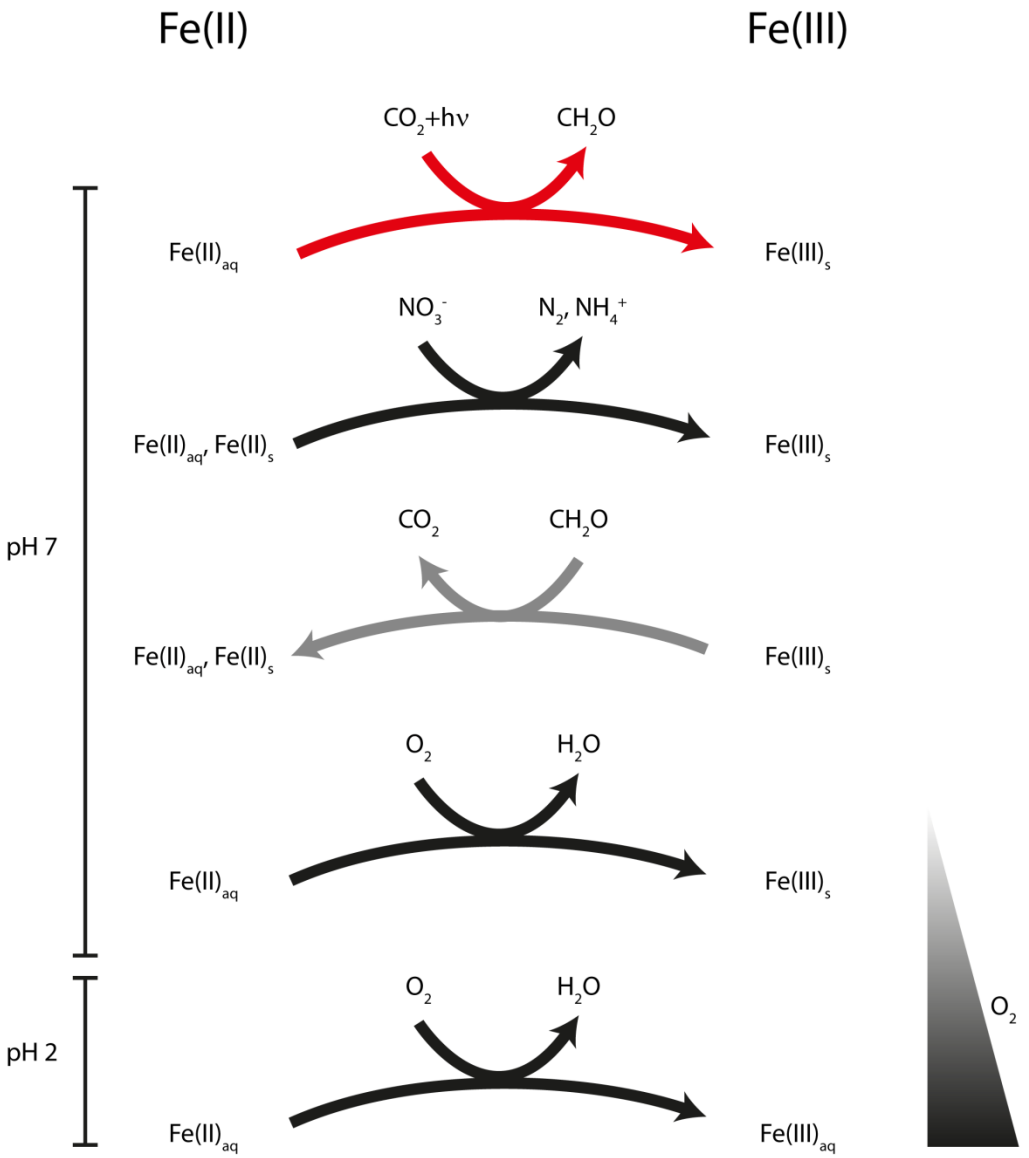

Figure 1.1: redox cycling of iron at different pH and O_2 concentrations.
From top to bottom are photoferrotrophy, nitrate-reducing iron oxidation, dissimilatory iron reduction, circumneutral aerobic iron oxidation and low-pH iron oxidation.

1.1.1 Microbial iron reduction

By the time respiratory metabolisms evolved on Earth, the variability of electron acceptors was limited (9, 10). One available electron acceptor was Fe(III) that resulted from abiotic photochemical oxidation of abundant Fe(II). This, together with the widespread of iron respiration in today's microorganisms, either in Bacteria or in Archea, suggests that Fe(III) respiration was one of the first respiratory metabolisms to evolve (11). Fe(III) is reduced mostly in anaerobic conditions either by strict anaerobes, like members of the genus *Geobacter*, or by facultative anaerobes, like members of the genus *Shewanella*. Both of which are Gram-negative bacteria. At circumneutral pH, the available Fe(III) can be in dissolved chelated form or in solid ferric minerals. The mentioned genera are able to use solid ferric minerals as terminal electron acceptors (12, 13), for which there is the need to transfer electrons to the

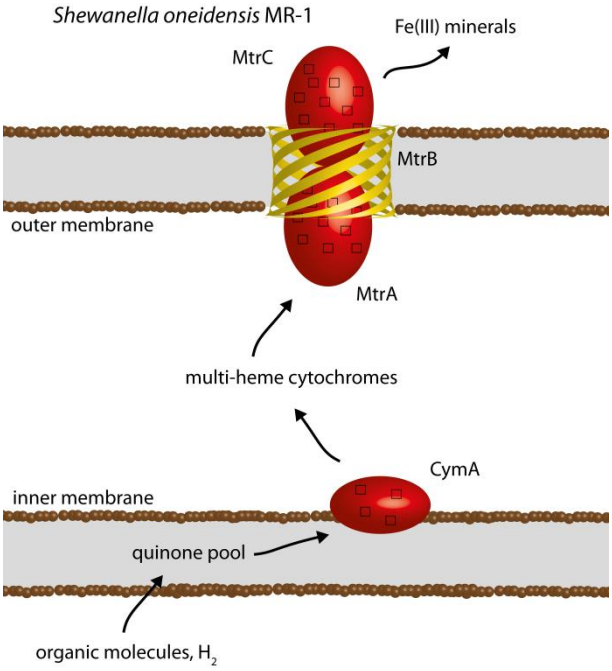

Figure 1.2: cartoon of ferric iron respiration by *Shewanella oneidensis* MR-1.

extracellular space. Depending on the species, electrons from oxidation of different organic compounds (acetate, lactate, palmitate, aromatic compounds) or H_2 in the cytoplasm are transferred through the periplasm, to terminal iron reductases in the outer membrane. This transfer is performed by a complex chain of inner membrane, periplasmatic and outer membrane multi-heme cytochromes (Figure 1.2) (14, 15). The reduction of ferrous minerals may lead to their solubilization and mobilization of iron.

1.1.2 Microbial iron oxidation

1.1.2.1 Aerobic iron oxidation

Low pH slows down autooxidation (equation 1-1) allowing the competition of microorganisms for Fe(II). Many acidophiles oxidize iron using O_2 as terminal electron acceptor (16, 17). The most studied organism performing this metabolism is the bacterium *Acidithiobacillus ferrooxidans* (18), a chemolithoautotroph belonging to the γ-proteobacteria. This microorganism is associated with acidified environments rich in iron and sulfur ores (19). Different strains of *A. ferrooxidans* seem to have different mechanisms of iron oxidation (20). For the type strain, *A. ferrooxidans* ATCC 23270^T, the proteins involved are coded by the *rus* operon (Figure 1.3) (21–23). Iron is oxidized extracellularly by the outer membrane *c*-type cytochrome Cyc2. The electrons are then transferred to the periplasmatic blue copper protein rusticyanin, where the path bifurcates. The electrons can follow an electrochemical downhill path through the cytochrome c_4 Cyc1 to the inner membrane aa_3-type terminal oxidase that couples the reduction of O_2 to the translocation of H^+ from the cytoplasm to the periplasm. This path helps keep the proton gradient that drives the ATP-synthase. In a parallel way, the electrons can follow an electrochemical uphill path through the cytochrome c_4 CycA1 to the

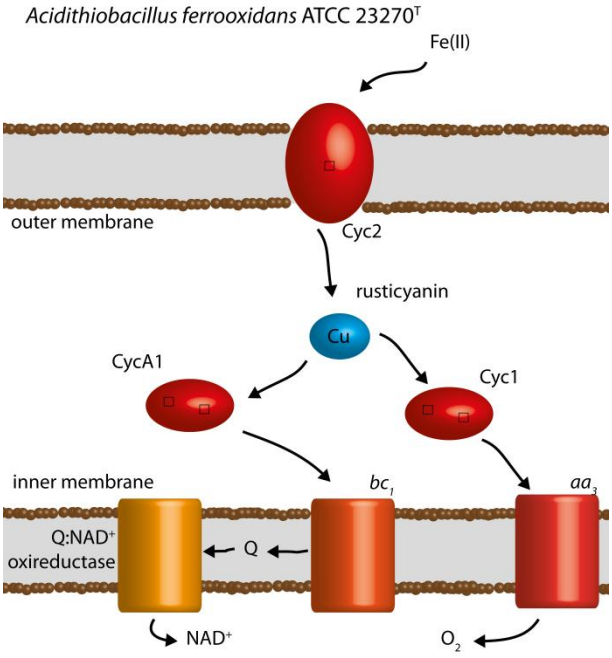

Figure 1.3: cartoon of ferrous iron oxidation by *Acidithiobacillus ferrooxidans* 23270^T.

bc_1 complex, the quinone pool and finally to the NADH dehydrogenase NADH1 ending in the reduction of NAD^+. This uphill path is driven forward by using the transmembrane proton gradient. *A. ferrooxidans* uses iron as source of energy and of reducing power.

Other identified acidophiles oxidizing iron (24) belong to the genera *Acidithiobacillus* (25), *Thiobacillus* (26) and *Acidiferrobacter* (27), which are all γ-proteobacteria, and to the genus *Ferrovum* (24), which belongs to the β-proteobacteria.

Recently, there has been increasing interest in the research of aerobic iron oxidizers that grow at circumneutral pH (17). In the presence of O_2, Fe(II) is rapidly autooxidized (equation 1-1). As such, microorganisms can only compete with autooxidation of iron in micro-aerobic Fe(II) rich conditions. These are found in habitats where Fe(II) rich anoxic water comes in contact with O_2, like

fresh water iron seeps (28–32), marine hydrothermal vents (33–35) or the rhizosphere of plants that grow in soils saturated with anoxic water (36–38). Because of these specific environmental conditions, the laboratory study of aerobic iron oxidizers at circumneutral pH requires techniques that mimic oxic-anoxic interfaces (39). So far, all characterized strains belong to the proteobacteria. The most common bacteria found in the described fresh water habitats belong to the β-proteobacteria genera *Gallionella*, *Leptothrix* or *Syderoxydans*. The bacterium *Gallionella ferruginea* is the most studied. It was first described in 1836 (40). The cells from this bacterium form stalks that are proposed to position the cell in the right Fe(II)/O_2 gradient and to provide a nucleation site for Fe(III) precipitation, thus preventing cell encrustation (17). Recently, the genome of the bacterium *Syderoxydans lithotrophicus* ES-1 was sequenced. Analysis of the genome and search for homologous of genes from iron oxidizers and reducers that are known to be involved in iron metabolism led to the proposal of an iron oxidation electron chain coded by a three gene operon (41). The first two genes, *mtoA* and *mtoB*, code for a periplasmatic deca-heme cytochrome and its associated outer-membrane β-barrel, respectively. These cytochromes are known to be able to transfer electrons between the periplasm and the extracellular space through the pore of the associated β-barrel (42). The third gene *cymA*, codes for a homologue of the inner-membrane associated tetra-heme cytochrome CymA, from the iron reducer *Shewanella oneidensis* MR-1. In the proposed iron oxidation mechanism MtoB allows access of MtoA to the extracellular space to receive electrons from ferrous iron, thus preventing ferric iron precipitation inside the cell. Through an unknown mechanism the electrons are then transferred to $CymA_{ES-1}$ and used to reduce the quinone pool (Figure 1.4).

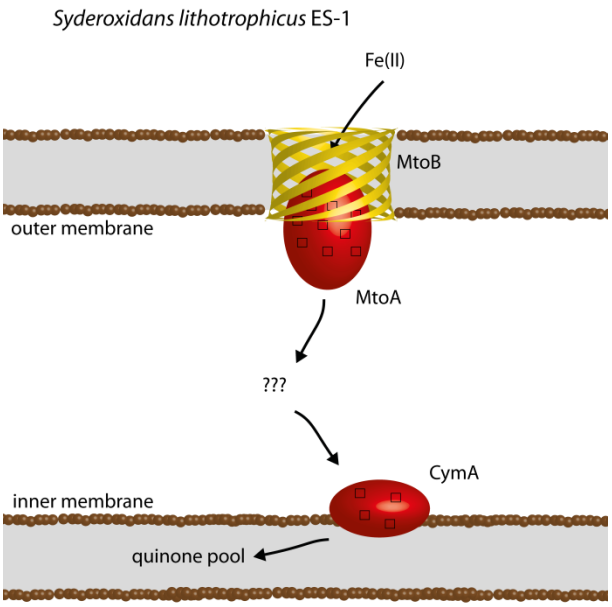

Figure 1.4: cartoon of ferrous iron oxidation by *Sideroxidans lithotrophicus* ES-1.

In marine environments, the best known neutrophilic aerobic iron oxidizer is the bacterium *Mariprofundus ferrooxydans*. This species and closely related clones from deep-sea environmental samples form the new proposed class ζ-proteobacteria (43). Based on the whole genome analysis of the type strain *Mariprofundus ferrooxydans* PV-1^T and analysis of protein expression patterns, a group of genes was suggested to be involved in iron oxidation (44). Among these are a molydopterin and 4Fe-4S cluster binding protein, a *c*-type cytochrome and two terminal oxidases, type ccb_3 and type *bd*. Experimental evidence supporting this hypothesis is still lacking.

1.1.2.2 Anaerobic iron oxidation

The reduction potentials of complexed iron species at pH 7 are below 400 mV. These values allow the utilization of electron acceptors with reduction potentials lower than oxygen (870 mV). The majority of anaerobic iron

oxidizers can be divided into photosynthetic (with the potential of the reaction center near 450 mV) and nitrate-reducing (with the potential of the NO_3^-/NO_2^- at 430 mV). The utilization of nitrate as final electron acceptor in iron oxidation was first detected in 1996 (45). Microorganisms performing this metabolism are phylogenetically spread in Bacteria and Archea (8). Several strains have been isolated from fresh-water, brackish-water or marine environments (45–49). Sustained growth of iron-oxidizing nitrate reducers is proposed to only occur in the presence of additional organic substrates, like acetate (50). This mixotrophic metabolism, even though present only in a small fraction of nitrate reducers, is widespread among this group of organisms and contributes significantly to iron oxidation in their habitats (50).

Photosynthetic bacteria that use oxidation of iron as electron source for photosynthesis form a second group of organisms that oxidize iron in anaerobic circumneutral environment. This metabolism is the focus of this thesis and is described in more detail.

1.2 Photoferrotrophy: shining light on iron oxidation

The oxidation of ferrous iron by anoxygenic photosynthetic bacteria was first proposed a few decades ago (51), as an hypothesis for the origin of Banded Iron Formations (BIF). These geological structures form the largest geological iron deposits in the planet but their origin is still debated. The activity of oxygenic photosynthetic cyanobacteria was proposed first to be the main cause that led to this iron oxidation and deposition. In the beginning of the 1990s photoferrotrophy was detected and photoferrotrophs were first isolated (4, 5). Current studies on the origin of BIFs suggest that both mechanisms had important roles in BIF formation in different times in the history of the planet (2).

Several photoferrotrophs have been isolated in the last twenty years. However, the identification of the molecular mechanisms of this iron oxidation was still stalled, probably due to the lack of genetically tractable organisms. This obstacle has recently been overcome twice (52, 53), opening the window for the biochemical study of photoferrotrophy.

1.2.1 Photoferrotrophs

Until today seven photoferrotrophs from different sources have been cultured and characterized. They are all Gram-negative bacteria that appear to have different strategies to oxidize iron.

1.2.1.1 *Rhodobacter ferrooxidans* SW2

Rhodobacter ferrooxidans SW2 (SW2) is among the first isolated organisms capable of using electrons from iron oxidation to feed photosynthesis (5), and it is one of the most studied. It was isolated from fresh water sediments, belongs to the α-proteobacteria and is a purple non-sulfur bacterium. It is able to grow photoheterotrophically on a variety of substrates (low molecular weight carboxylates, saccharides and amino acids). In the dark it can grow on oxygen.

The SW2 operon *foxEYZ* was identified as possibly responsible for

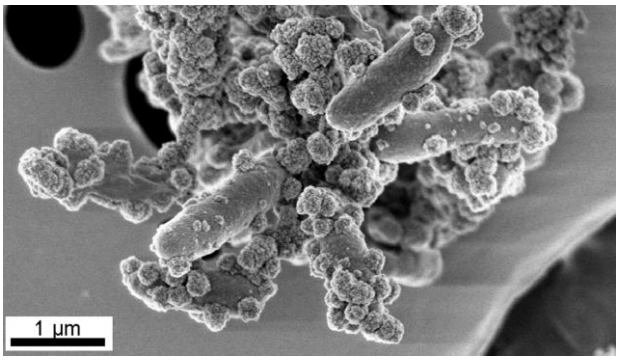

Figure 1.5: scanning electron microscopy micrograph of SW2. Fe(III) minerals are visible around the cells (131).

photoferrotrophy, as it was shown to enhance phototrophic iron oxidation in the related bacterium *Rhodobacter capsulatus* SB1003 (53).

1.2.1.2 *Rhodomicrobium vannielii* BS-1

BS-1 was also isolated from fresh water sediments and is an α-proteobacterium (54). Iron oxidation by BS-1 is enhanced by the addition of organic co-substrates like acetate, butyrate, malate, succinate and pyruvate. This organism, upon oxidizing Fe^{2+}, becomes encrusted in Fe^{3+} minerals that inhibit further growth. The authors state that phototrophic iron oxidation has little physiological importance in BS-1 metabolism.

1.2.1.3 *Chlorobium ferrooxidans* KoFox

KoFox was also isolated from fresh water sediments, but, unlike the previous organisms, it is a green sulfur bacterium belonging to the Chlorobia (55). Iron oxidation is accelerated by additional substrates either organic (pyruvate, fumarate, acetate and cysteine) or inorganic (H_2, $S_2O_3^-$). KoFox grows in co-culture with the bacterium *Geospirillum* strain KoFum. KoFum does not oxidize iron but it becomes incrusted in ferric iron precipitates from the activity of KoFox, suggesting that photoferrotrophs have specific properties to avoid incrustation.

1.2.1.4 *Rhodovulum iodosum* N1 and *Rhodovulum robiginosum* N2

These two bacteria are the only marine photoferrotrophs isolated so far (56). They are also α-proteobacteria and have a versatile metabolism being able to grow photoheterotrophically with a variety of small organic molecules and also in the dark with oxygen as final electron acceptor.

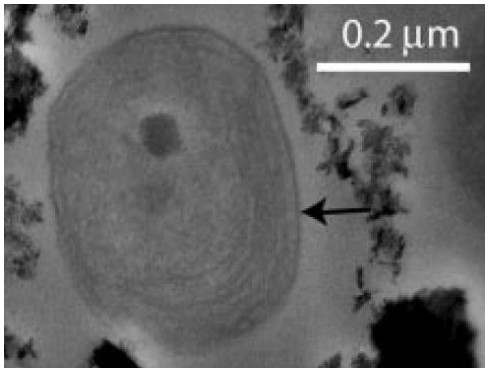

Figure 1.6: transmission electron microscopy micrograph of TIE-1.
The arrow indicates inner cytoplasmatic membrane structures (59).

1.2.1.5 *Thiodictyon* strain F4

F4 belongs to the γ-proteobacteria and was isolated from a fresh water marsh. It is a purple sulfur bacterium (57). This organism has shown the highest iron oxidation rates so far (58).

1.2.1.6 *Rhodopseudomonas palustris* TIE-1

TIE-1 is also a purple non-sulfur bacterium from the α-proteobacteria, but is phylogenetically apart from strains SW2, N1 and N2 (Figure 1.6) (59). It was isolated from fresh water sediments. This bacterium has a very versatile metabolism being able to grow photoauto-, photohetero-, chemohetero- and chemoautotrophycally. This organism has the particularity of being genetically tractable. This allowed the identification of the *pioABC* operon, as required for photoferrotrophy (52).

1.2.2 Photoferrotrophic genes

Despite the biological and geological importance of photoferrotrophy, genes responsible for this metabolism were identified in two organisms only recently. In *Rhodopseudomonas palustris* TIE-1, which is genetically tractable, a three gene operon was identified by analysis of protein expression patterns in cultures grown with or without Fe^{2+} as electron source (52) (Figure 1.7). In Fe^{2+} oxidizing conditions a *c*-type cytochrome was detected to be differently expressed. The identification of this protein by mass spectroscopy and subsequent sequence analysis led to the identification of the *pio* operon. The first gene, *pioA*, codes for a 540 amino acid protein with ten canonical *c*-type heme binding sites (CXXCH). It has a Sec system peptide signal for co-translational translocation to the periplasm, as is required for the maturation of *c*-type cytochromes (60). By studying the effect on iron oxidation of individual deletions of the *pio* genes, PioA was predicted to be the iron oxidase. In BLAST runs of PioA the first half of the sequence hits only proteins from other strains of the *R. palustris* species and has no predicted function. The second half of the PioA sequence, which contains the ten heme binding sites, falls into the deca-heme *c*-type cytochrome family. One member of this family, MtrA, is involved in ferric iron reduction by *Shewanella oneidensis* MR-

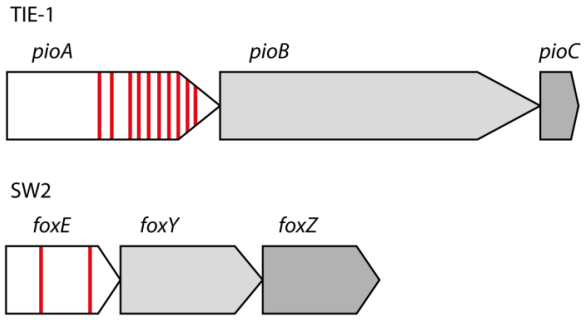

Figure 1.7: genes involved in photoferrotrophy in *Rhodopseudomonas palustris* TIE-1 and *Rhodobacter ferrooxidans* SW2.
In red are indicated the canonical heme biding sites (CXXCH).

1. This suggests a common evolutionary path between iron oxidation and iron reduction (61). The second gene of the *pio* operon, *pioB*, codes for an 811 amino acid protein also with a Sec system peptide signal. A BLAST run of PioB places it in a deca-heme associated outer-membrane β-barrel family (Figure 1.8). To this family belongs the beta-barrel MtrB, which is coded in the same operon of MtrA in *Shewanella oneidensis* MR-1. It was shown that these β-barrels allow the transfer of electrons from their associated periplasmatic deca-heme cytochromes, through the outer membrane, to electron acceptors on the outside of the cells (42). This interaction allows the reduction of extracellular solid minerals. In the case of MtrAB, this association ultimately allows the reduction of ferric minerals with electrons gathered from different donors in the cytoplasm. Again, these data suggest a common evolutionary path for iron oxidation and reduction. The third gene, *pioC*, codes for a High

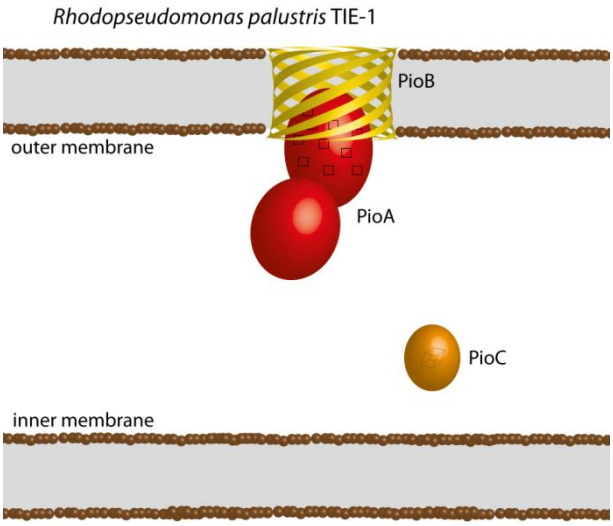

Figure 1.8: predicted location of the products of the *pio* operon based on sequence analysis.
PioA has the two domains represented, with the deca-heme cytochrome domain interacting with PioB in the outer membrane as it happens with this family of proteins. All the predicted co-factors are represented.

Potential Iron-Sulfur protein (HiPIP). These proteins are commonly seen in photosynthetic electron transfer pathways. PioC has a Tat system peptide signal for post-folding translocation to the periplasm, as is common in iron-sulfur proteins. This protein has similarity with several other annotated HiPIPs, including a HiPIP from the acidophilic iron oxidizer *Acidithiobacillus ferrooxidans*, which shows a precedence of the involvement of HiPIPs in iron oxidation.

Because SW2 is not genetically tractable, a different strategy was used to identify the genes involved in photoferrotrophy (53). A cosmid library of SW2 genome was expressed in *Rhodobacter capsulatus* SB1003. This bacterium is related to SW2 but is not capable of growing photoautotrophically exclusively on Fe^{2+}. The cosmids that led to enhanced iron oxidation by SB1003 allowed the identification of the *fox* operon as the probable responsible for photoferrotrophy in SW2 (Figure 1.7 and Figure 1.9). The first coded gene, *foxE*, is a di-heme *c*-type cytochrome with 291 amino acids. Expressing this

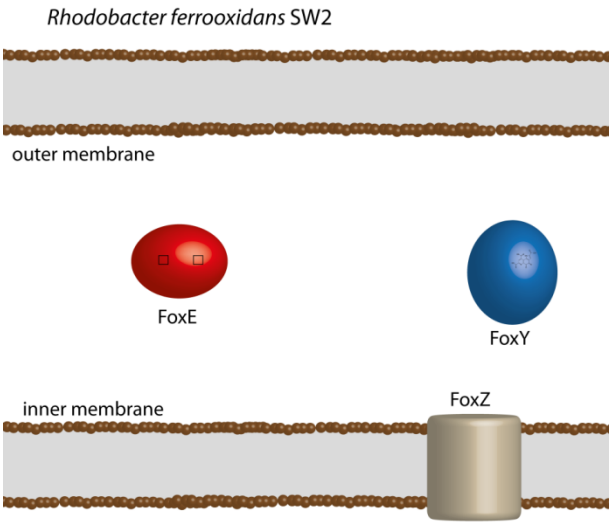

Figure 1.9: predicted location of the products of the *fox* operon based on sequence analysis.
All the predicted co-factors are represented.

gene alone in SB1003 enhances iron oxidation. Therefore, a *c*-type cytochrome was again predicted to be the iron oxidase. A BLAST run of FoxE has no significant hits, indicating a new member of the diverse cytochrome family. The second gene *foxY*, codes for a 362 amino acid protein with a Sec system peptide signal. A BLAST run suggests that this protein binds a pyrroloquinoline quinone (PQQ) redox cofactor. As such, FoxY may be involved in electron transfer between FoxE and the other components of the cyclic photosynthetic electron transfer chain. The last gene, *foxZ*, codes for a 301 amino acid protein with a Sec system signal. Comparison with the databases suggests that this protein is a cytoplasmatic membrane protein with unknown transport function.

In order to try to predict genes that may be involved in photoferrotrophy in the other organisms described here, the protein sequences of the *pio* and *fox* operons were blasted against the available genomes. Only the genomes of the bacteria *Chlorobium ferrooxidans* KoFox and of the type strain of the *Rhodomicrobium vannielii* species, which is also capable of iron oxidation, are available. KoFox has no significant homologues of the Fox or Pio proteins. *Rhodomicrobium vannielii* however, has three consecutive genes (Rvan_3213, Rvan_3214 and Rvan_3215) that have significant homology to the *pioABC* operon and encode a deca-heme cytochrome, its associated outer membrane β-barrel and a hypothetical periplasmatic HiPIP, respectively. The products of these three genes might be able to oxidize iron and transfer electrons to the reaction center as predicted for TIE-1. However, the iron oxidation activity in *Rhodomicrobium vannielii* has little importance in its metabolism, and the primary function of these proteins might be different.

1.3 Multi-heme *c*-type cytochromes

The proteins predicted to be iron oxidizers in TIE-1 and SW2, PioA and FoxE respectively, are multi-heme *c*-type cytochromes. Cytochromes are electron transfer proteins containing a heme cofactor. This cofactor is composed of an iron atom coordinated by a porphyrin ring. Cytochromes can be classified as *a*, *b*, *c* or *d* according to the substituents of the porphyrin ring (62). *c*-type cytochromes are the only in which the porphyrin ring is covalently bound to the polypeptide chain. These connections are thioether bonds between substituents 3 and 8 and the cysteine residues of the binding motif CXXCH, in which the histidine is the proximal ligand to the iron. The distal ligand is found in an unpredictable region of the polypeptide and, in most cases, is another histidine or a methionine, or a less common ligand like lysine, tyrosine, cysteine, asparagine or the N-terminal. Several factors determine the reduction potential of a heme. Depending on protein fold, nature of the axial ligands or the geometry of the cofactor, *c*-type hemes have a reduction potential between -400 and 450 mV (63).

The number of hemes present in a *c*-type cytochrome varies considerably. The protein with the highest number of hemes per peptide to have its structure solved has sixteen *c*-type hemes (64) and the available genomic sequences show that cytochromes can have up to 58 heme binding motifs (65). Some of these numbers are more common like two, three and four hemes. Frequently, the folding of these smaller cytochromes is repeated in tandem in larger cytochromes, probably due to gene duplication and fusion.

Multi heme *c*-type cytochromes are present in almost all groups of Bacteria and Archea. In some groups, the number of different multi-heme cytochromes makes up a substantial part of their proteomes, providing a versatile metabolic capacity. For instance, the different cytochromes in the bacteria of the genus

Shewanella provide the ability to use many different electrons acceptors (66–69).

The covalent binding of several hemes to their apo-protein is a complex process that requires several enzymes in sequential steps. The enzymatic machinery used by the organisms studied in this thesis is the product of the *ccm* operon (60). This operon codes up to nine membrane and periplasmatic proteins that, in a stereo specific way, attach the hemes to their binding sites after the polypeptide is translocated to the periplasm by the Sec pathway. As a consequence, no cytoplasmatic *c*-type cytochromes have been found.

In order to fully understand the functional mechanisms of multi heme cytochromes, a detailed characterization of the role of each individual heme is required. This means determining the heme intrinsic reduction potentials and electron transfer rate constants and understanding how the several cofactors interact. This detailed characterization has been performed for several cytochromes (70–83).

1.3.1 Functional mechanism

With each heme having 2 possible redox states, a multi-heme cytochrome having n hemes has 2^n possible ways of electron distribution, each way defining a redox microstate. These microstates can be thermodynamically described by considering the individual reduction potentials of its reduced hemes. However, due to the close packing of the redox centers, there are electrostatic interactions between hemes. This results in anti-cooperativity in heme reduction due to electron repulsion, and these interactions need to be considered in the functional characterization of a multi-heme cytochrome (84). What also affects the reduction of a heme is thermodynamic coupling to acid-base centers titrating at the physiological pH range (redox-Bohr effect). This interaction results from attraction between the electron and proton and is

therefore cooperative. The heme is not only a redox co-factor but also has two propionate groups that are important in the redox-Bohr effect (76). Taken together the *n* hemes and *m* acid-base centers, there are 2^{n+m} possible microstates. Each of these can be thermodynamically defined by a set of *n* reduction potentials, *m* pK_a values, corresponding heme-heme interactions and redox-Bohr effects (85). Through the characterization of several multi-heme cytochromes, these parameters were shown to be defined in order to originate only a few thermodynamically favorable microstates (84). That is in the activity of a multi-heme cytochrome, instead of 2^{n+m} possible microstates, only a few are significantly populated in physiologically significant conditions (76). This gives specificity to the cytochrome by allowing only the population of microstates that have a physiological and functional meaning. This is illustrated by the c_7 tri-heme cytochrome family. These cytochromes having similar structures have different functional roles, which are dictated by the different sets of favorable microstates (71, 72, 86). Another example is the cytochrome c_3 family. Due to the redox-Bohr effect, only specific microstates are populated that result in energy transduction by converting weakly acidic protons into more acidic protons through coupling with electron transfer (87).

Another important consequence of the close packing of the hemes in multi-heme cytochromes is that it allows for a fast intramolecular electron transfer. This means that, upon the entry or exit of an electron, there is rapid equilibrium between the possible different microstates (88). Therefore, whatever heme receives or donates an electron, only the thermodynamically favorable microstates remain significantly populated. The functional consequences of this rapid equilibrium are illustrated by the small tetra-heme cytochromes (STC) from the bacteria *Shewanella oneidensis* and *Shewanella frigidimarina* (82). In these cytochromes electrons enter the protein only through heme I, in *S. oneidensis*, and mostly through heme IV, in *S.*

frigidimarina. However, the rapid equilibrium in the distribution of electrons in the cytochrome keeps the microstates, in which these hemes are reduced, scarcely populated. This allows the proteins to be ready to receive more electrons until full reduction.

1.4 High potential iron-sulfur proteins (HiPIP)

The third gene present in the *pio* operon is a HiPIP. HiPIPs together with ferredoxins form a group of proteins that contain a 4Fe-4S cluster arranged as a cubane and coordinated by four cysteine residues. Under physiological conditions this cluster in HiPIPs changes between +2 and +3 oxidation states (89) and its reduction potential ranges from 50 to 500 mV (90). In Ferredoxins it changes between oxidation states +1 and +2 and has an average reduction potential of -400 mV (89). What defines the accessible oxidation states of these two protein families is still debated, but exposure to the solvent and hydrogen-bond network are important aspects (91). The 4Fe-4S clusters are assembled in the cytoplasm of bacteria and the holoprotein is then translocated folded by the Tat translocation system to the periplasm where it functions.

1.4.1 Biological function

HiPIPs are single electron transfer proteins. Having a high reduction potential HiPIPs are primarily found in purple photosynthetic bacteria where they function as electron mediators between the cytochrome bc_1 and the reaction center tetra-heme cytochrome in cyclic photosynthesis (92, 93). A few exceptions are the case of *Rhodothermus marinus* (94, 95) or of *Acidithiobacillus ferrooxidans* (96, 97) where the HiPIPs are involved in respiration.

1.4.2 HiPIP structure

HiPIPs are small proteins without highly conserved sequences. According to the Protein data Bank the structure of HiPIPs of eight different organisms has been solved, either by X-ray diffraction or NMR spectroscopy (*Allochromatium vinosum*, *Thermochromatium tepidum*, *Halorhodospira halophila*, *Rhodocyclus tenuis*, *Marichromatium purpuratum*, *Rhodoferax fermentans*, *Ectothiorhodospira shaposhnikovii* and *Rhodothermus marinus*). All these are photosynthetic Proteobacteria with the exception of *Rhodothermus marinus*, which belongs to the Bacteroidetes group. Even though the sequences of HiPIPs are not highly conserved, all the structures have a common folding around the cluster. The 4Fe-4S cluster is secluded from the solvent and surrounded by aromatic residues that contribute to its stabilization (98, 99). Another common feature is an alfa-helix near the N-terminal. Away from the cluster, HiPIPs present loops of variable length originated by non-conserved insertions.

1.5 Biotechnological applications

Besides the described biological and geological relevance of the study of photoferrotrophy, studying this metabolism will ultimately lead to biotechnological relevant information. The organisms under study have versatile metabolisms with potential to be used in different biotechnological applications.

1.5.1 Hydrogen production

Given the current world population growth and the evidence for climate change, finding new sustainable and clean energy sources is a priority. Hydrogen is a viable alternative fuel as it causes no CO_2 emissions and has a higher energy yield than current fossil fuels. Currently most H_2 is produced

from fossil fuels, and as demand for H_2 increases (100) sustainable production mechanisms are required. Several sustainable approaches are currently researched (101), including biological photosynthetic production (102).

In phototrophs H_2 is produced by hydrogenases and nitrogenases, which are O_2 sensitive enzymes. In oxygenic phototrophs this creates the requirement for approaches that separate photosynthesis and H_2 production either spatially or temporally (103, 104). Anoxygenic phototrophs, like the ones under study here, have the advantage of not having to deal with oxygen. In these organisms, H_2 is produced mostly by nitrogenases. These enzymes catalyze the reduction of N_2 and have H_2 as an obligate product, being able to produce only H_2 in the absence of N_2. In the genomes of the organisms under study two different nitrogenases are coded: Fe-Fe and Mo-Fe nitrogenases. Several different strains of *R. palustris* have been used in H_2 production (105–107), as well as different species of the genus *Rhodobacter* (108–110). This makes TIE-1 and SW2 good candidates for H_2 production, in particular TIE-1 as it is genetically tractable.

1.5.2 Bioremediation

Bioremediation is the utilization of an organism's metabolism for the removal or treatment of pollutants. The bacteria under study in this work have a versatile metabolic capacity, being able to feed on a variety of organic and inorganic substrates. In their genomes they code for several enzymes involved in the degradation of aromatic pollutants (111, 112) and also several cytochromes P450 (113) and S-transferases (114), enzymes involved in degradation of xenobiotics. This makes them good candidates for bioremediation applications.

The iron precipitation process also has potential applications. The precipitation of ferric iron promotes co-precipitation of other molecules and ions in solution. This has been suggested as strategy to clean contaminated waters (24).

1.5.3 Microbial fuel cells

Microbial fuel cells (MFC) are a rising technological field with clean energy production potential (115) combined with the capacity to perform bioremediation. An MFC is a bioelectrochemical device that uses the metabolism of bacteria to produce electrical current (Figure 1.10). Bacteria gather energy by transferring electrons from low potential substrates to high potential ones. In a MFC an electrical circuit is placed in this electron flow in order to harness electrical energy. The bacteria in a MFC feed on different substrates, preferably organic or inorganic wastes, and use an anode as an electron acceptor. The electrons then flow through the electrical circuit to a cathode and are ultimately transferred to a terminal electron acceptor.

Many advances have been made in this technology, and several issues are research targets for optimization. Although MFCs have a theoretical potential that depends on the standard potentials of the substrates and final electron acceptors being utilized, these values are never reached. These potential losses are due to ohmic losses and overpotentials, which depend on the design of the cell and on the choice of final electron acceptor and microbial culture at the anode. Different cultures, either axenic or mixed, can be used at the anode (116). Depending on the working conditions of the cell, different species thrive at the anode. Important factors in this adaptation are inoculum source, the fed substrates or the anode potential (117).

The electron transfer mechanism from the cells to the anode is also debated. Different bacteria seem to have different mechanisms of electron transfer.

Some species use small organic electron shuttles (118–120). These molecules are reduced by the cells, then diffuse to the anode to deliver the electrons and are then reused. Another strategy is the production of electron conducting nanowires that connect the different cells in a biofilm and the electrode (121, 122). A third mechanism is the direct electron transfer from the cells to the electrode through outer-membrane bound electron transfer proteins, a mechanism that requires a close interaction between the cells and the electrode (42, 123). A better understanding of these electron transfer mechanisms will allow an optimization of this step in the electron flow, thus limiting potential losses.

Another aspect is the choice of terminal electron accepter at the cathode. The most used acceptor is O_2. Oxygen has several advantages: it has a high reduction potential, it is easily available and it is free. It has the disadvantages of having slow reduction kinetics, creating the need for expensive catalysts, like platinum, and of being able to diffuse into the anode chamber and inhibit bacterial activity. Another commonly used acceptor is ferricyanide. This molecule has low overpotential and has allowed a higher power density then oxygen (115). However, it needs to be regularly replaced, as it is insufficiently reoxidized by oxygen. It is also possible to reduce protons at the cathode producing H_2 (124). So far the potentials in MFC do not allow the reaction without an increase in potential through an external source, but production of H_2 is a promising option in MFCs (125, 126). Another approach is the utilization of a second bacterial culture that receives the electrons at the cathode (127). Biocathodes where Mn (128) or Fe (129) are oxidized have been studied. In this last approach the acidophilic iron oxidizer *Acidithiobacillus ferrooxidans* was utilized with the electrons ultimately transferred to O_2.

As photosynthetic bacteria that oxidize iron, the bacteria studied in this thesis are good candidates for being used in the cathode of MFCs. Being

photosynthetic these organisms would have the advantage of using CO_2 as final electron acceptor, thus creating an MFC that should be CO_2 neutral. The understanding of molecular mechanisms of photoferrotrophy should allow determining if this metabolic capacity can be used in this biotechnological application and to determine how a prototype could be optimized.

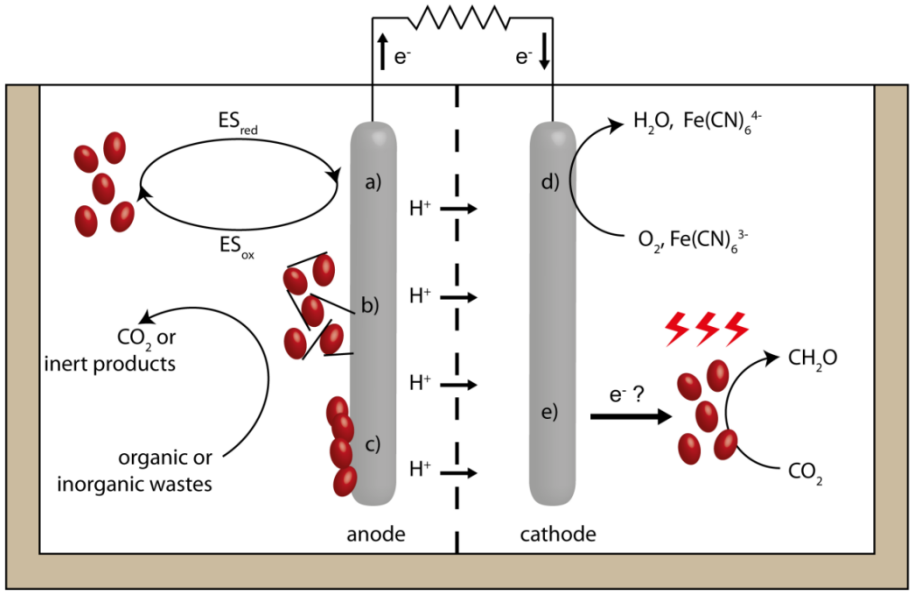

Figure 1.10: schematic representation of an MFC.
Bacteria at the anode chamber feed on organic or inorganic wastes and transfer electrons to the anode through: a) electron shuttles (ES), b) nanowires or c) directly through outer membrane cytochromes. The protons produced flow through the selectively permeable membrane (dashed line) to the cathode chamber and the electrons flow through an electrical circuit to the cathode. The electrons are then transferred to the final electron acceptor. This can be d) abiotic or e) biotic. In the present case, the utilization of a photoferrotroph is suggested.

2

The FoxE iron oxidoreductase of *Rhodobacter ferrooxidans* SW2

The work presented in this chapter was published in:

- Ivo H. Saraiva, Dianne K. Newman, Ricardo O. Louro. 2012. Functional characterization of the FoxE iron oxidoreductase from the photoferrotroph *Rhodobacter ferrooxidans* SW2. *J Biol Chem*. doi:10.1074/jbc.M112.360636
  Ivo H. Saraiva designed and performed all the experiments and participated in the writing of the manuscript

- Luís Pereira, Ivo H. Saraiva, Ricardo Coelho, Dianne K. Newman, Ricardo O. Louro, Carlos Frazão. 2012. Crystallization and preliminary crystallographic studies on FoxE from *Rhodobacter* ferrooxidans SW2, a Fe(II) oxidoreductase involved in photoferrotrophy. *Acta Crystalogr F*. *In press*.
  Ivo H. Saraiva performed the purification of FoxE.

- will be published in a further manuscript in preparation

2 The FoxE iron oxidoreductase of *Rhodobacter ferrooxidans* SW2

2.1 Introduction

Despite the importance of photoferrotrophy for understanding the co-evolution of life and Earth, little is known about its molecular mechanisms. *Rhodobacter ferrooxidans* SW2 has been a subject of studies aiming to understand biologically induced mineralization because ferric (hydr)oxides precipitate away from the cell and no mineral is found inside the cells or encrusting the cell surface (130–132). It is also known that SW2 utilizes only soluble Fe(II) compounds as the electron source for photoferrotrophy and does not actively dissolve Fe(II) minerals (132), suggesting that iron oxidation does not occur at the cell surface. Recently, the operon *foxEYZ* from SW2 was found to stimulate light-dependent Fe(II) oxidation by the bacterium *Rhodobacter capsulatus* SB1003 (53). This operon is composed of three genes: *foxE,* that encodes a 29 kDa protein containing two canonical heme *c* binding sites, *foxY,* that encodes a predicted pyrroloquinoline quinone binding protein, and *foxZ,* that encodes a predicted inner membrane transport protein. FoxE was predicted to be the iron oxidoreductase and to perform the main step in photoferrotrophy because its expression alone is enough to significantly enhance light-dependent Fe(II) oxidation activity on SB1003 (53). This *c*-type cytochrome has no significant sequence homology with other predicted proteins in the genomic databases, which suggests a novel protein fold and cofactor organization. It has also no predicted transmembrane domains or lipoprotein attachment sites typical of outer-membrane associated proteins. The lack of obvious membrane attachment suggests a periplasmatic location

for FoxE that is in agreement with the requirement of soluble Fe(II) for the photoferrotrophic metabolism of SW2 (132). However, this cellular location implies the occurrence of mechanisms to avoid iron precipitation in the periplasm. Detailed characterization of the iron oxidoreductase FoxE is crucial for the understanding of this photosynthetic metabolism.

To investigate the first step of photoferrotrophy in SW2, detailed functional and structural characterization of FoxE was performed.

2.2 Experimental procedures

Cloning

The *foxE* gene was amplified by PCR from the plasmid pfoxE (53) and cloned without its periplasmic signal sequence (predicted with SignalP) into the NcoI/EcoRI sites of the pET20b(+) plasmid, which contains the periplasmic signal sequence pelB from E. coli. The fragment pelB:foxE was amplified by PCR and cloned into the BglII/EcoRI restriction site of plasmid pUX19 (133). The resulting plasmid was used to transform E. coli JCB7123 cells containing the pEC86 plasmid (134), which codes for the c-type cytochrome maturation (ccm) operon that allows E. coli to produce cytochromes in aerobic conditions. All constructs were confirmed by DNA sequencing.

Expression and growth

Cells were grown in Lysogeny Broth (LB) supplemented with 50 $\mu g.mL^{-1}$ kanamycin and 34 $\mu g.mL^{-1}$ chloramphenicol to maintain selective pressure for the pUX19 and pEC86 plasmids respectively. Frozen stocks of E. coli JCB7123 containing both plasmids were used to inoculate 200 mL of LB. The culture was grown for 24 h at 30° C and stirred at 140 rpm. The resulting cell culture was used for a 1% inoculum of four 5 L conical flasks with 3.5 L of LB each and the same growth conditions were used. After cell harvesting, cell pellets were resuspended in 300 mL of extraction solution (0.5 M sucrose, 0.2 M TrisHCl, 0.5

mM EDTA, 100 mg.L^{-1} lysozyme, pH 8) and incubated in ice for 30 min with gentle stirring. The resulting spheroplasts were pelleted and the supernatant, containing the periplasm, was cleared by ultracentrifugation at 138000 g for 30 min and then frozen at -80° C.

Purification

The periplasmic fractions of four growth batches were pooled, concentrated in an ultrafiltration cell with a 30 kDa cut-off membrane and dialyzed twice against 20 mM TrisHCl pH 7.6 for 12 h. The resulting fraction was loaded into a DEAE chromatography column equilibrated with 20 mM TrisHCl pH 7.6. A step gradient with 20 mM TrisHCl, 1 M NaCl, pH 7.6 was used to elute the bound proteins and FoxE was eluted at 150 mM NaCl. The presence of the cytochrome was determined by UV-visible spectroscopy and SDS-PAGE stained to detect hemes (135). Fractions containing FoxE were pooled, concentrated and washed with 5 mM potassium phosphate buffer at pH 7 in an ultrafiltration cell with a 30 kDa cut-off membrane. The resulting fraction was loaded into a hydroxylapatite chromatography column equilibrated with 5 mM potassium phosphate buffer at pH 7. Bound proteins were eluted with a step gradient and FoxE was eluted at 50 mM potassium phosphate buffer at pH 7. The pure protein yield was 1.5 mg per liter of culture medium. Both chromatography steps were performed in a GE Äktaprime Plus purification system.

The binding of two heme groups to the FoxE polypeptide was confirmed by mass spectrometry (MALDI-TOF) analysis.

Dynamic light scattering

Dynamic light scattering (DLS) experiments were performed in a Malvern Instruments Zetasizer Nano at 25 °C. FoxE samples were prepared in 50 mM potassium phosphate buffer at pH 7. The molecular weight of the FoxE particle was estimated using the manufacturer's software.

UV-visible spectroscopy

UV-visible spectra were recorded in a Shimadzu UV-1700 spectrophotometer at room temperature (~25°C).

EPR spectroscopy

EPR spectroscopy was performed in a Bruker EMX spectrometer equipped with an ESR-900 continuous-flow helium cryostat. The spectrum was recorded under the following conditions: microwave frequency, 9.391 GHz; microwave power, 2 mW; modulation frequency, 100 kHz; modulation amplitude, 1 mT; temperature, 13 K. FoxE was prepared in 50 mM potassium phosphate pH 7 buffer and oxidized with potassium hexachloroiridate(IV).

NMR spectroscopy

^{1}H-NMR spectroscopy was performed in a 500 MHz Bruker Avance II+ spectrometer at 25 °C. FoxE samples in 50 mM potassium phosphate buffer pH 7 were lyophilized twice and solubilized in D_2O before spectra acquisition. The residual water signal was suppressed by pre-saturation. The sample was reduced with small amounts of sodium dithionite or sodium ascorbate and oxidized with potassium ferricyanide. A 2D NOESY spectrum of a 4.9 mM FoxE sample was obtained with 8192x144 points, 512 scans, a 45kHz sweep width and a mixing time of 25 ms. Longer mixing times caused the loss of cross peaks. A superWEFT 180° pulse was used to suppress the water signal and reduce the intensity of sharp diamagnetic signals (136).

Redox titration

Redox titrations were performed at 25 °C inside an anaerobic glove box (Coy Laboratory Products, Inc.) in an OTTLE cell using a potentiostat (CH Instruments) with a three electrode system: two platinum wire meshes comprised the working electrode, a platinum wire was used as counter electrode and a saturated calomel electrode was used as the reference electrode. Potential values were converted to standard hydrogen electrode

(SHE) by adding 241 mV to the imposed potentials. The FoxE concentration was 20 μM prepared in 50 mM phosphate buffer with 300 mM KCl. A mixture at 40 μM of each of the following mediators was used: potassium ferricyanide, n,n-dimethyl-p-phenyldiamine, p-benzoquinone, 1,2-naphtoquinone-4-sulphonic acid, 1,2-naphtoquinone, trimethyl hydroquinone, phenazine methosulphate and 1,4-naphtoquinone. Different mediator concentrations were used to check for their possible interference with FoxE. No effects in the reduction potentials were detected. Data were collected in reductive and oxidative directions and were reproducible within 10 mV.

Stopped-flow

Stopped-flow experiments were performed in a KinetAsyst SF-61DX2 Hitech Scientific apparatus placed inside an anaerobic glove box (MBraun 150-GI). FoxE at 1 μM (after mixing) in 50 mM phosphate buffer with 300 mM KCl was reduced with Fe(II)-EDTA at different concentrations (150, 100 and 50 μM after mixing). Reduction of FoxE was followed at the Soret band (417 nm) and the reduction fractions were calculated by normalization using the fully reduced and fully oxidized absorbance values. Fe(II)-EDTA was prepared by mixing $FeSO_4$ and NaEDTA in a 1:1.5 ratio inside the anaerobic glove box. Speciation in solution was calculated using the PHREEQC Interactive 2.18.5314 software with the minteq.v4.dat database (137). Fe(II)-EDTA was always the dominant species in solution (Table 2.1).

Table 2.1: Speciation and reduction potential of FeEDTA.
Values were determined with the minteq.v4.dat database for the experimental conditions used.

	% of $Fe(EDTA)^{2-}$	E_m of FeEDTA
pH 6	99%	130 mV
pH 7	89%	114 mV

Kinetic analysis

The kinetics of reduction of FoxE was analyzed considering a collisional model, in which the association and dissociation of the electron donor and the protein are in fast equlibrium. Therefore:

$$rate_i = K_i[Fe(II)EDTA][heme_i] \quad \text{2-1}$$

Experiments were performed in pseudo-first order conditions. A linear dependence of the pseudo-first order rate constants with Fe(II)-EDTA concentration allowed the determination of second order rate constants. According to Marcus theory the rate constants depend on the driving force, on the reorganization energy and on structural factors. To separate the structural factors from the contribution of the driving force, the reduction rate constants (K_i) of each heme i were described by the following equation:

$$K_i = k_i \exp\left[-\frac{\left(\lambda - F\Delta E_i^0\right)^2}{4\lambda RT}\right] \quad \text{2-2}$$

where k_i is the intrinsic rate constant that accounts for the structural factors of the i^{th} heme, ΔE^0_i is the potential of reduction of the i^{th} heme by the electron donor , F is the Faraday constant, R is the gas constant, T is the temperature and λ is the reorganization energy, taken as 1 eV (88). The reorganization energy and the structural factors were considered constant during reduction. The kinetics of the reduction of FoxE were analyzed considering the two hemes independent and therefore described by the sum of two exponentials. The model was implemented in Matlab and fit to the experimental data using the Nelder-Mead simplex algorithm (138). Standard errors of the fit parameters were obtained from the diagonal elements of the covariance matrix (139).

X-ray crystal structure

Crystallization and structure determination are described elsewhere (140).

2.3 Results

The purity of FoxE was assessed by SDS-PAGE (Figure 2.1). The UV-spectrum of FoxE as purified has maxima at 553, 523, 416, 319 and 274 nm. The cytochrome was considered pure with a ratio $Abs_{416/274}$~5. The presence of the peaks at 553 and 524 nm, the α and β bands respectively, indicate partial reduction of the cytochrome during purification, even though all procedures were performed in aerobic conditions. Full reduction with sodium ascorbate originates peaks at 553 nm for the α band, 523 nm for the β band and 417 nm for the Soret band. In the fully oxidized state, obtained by adding potassium ferricyanide, the Soret band shifts to 411 nm and the α and β bands become broad, typical of the low spin hexacoordinated hemes.

The degree of homogeneity of the sample was determined by DLS. The results indicate that the sample is monodispersive with a diameter of 8.3 nm. Assuming a globular shape, this translates into an approximate molecular weight of 99.4±10.1 kDa. This is approximately three times the molecular

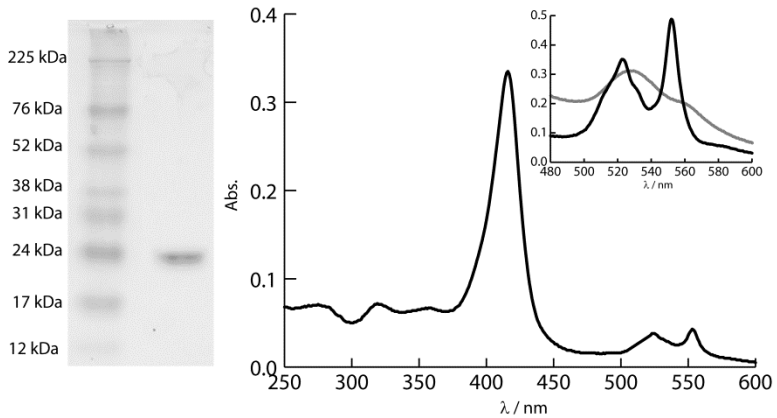

Figure 2.1: SDS-PAGE and UV-visible spectrum of FoxE.

The gel shows a single band from FoxE. The spectrum is from FoxE as purified and the inset shows the fully reduced (black) and fully oxidized (gray) spectra of FoxE in the alpha and beta region.

weight deduced from the annotated sequence plus two hemes (29 kDa).

The preliminary structural model of FoxE was determined by X-ray crystallography. For the crystallization conditions used FoxE forms a homotrimer complex (Figure 2.2A). Each monomer has two domains, where each domain binds a *c*-type heme (Figure 2.2B). The hemes were numbered according to the order by which their respective binding site appears in the amino acid sequence. The secondary structure is composed of α-helices and loops. Monomer contacts are performed mostly through the Heme I domain plus two N-terminal α-helices that form an arm embracing the neighboring monomer. Even though the two domains have little sequence homology, they present the same structural folding (Figure 2.2C). The Heme II domain is sequentially inserted in the Heme I domain, and the two hemes have similar coordination, with the distal ligands of Heme I and II being M230 and M116, respectively. The hemes have a similar binding cavity, with the exception of the two N-terminal α-helices that form part of the binding cavity of the Heme I from the neighboring monomer. The distance between redox cofactors is an important factor controlling electron transfer. The intra monomeric heme-heme distance is 18 Å, with the shortest inter monomeric heme distance being 25 Å between Hemes I. Additionally, the Heme I domain shows one intra monomeric disulfide bond between C80 and C258, at 16 Å from Heme I and 32 Å from Heme II.

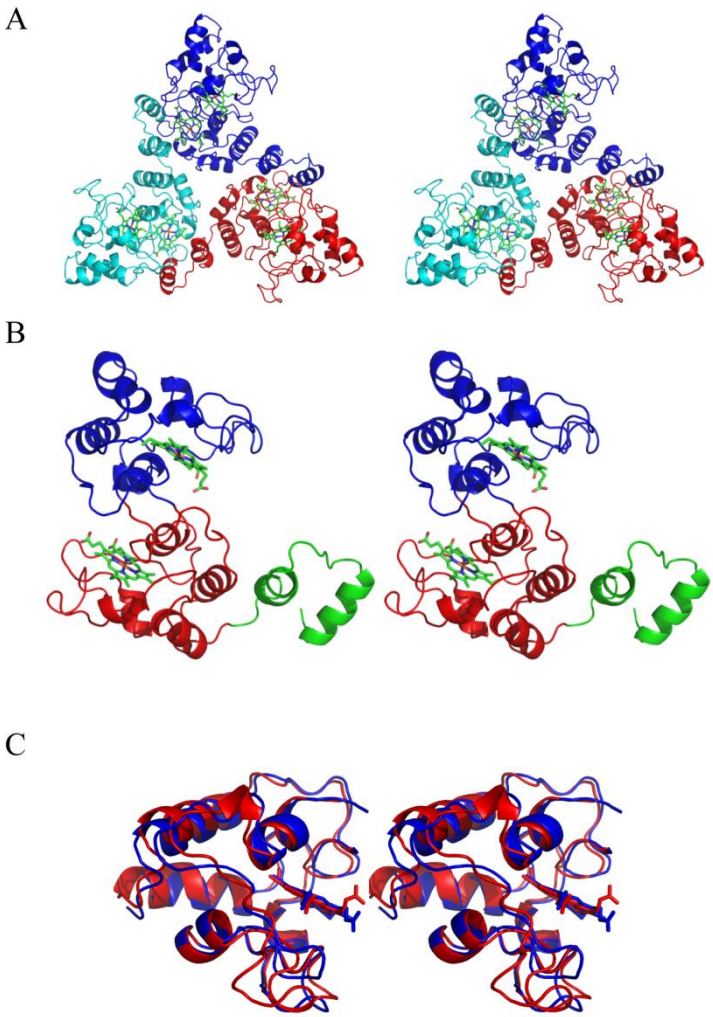

Figure 2.2: X-ray crystal structure model of FoxE.
A) Stereo view of the FoxE trimer showing the three monomers in different colors, with the hemes in stick representation. B) Stereo view of the FoxE monomer with the Heme I domain in red, the Heme II domain in blue, and the N-terminal α-helices in green. C) Stereo view of the superposition of the Heme I domain (blue) and the Heme II domain (red).

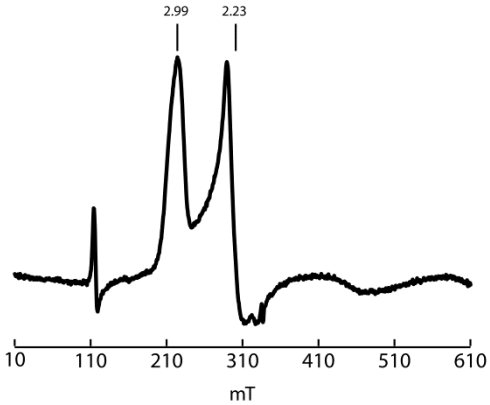

Figure 2.3: X-band EPR spectrum of fully oxidized FoxE.
The background from the cavity has been subtracted. On top the g-values of the main features of the spectrum are indicated.

EPR spectroscopy was performed to evaluate the spin state and coordination of FoxE (Figure 2.3). The spectrum suggests that both hemes are low-spin, rhombic and hexacoordinated and agrees with typical His-Met coordinated hemes (141).

1D ^{1}H-NMR spectra of FoxE were collected with the sample poised at various partially oxidized conditions (Figure 2.4). In the reduced state both hemes are diamagnetic and in the oxidized state they are low-spin paramagnetic without

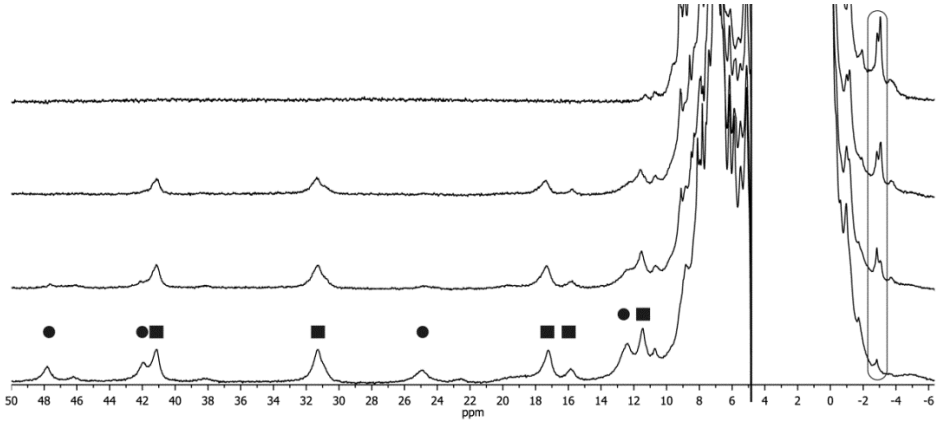

Figure 2.4: 1D ^{1}H-NMR spectra of FoxE poised at different degrees of oxidation.
Spectra from fully oxidized (bottom) to fully reduced (top) are presented. Signals identified with a circle belong to the HP heme and signals identified with a square belong to the LP heme. The rounded box at approximately -3 ppm highlights the signals tentatively assigned to the heme axial methionines.

any visible evidence of high-spin, in agreement with the low temperature EPR data. The signals in both oxidation states are much broader than expected for a protein with 29 kDa in agreement with the formation of a trimer (79).

Ferricyanide oxidized FoxE shows two sets of paramagnetically shifted signals in the spectral region where heme methyls and propionate CH_2 protons are found (142). These two sets are differentiated by line width (Figure 2.4): a set of sharper signals from one heme and a set of broader signals from the other heme. This indicates that although the sample is homogeneous, as deduced from the DLS data, there appears to be microscopic heterogeneity in the environment of one of the hemes that causes broadening of its signals. Progressive reduction of FoxE with sodium ascorbate or sodium dithionite causes the concerted decrease and disappearance of the set of signals with broader line width. This indicates that these signals belong to the same heme, which has the highest reduction potential (HP), being the first to be reduced. Further addition of reducing agent causes the decrease and disappearance of the sharper signals that belong to the heme with the lowest reduction potential (LP). There is no spectral discrimination between the hemes of different monomers of FoxE, as expected from a homo-oligomer that necessarily must display symmetry in the arrangement of the monomeric units. The spectra in Figure 2.4 also show appearance of two signals close to -3 ppm upon reduction of the cytochrome. These can be tentatively assigned to the methyl groups of heme axial methionines. In diamagnetic hemes coordinated by methionine this group shows a signal in this region due to ring currents of the porphyrin ring (143). From the order of appearance of those signals during the progress of the titration, the signal at -2.84 ppm can be assigned to the axial methionine of the HP hemes and the signal at -3.05 ppm can be assigned to the axial methionine of the LP hemes. Also in this case, the signal assigned to the methyl of the methionine attached to the HP heme is broader.

Progressive re-oxidation of ascorbate reduced FoxE restores the LP signals followed by the HP signals. However, re-oxidation of dithionite reduced FoxE only restores the LP signals that appear with a small shift (Figure 2.5). In these experiments no high-spin signals were detected between 40 and 100 ppm, where high-spin heme signals appear. The EPR spectrum of oxidized FoxE previously reduced with dithionite indicates a change in the coordination environment of one of the hemes but not of spin state. The data suggest that the HP heme NMR signals are broadened beyond detection due to chemical exchange. Full oxidation of the sample was confirmed by UV-visible spectroscopy and no changes in the spectrum were observed. This indicates that reduction by sodium dithionite induces an irreversible conformational change in the protein that mostly affects the environment of the HP hemes.

To determine the reduction potentials of the hemes, redox titrations of FoxE were followed by visible spectroscopy (Figure 2.6). The data was fit with two independent Nernst equations resulting in potentials of 207 mV and 270 mV at pH 7 and potentials of 253 mV and 309 mV at pH6. The potentials of both hemes in each monomer increase with a decreasing pH.

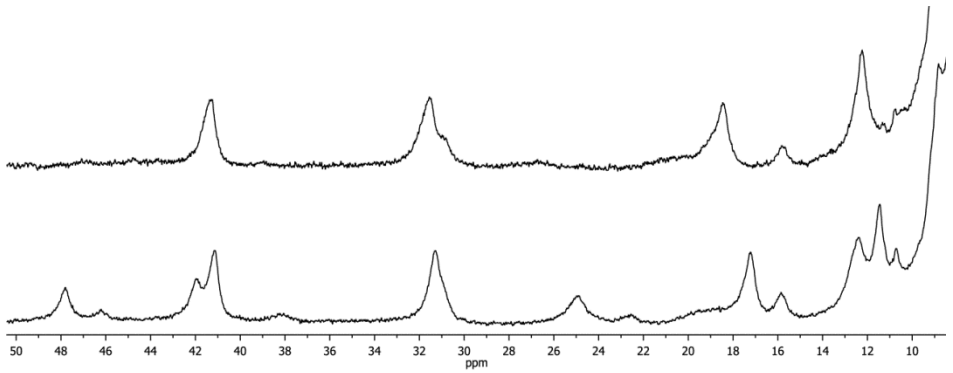

Figure 2.5: 1D ^{1}H-NMR spectra of FoxE fully re-oxidized with $K_3Fe(CN)_6$.
FoxE was reoxidized after reduction with sodium dithionite (top) or sodium ascorbate (bottom). Full oxidation of both samples was independently confirmed by UV-visible spectroscopy

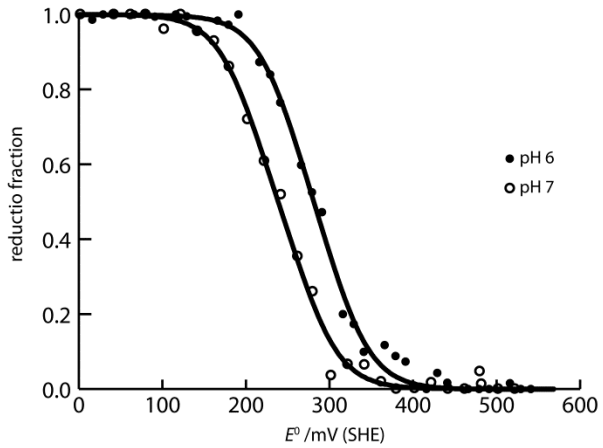

Figure 2.6: redox titrations of FoxE at pH 6 and pH 7 at 25°C. The solid lines represent the best fits of the data.

Kinetic measurements of FoxE reduction by Fe(II)-EDTA were performed in pseudo-first order conditions at three different Fe(II)-EDTA concentrations. These measurements yield a biphasic trace with each phase corresponding to 50% of FoxE reduction (Figure 2.7). The pseudo-first order rate constants of each phase show a linear dependence with Fe(II)-EDTA concentration. Experiments were performed at pH 6 and pH 7. The biphasic behavior was maintained at both pH values and FoxE reduction was faster at the more acidic pH (Table 2.2). Measurements starting with partially reduced FoxE have decreased amplitude of the fast phase of reduction at both pH values.

Table 2.2: reduction potentials of the two hemes of FoxE and kinetic parameters for the reduction of FoxE determined at pH 6 and pH7 at 25°C.
Values between parentheses indicate the standard error determined from the diagonal elements of the covariance matrix.

	pH 7	pH 6
E_m^{LP} (*mV*)	207(4)	253(4)
E_m^{HP} (*mV*)	270(4)	309(4)
k_{LP} ($s^{-1}\mu M^{-1}$)	2.0(0.2)	1.8(0.3)
k_{HP} ($s^{-1}\mu M^{-1}$)	8(2)	18(3)
K_{LP} ($s^{-1}mM^{-1}$)	0.67(0.05)	1.0(0.2)
K_{HP} ($s^{-1}mM^{-1}$)	8(1)	26(4)

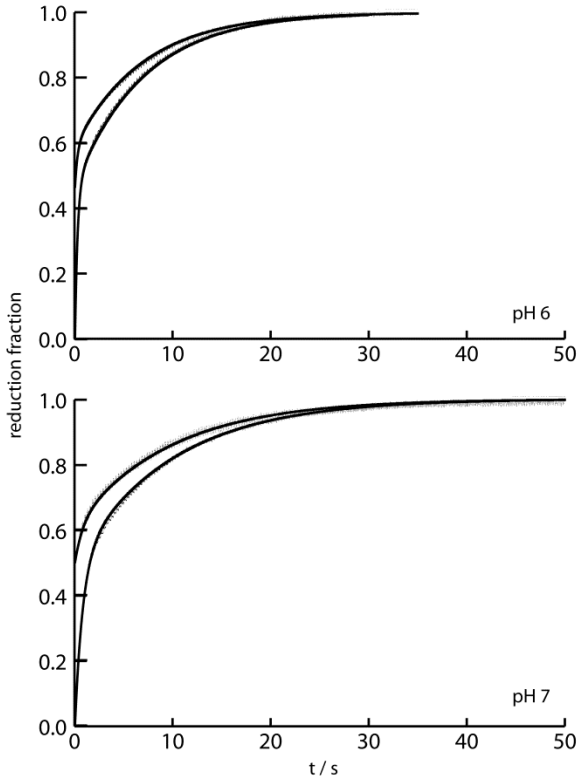

Figure 2.7: kinetic traces of FoxE reduction with Fe(II)-EDTA at pH 6 and pH 7 at 25°C. At each pH FoxE was reduced starting from totally or partially oxidized. The solid lines represent the best fit of the data.

2.4 Discussion

c-type cytochromes are ubiquitous redox proteins present in all domains of life. Depending on many factors such as solvent exposure or the nature of iron distal coordination, *c*-type cytochromes display reduction potentials that range from approximately -550 to 450 mV (63). This large range allows for their involvement in diverse bioenergetic pathways, including Fe(II) oxidation. A multi heme cytochrome that is the putative Fe(II) oxidoreductase from *Rhodobacter ferrooxidans* SW2, FoxE, was successfully produced in *E. coli* and was functionally and structurally characterized *in vitro*.

The determined crystal structure of FoxE shows a new folding in the *c*-type cytochrome family. The hemes, with His-Met coordination, are enclosed by α-helices and inter helices loops. This folding is repeated 6 times in a trimer complex with a "bowl" like structure. The Heme I domains form a ≈25 Å equilateral triangle at the base and the Heme II domains form a ≈40 Å equilateral triangle at the "bowl" rim. All domains function independently, at least at the *in vitro* experimental conditions used.

According to the EPR spectrum of FoxE, the two heme types have similar rhombic magnetic tensors and the observed g-values are in agreement with the distal ligand of the hemes being a methionine. The magnetic properties in hexacoordinated His-Met hemes are determined by the orientation of the axial ligands. It is this geometry that determines the shape of the heme frontier molecular orbitals occupied by the unpaired electron. In both hemes of FoxE the His imidazole plane is parallel to the Met δS-εC bond and the ligands have the same orientation in relation to the hemes. This geometry originates the observed rhombic tensors and is in agreement with the dispersion of the NMR paramagnetic signals, which depend on the unpaired electron density around the ring (144).

Mechanistic insights into FoxE reduction were obtained from NMR experiments. The progressive reduction of FoxE followed by NMR spectroscopy showed that the two hemes are reduced at different poised potentials. This can arise from different intrinsic reduction potentials or from a large negative cooperativity between the hemes. The latter option implicates a close proximity between the hemes or a substantial conformational change in the heme environments. According to the crystal structural model all hemes are more than 18 Å apart. At this distance electrostatic interactions are negligible and cannot cause significant negative cooperativities (145). 1D NMR spectra of partially-reduced FoxE present no shifts of the LP signals towards the diamagnetic chemical shift position of the reduced state (Figure 2.4). This suggests that intra molecule electron transfer is slow in the NMR timescale (76). Considering the relationship between distance and electron transfer rate (146), slow electron transfer is in agreement with the inter heme distances determined in the structural model, both for the two hemes within each monomer and also across monomers. These data suggest that all the hemes in the oligomer are reduced independently, with the HP and LP hemes being found in different electrostatic environments. Also, substantial conformational rearrangement of the heme environment would change the chemical shift pattern of the paramagnetic heme signals, which are exquisitely sensitive to conformational changes. This is not observed in the experimental data. Given the evidence for lack of significant electrostatic interactions between hemes and rearrangement of the hemes regions, the data from the redox titrations of FoxE were fit by adding two Nernst equations providing the reduction potentials of the HP and the LP hemes.

The influence of pH on the reduction potentials of the hemes was also studied. It was observed that lowering the pH from 7 to 6 results in an increase in the reduction potential of all hemes (46 mV for the LP hemes and 39 mV for the HP

hemes). This influence of pH (redox-Bohr effect) indicates that electron transfer is thermodynamically coupled to proton transfer in the physiological pH range. In other multi-heme cytochromes the heme propionates are often identified as the major contributors to this effect (76). In environments with circumneutral pH, ferrous iron has many different forms with reduction potentials ranging from -200 mV to almost 400 mV (147). The potentials of the hemes of FoxE are positioned to make the oxidation of many of these iron forms thermodynamically favorable and enable FoxE to perform its predicted task of capturing electrons from Fe(II) to deliver to the photosynthetic reaction center, either directly or via a relay of other electron transfer partners (Figure 2.8).

Having shown that FoxE is thermodynamically suitable for physiologically harvesting electrons from soluble ferrous iron to support anoxygenic

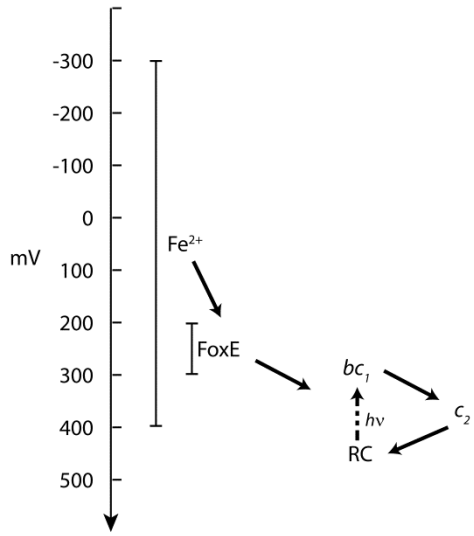

Figure 2.8: electron flow diagram in the periplasm of SW2.
The vertical bar represents reduction potential. The solid arrows indicate electron flow. FoxE can potentially reduce any of the components of the cyclic photosynthesis electron chain: bc_1, cytochrome bc_1; c_2, cytochrome c_2; RC, photosynthetic reaction center. The dashed arrow indicates the ET through the quinone pool from the light excited RC to the cytochrome bc_1. The vertical Fe^{2+} line indicates the reduction potential range of Fe^{2+} species at circumneutral pH.

photosynthesis, the electron transfer kinetics was investigated. In the stopped-flow experiments Fe(II)-EDTA was used as the electron donor for three reasons: it is soluble and thus is a suitable mimic of the physiological iron forms used by SW2; its reduction potential is within the range of values for iron compounds likely to be found in the habitat of SW2 (148) and; in the pH range corresponding to optima for SW2 growth (58) a single species is dominant, therefore facilitating the kinetics analysis. Reduction of fully oxidized FoxE by Fe(II)-EDTA is a biphasic process (Figure 2.7). The fast phase and the slow phase constitute approximately 50% of total reduction, each. The NMR data established that the intra molecule electron transfer is slow, which means that the hemes are independently reduced by Fe(II)-EDTA and each phase corresponds to the reduction of each heme type. As such, the amplitude of each phase is proportional to the initial oxidation fraction of the respective heme type. In order to assign each phase to specific hemes, stopped-flow experiments were performed with FoxE poised in a partially reduced state (Figure 2.9). Because the two heme types have different reduction potentials, in partially reduced FoxE they will have different oxidation fractions. In these experiments the fast phase has smaller amplitude than the slow phase. This observation identifies the HP hemes, which have a smaller initial oxidation fraction, as those reduced in the fast phase. The LP hemes are reduced in the slow phase.

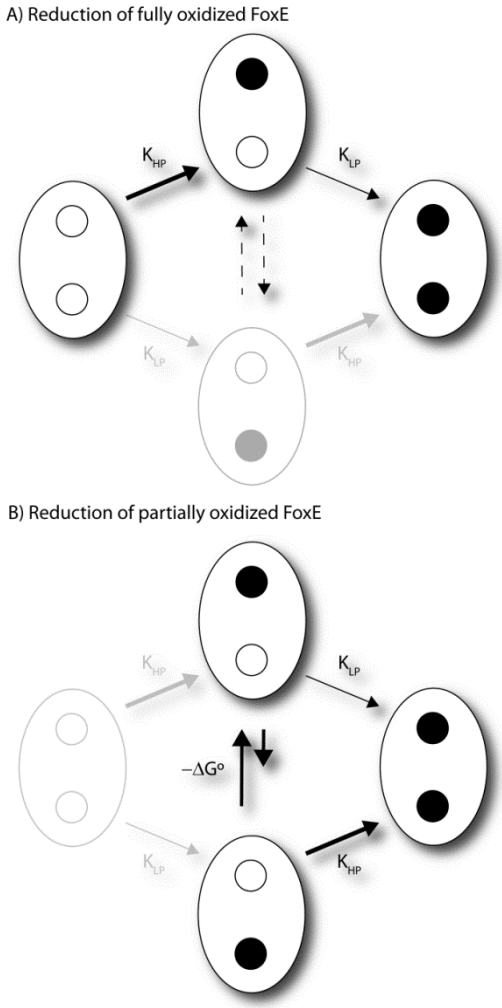

Figure 2.9: schematic representation of reduction of each FoxE monomer. Open circles represent oxidized heme and closed circles represent reduced hemes. Indicated are the reduction rate constants present in Table 2.2. A) Conditions where the cytochrome is fully oxidized at the beginning of the kinetic experiment. The dashed lines indicate slow intra monomer electron transfer. Because K_{LP} is faster than the intra monomer electron transfer the bottom microstate has a negligible contribution in the kinetic experiment. B) Conditions when the cytochrome is partially reduced at the beginning of the kinetic experiment. The system has reached equilibrium between the two intermediate microstates before the reaction with Fe(II)-EDTA is initiated.

Having established that the reduction potentials are pH dependent, the influence of pH on the kinetics of the iron oxidizing activity of FoxE was investigated by measurements made at pH 6 and 7. Increasing the pH from 6

to 7 causes a decrease in the reduction rate constants (K_i). In order to understand the role of the driving force in this change, intrinsic rate constants (k_i) were calculated according to equation 2. These are rate constants that are independent of driving force and depend only on structural factors of the reaction. It is possible to observe that for the LP hemes the decrease in reduction rate constant is caused exclusively by a decrease in driving force, as the corresponding intrinsic rate constant (k_{LP}) remains approximately constant with pH variation. For the HP hemes a decrease in intrinsic rate constants (k_{HP}) from pH 6 to 7 contributes to the decrease in rate constant (K_{HP}) but the driving force is again the dominating contribution. Therefore, the data show that pH modulates the rates of iron oxidation by an increase in the driving force of the reaction at more acidic pH values. A similar approach was followed in the kinetic characterization of iron reduction by the MtrC and OmcA iron reductases from the bacterium *Shewanella oneidensis* MR-1 (149). At pH 7 the second order rate constants of iron oxidation by FoxE are one to two orders of magnitude below the lower values obtained for iron reduction by MtrC and OmcA. At pH 6 however, the second order rate constant for the HP hemes fall within the same order of magnitude as those determined for OmcA.

Based on the reduction potentials and intrinsic rates constants it is possible to make some structural considerations about the heme environments. The higher potential of the HP hemes suggests a more hydrophobic environment. Considering the lower exposure of Heme I to the solvent, this higher reduction potential suggests that the HP heme could be assigned to Heme I. Despite the lower predicted solvent exposure of the HP hemes, the intrinsic rate constants indicate that Fe(II)-EDTA has more access to these hemes. This could arise from a surface region near the HP hemes with favorable shape and electrostatic properties towards Fe(II)-EDTA. Also, as suggested by the broader NMR signals of the HP hemes, the HP heme region seems to be more flexible. This

increased mobility might contribute to the higher intrinsic rate constant of reduction of this heme. Another structural consideration can be made based on the effects caused by dithionite on the NMR spectra of FoxE. These changes suggest that FoxE has redox dependent structural changes that are triggered by dithionite but not by ascorbate or other reducing agent with higher reduction potential. With a low reduction potential, dithionite can reduce disulfide bonds, and reduction of the C80-C258 bond might be the cause of these changes. As this bond is found near Heme I and the structural changes affect mainly the HP hemes, this would again assign the HP heme as Heme I. Because reduction of the C80-C258 bond only occurs at negative potentials, unsuitable for oxidation of Fe(II) compounds (Figure 2.8), this disulfide bond is unlikely to be relevant for the physiological activity of FoxE and instead play a structural role.

This work shows that the FoxE cytochrome is thermodynamically and kinetically competent for oxidizing iron in the periplasm of SW2. This implies that SW2 has a strategy to prevent Fe(III) precipitation in the periplasm and on the cell surface. Different iron oxidizing bacteria appear to have different mechanisms to avoid precipitation (131) and some, such as *Rhodomicrobium vannielii*, cannot escape becoming encrusted by iron minerals (54). Iron chelators produced by the cells have been suggested to solubilize Fe(III) and it is known that the growth of SW2 increases the solubility of Fe(III) in the supernatant of the culture medium (148). However, no strong siderophores were detected in SW2 spent medium and the energetic cost of producing such a molecule would likely be prohibitive (132). An alternative strategy for keeping Fe(III) soluble is the creation of a low pH microenvironment around the cell to promote precipitation away from the cell both thermodynamically and kinetically (131, 132, 150). This implies a tight pH control of the iron oxidation step. The kinetic data reported in this work show that in the

physiological pH range for SW2, the rates of iron oxidation by FoxE increase with lower pH. This modulation of the rate of iron oxidation is made mostly by changing the reduction potential of the hemes and not by the adjustment of the structural factors involved in the electron transfer. Modulating the reaction rate by the driving force favors adaptation to an environment where ferrous iron can be available in multiple forms. Manipulating the driving force generates a similar outcome for all possible Fe(II) forms whereas adjusting structural factors could have different outcomes depending on the specific molecular nature of Fe(II). Given our results, the iron oxidation activity by FoxE appears optimized to work in the low pH microenvironment found in the vicinity of colonies of SW2 (132), which would be consistent with a pH strategy to minimize Fe(III) precipitation.

The experimental evidence points to the formation of a trimer in solution. This result does not have implications on the iron oxidation activity measured here. However, it has implications on how FoxE interacts with its physiological partners. A related issue raised by the obtained results is the long inter heme distances that result in six independent redox centers, without relevant electron transfer or cooperativity between them. Several hypotheses can be put forward concerning these issues. Even though the experimental evidence suggests a homo-trimer in the used experimental conditions, there is the possibility of higher order oligomers of FoxE *in vivo*. A higher order oligomer might have a higher conformational space that could allow cooperativity between the several domains, a cooperativity that is missing in the observed trimer. A second hypothesis is the formation of allosteric sites. A homo-trimer might allow the creation of a single allosteric site that would regulate six redox cofactors. To avoid Fe(III) precipitation a tight control of the iron oxidoreductase is required. Beyond the pH regulation shown here, an allosteric site would allow a tighter regulation. Possible allosteric effectors might be

Fe(III) itself, which would inhibit the activity of FoxE, or a Fe(III) chelator that would not be used to export Fe(III) in a soluble form but only to inhibit the activity of FoxE. A last hypothesis to consider is the formation of a bigger protein complex between FoxE and its physiological partners. *In vivo*, FoxE may perform its function bound to other proteins, and this interaction might give answers to these issues. The binding pockets of the two hemes in each monomer of FoxE appear to display different dynamics, at least when the protein is isolated, and may suggest points of partner docking. For exploring these issues, structural studies of the proteins involved must be pursued.

In summary, we have functionally and structurally characterized an iron oxidoreductase from a contemporary photoferrotrophic bacterium. The biochemical properties of FoxE show that it is thermodynamically competent to perform physiological Fe(II) oxidation and intrinsically regulate its activity to support the avoidance of Fe(III) (hydr)oxide precipitation within the cell. This is the first structural and molecular characterization of this ancient form of phototrophy, which has been implicated in leaving profound signatures in the geological record at early periods in Earth history.

3

PioC: a photoferrotrophic HiPIP

This work will be published in two manuscripts in preparation.

Ivo H. Saraiva designed and performed all the experiments.

3 PioC: a photoferrotrophic HiPIP

3.1 Introduction

PioC is a single electron transfer protein that probably belongs to the electron transfer (ET) chain connecting Fe(II) to the reaction center (RC). HiPIPs are proteins containing a $[4Fe\text{-}4S]^{3+/2+}$ cubane cluster coordinated by four cysteine residues and are present in many photosynthetic bacteria (92). Their high potential makes them suitable to transfer electrons to the RC and they are commonly seen in this function either alone or together with other ET proteins. This suggests that PioC might be responsible for the last ET step to the RC in photosynthetic iron oxidation in *R. palustris* TIE-1. These iron sulfur proteins assume relevant roles in many organisms but the fact that they sometimes seem to have redundant roles with cytochromes remains puzzling (151). Also, in the published kinetic studies on ET between HiPIPs and the RC the ET is made through the RC associated tetra-heme cytochrome (93, 152–154). This protein is not present in *R. palustris* TIE-1 RC complex, which raises the possibility for the need of an alternative intermediary between the PioC and the RC.

PioC is a HiPIP involved in photoferrotrophy by TIE-1 but its specific role in this metabolism and its position in the electron transfer chain between Fe(II) and the RC is still unknown. To try to answer these questions a functional and structural characterization of this protein was performed.

3.2 Experimental procedures

Expression and purification

PioC was expressed in *E. coli* BL21 with a pET32h plasmid. The signal sequences predicted with TatP (155) were excluded from the resulting construct: thioredoxin – 6xHis – thrombin cleavage site – PioC. *E. coli* expressing

producing PioC was grown in LB medium at 37 °C. At an $O.D._{600nm}$ of 1 expression was induced with 0.5 mM of IPTG at 30 °C. After 4 hours cells were harvested by centrifugation and resuspended in binding buffer (50 mM phosphate buffer, 300 mM NaCl, pH 8). Cells were lysed with a Thermo Scientific french-press and cell debris was removed by centrifugation. To produce isotopically labeled PioC the same strain was grown in the same conditions until an $O.D._{600nm}$ of 1. Cells were then collected by centrifugation, washed twice with M9 minimal medium salts and finally resuspended in 0.25 L of M9 minimal medium containing $^{15}NH_4Cl$ and D-glucose-^{13}C for each liter of LB medium. Cells were incubated under the same conditions for one hour, to deplete non-labeled nutrients, and induction and harvesting were performed as before.

The supernatant resulting from cell lysis was loaded into a Qiagen Ni-NTA agarose column equilibrated with binding buffer. Unbound proteins were discarded and bound proteins were eluted with elution buffer (50 mM phosphate buffer, 300 mM NaCl, 250 mM imidazole, pH 8). After elution, the bound fraction was incubated with GE Healthcare thrombin overnight according to the manufacturer protocol. The enzymatic digest was dialyzed against binding buffer and reloaded into the re-equilibrated Ni-NTA column. Target protein did not bind to the column and was collected in the flow-through. N-terminal sequencing showed that the obtained protein was correctly digested by thrombin.

EPR spectroscopy

EPR spectra of pure PioC were recorded on a Bruker EMX spectrometer equipped with a dual-mode cavity and an Oxford Instruments continuous flow cryostat. The experimental conditions were: temperature 10 K; microwave frequency 9.655 GHz; microwave power 6.346 mW; modulation amplitude 0.5

mT; receiver gain 1.00 x 10^5. HiPIP concentration was 200 μM in 100 mM potassium phosphate buffer, 400 mM KCl, pH 8. Sample oxidation was achieved by addition of potassium ferricyanide.

1D NMR spectroscopy

1D ^{1}H-NMR spectrocopy was performed in a Bruker AVANCE II 500 MHz spectrometer. Protein concentration was 0.5 mM in 50 mM phosphate buffer with 300 mM NaCl pH 8. Spectra were made in H_2O + 10% D_2O at 25 ºC. The temperature of each spectrum was calibrated with either 4% MeOH in [D_4] methanol or 80% 1,2-ethanediol in [D_6] DMSO.

Cyclic voltammetry

Cyclic voltammograms were recorded using an Autolab PSTAT10 potentiostat. The working electrode was a pyrolytic graphite-edge disc, a platinum wire was used as counter electrode and a Ag/AgCl (1M KCl) electrode was used as reference. Reduction potentials are reported versus standard hydrogen electrode (SHE) by adding +222 mV to the experimental readings made at 25 ºC. Prior to each experiment the working electrode was washed with Millipore water (18 MΩ.cm). For each voltammogram 20 μL of HiPIP at 5 μM in 50 mM TrisHCl, 300 mM NaCl, pH 9 buffer were used. The scan rate was 1 mV.s^{-1}. An initial potential of 750 mV was applied to the sample for 10 min before recording of each voltammogram. Data was processed with SOAS using a noise filter with automatic threshold and subtraction of the background current (156).

Multi-dimensional NMR, signal assignment and solution structure determination

All spectra of a double-labeled 1 mM PioC sample in 50 mM potassium phosphate buffer pH 6.3 were acquired with an Avance Bruker spectrometer at 800 MHz at 25 °C. Heteronuclear 2D spectra ^{1}H-^{15}N-HSQC and ^{1}H-^{13}C-ctHSQC (157) consisted of 2k data points in the ^{1}H dimension and 256 experiments in the heteronucleus dimension. For the sequential assignment of the PioC signals a set of BEST triple-resonance experiments (158) was used: HNCA, HNCACB, HNcoCACB and HNCO. Each experiment was acquired with 1k(^{1}H)x40(^{15}N)x112(^{13}C) data points. For the identification of spin systems and side chain assignment a hCCH-TOCSY acquired with 2k(^{1}H)x72(^{13}C)x128(^{13}C) data points was used. To obtain distance restraints a ^{1}H-^{1}H-NOESY of a non-labeled 3 mM sample in the same buffer was acquired with 4kx2k data points. The NOESY spectrum was processed with a squared cosine function with an SSB of 3 in both dimensions and forward linear prediction in the second dimension.

The analysis of the spectra, including peak integration, was performed with the CCPNMR Analysis software (159). A NOESY peak list was exported in CYANA format for use in the structure calculation and automatic peak assignment with CYANA (160). To define the iron-sulfur cluster in the calculation a previous approach (161) was followed. The ligand cysteines were replaced by a new cysteine like amino acid (CFS) in which the HG atom is replaced by the bound atoms -Fe-S. These two extra atoms are used to construct the cluster by covalent bonds defined in CYANA.

3.3 Results

To heterologously express and purify PioC a fusion with His-tagged thioredoxin was used. Because thioredoxin was placed at the N-terminal, the periplasmatic

Tat signal sequence of the HiPIPs was removed in the cloning and the fusion protein was accumulated in the cytoplasm. This approach, followed by affinity chromatography and proteolytic cleavage of thioredoxin, resulted in pure HiPIPs with a yield of 3 mg per liter of culture.

EPR spectroscopy

Reduced HiPIPs have a diamagnetic ground state. Since only the ground state is occupied at the temperature of the EPR experiments, PioC was EPR silent in the reduced form (not show). In the oxidized form the ground state is paramagnetic and HiPIPs have a typical complex EPR signal pattern (94, 162) shown in the spectrum (Figure 3.1). The main features of this signal have g values of 2.12, 2.08 and 2.03.

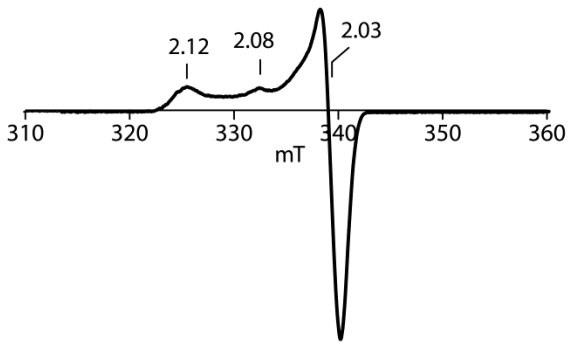

Figure 3.1: X-Band EPR spectrum of oxidized purified PioC.
Spectrum was obtained at 10 K. The g-values of the main features of are indicated.

NMR spectroscopy

Although the ground state of reduced HiPIPs is diamagnetic, at 25 °C there are paramagnetic excited states that are thermally populated. These states give origin to paramagnetic shifts, which are clearly visible for the β protons of the

cysteine ligands of the cluster, as some of them appear outside the protein crowded region of the spectrum. Like other HiPIPs, PioC shows these characteristic cysteine β proton signals between 10 and 20 ppm (Figure 3.2). The temperature dependence of these signals was monitored and showed the expected anti-Curie behaviour characterized by a linear dependence of the shifts with reciprocal temperature.

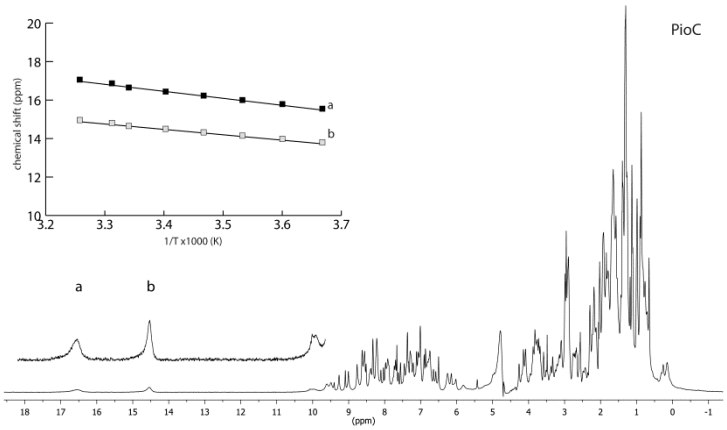

Figure 3.2: ^{1}H-NMR spectrum of PioC at 25 °C.
The region containing the paramagnetic signals of the β protons belonging to the cysteine ligands of the cluster is enhanced 10x and the signals are labeled. The inset shows the temperature dependence of the paramagnetic signals of the β protons from the ligand cysteines that are clearly visible in the spectra.

Cyclic voltammetry

The reduction potential of PioC was determined by cyclic voltammetry (Figure 3.3) at 1 mVs^{-1} scan rate and pH 9. The protein shows reversible reaction with midpoint potentials of 450 mV. Faster scan rates resulted in irreversible reactions.

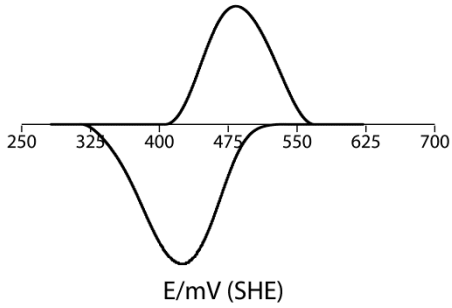

Figure 3.3: cyclic voltammogram of PioC.
The experiments were performed at 25 °C with a 1mVs^{-1} scan rate in 50 mM TrisHCl buffer, 300 mM NaCl, pH 9.

Solution structure determination

To help understand the role of PioC in the TIE-1 cell, a preliminary solution structure of this HiPIP was determined by NMR spectroscopy. Sequential assignment of PioC was achieved for 71% of the polypeptide. Analysis of the hCCH-TOCSY spectrum allowed the identification of 93% of the spin systems, even those for which no NH was assigned. Of the 53 backbone NHs in PioC, 45 were assigned. No assignment for the backbone of residues C25, Q30, F36, T39, V40, C50, L52 and A54 was possible. NOESY spectra were gathered to obtain structural information on PioC. Probably due to enhanced relaxation caused by the paramagnetic center, few distance restraints were obtained, and only an average of 10 restraints per amino acid were available to calculate the final structural models (Figure 3.6). Due to lack of long range NOEs for the first 6 amino acids of PioC, no specific tertiary structure was determined for the N-terminal. Despite the restricted structural information in the NMR spectra, the overall fold of PioC was determined (Figure 3.4, Table 3.1). The fold of this HiPIP is similar to the conserved fold observed for other HiPIPs. The iron-sulfur cluster is buried inside the protein, secluded from the solvent. Structurally

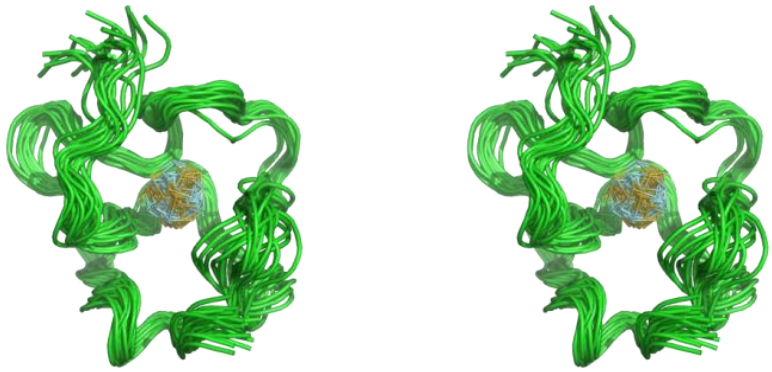

Figure 3.4: superposition of the backbone of the 20 best solutions of the CYANA calculation of the structure of PioC.
The cluster is represented with blue and yellow lines. Stereo cross-eyed view.

conserved residues present in all other HiPIPs are also present in PioC. Experimental data put some of these, W49 or F31, in their conserved positions in the structure. For others, which are close to the center or form conserved H-bonds with the ligand cysteines, no NOESY cross peaks were observed and their conformations were not experimentally determined. The same is observed for the ligand cysteines. Due to lack of NOEs for these residues and their neighbors, the environment close to the iron-sulfur cluster could not be experimentally well defined, as illustrated by high local rmsd values (Figure 3.5).

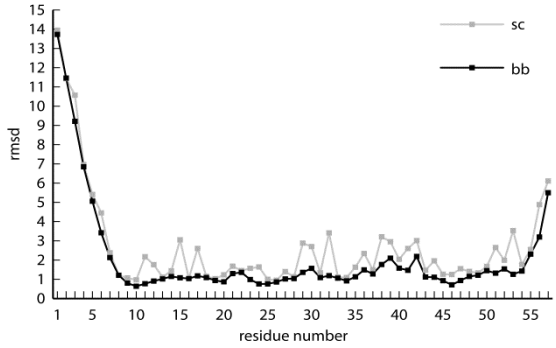

Figure 3.5: rmsd values of the models present in Figure 3.4.
bb, backbone; sc, sidechains.

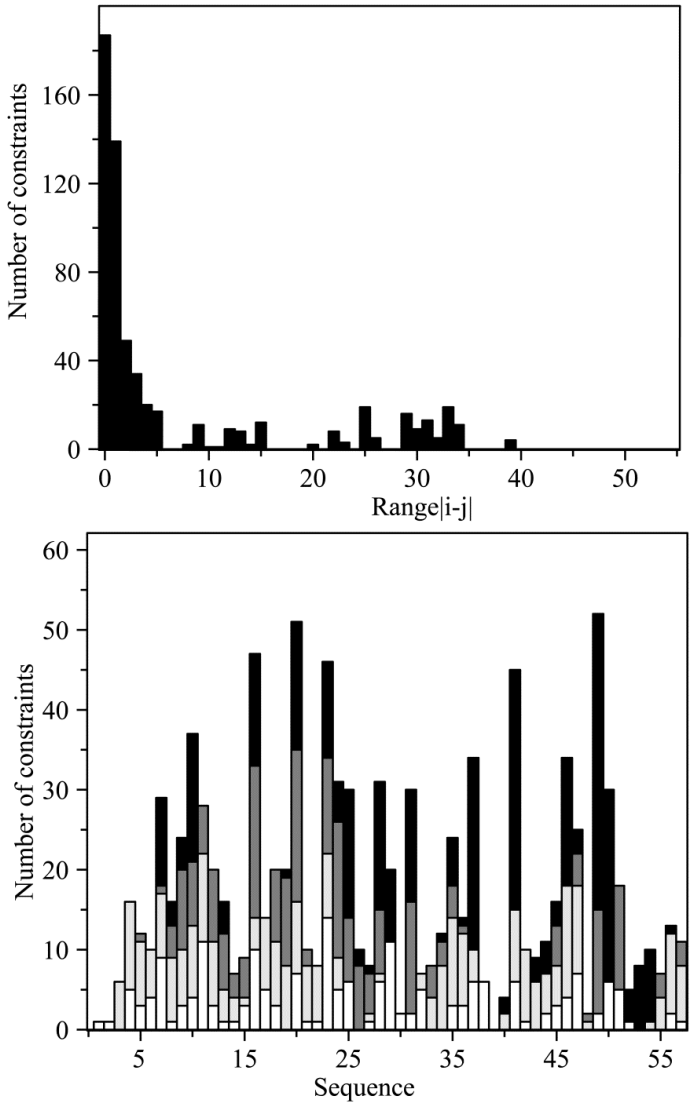

Figure 3.6: distance restraints used in the calculation of the structural model of PioC. From white to black the bars in the lower panel indicate intra-residual, sequential, medium-range (|i-j|<5), and long range(|i-j|>5) restraints, respectively.

3.4 Discussion

In this chapter a functional and structural characterization of PioC is presented. Spectroscopically, PioC shows the usual NMR and EPR features originated by the iron-sulfur cluster and no new feature is observed. The reduction potential determined by cyclic voltammetry can help understand the role of this HiPIP. PioC has a reduction potential of 450 mV, a value that falls in the range of other studied HiPIPs. To place PioC in the photoferrotrophic electron transfer chain, the two reduction potential extremes of the chain must be defined. The reduction potentials of the RCs of purple bacteria are between 450 and 500 mV (163). The potentials of common Fe(II) species at circumneutral pH are between -300 and 400 mV (147). The value determined places PioC within the predicted range of values for the RC and suggests that it can donate electrons directly to it. Arguing against direct electron transfer to the RC is the fact that TIE-1 does not have a tetra heme cytochrome in its genome, a RC subunit that usually mediates electron transfer between HiPIPs and the RC.

Another issue that needs consideration is the spatial distribution of the proteins involved. The RC is found in the inner cytoplasmic membrane, a photosynthetic lamellar structure stacked in the cytoplasm (Figure 3.7). Even though the periplasm and these structures are connected, the free diffusion of

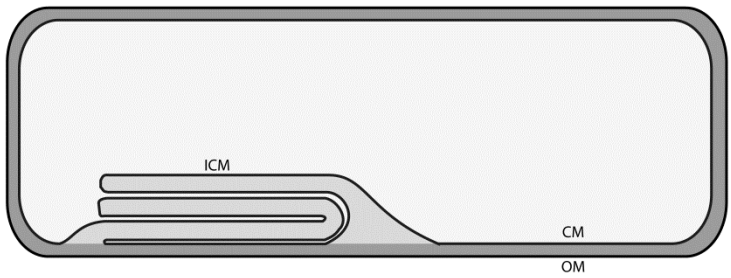

Figure 3.7: organization of the membrane structures of *R. palustris*. CM, cytoplasmatic membrane; OM outer membrane; ICM, inner cytoplasmatic membranes. The periplasm is in dark grey, the cytoplasm in white and the lumen of the ICM in light grey. Based on reference (186).

PioC or other proteins between these two cellular compartments is not obvious. If PioC is not able to transfer electrons directly to the RC due to spatial separation or due to the lack of tetra-heme cytochrome, another protein, with a high reduction potential, must be involved. Another common RC electron donor is cytochrome c_2. In other *R. palustris* strains this protein has a reduction potential of 365 mV (164). However, in other species values up to 470 mV have been determined (165). This raises the hypothesis of c_2 being the downstream electron transfer partner of PioC.

Fundamental to the characterization of a protein is the knowledge of its molecular structure. To obtain a structural model of the 6.5 kDa PioC, NMR spectroscopy was used. This technique has successfully been used before in solving several structures of HiPIPs in the oxidized (166) and reduced states (161, 167). Even though the experimental structural data on several residues of PioC are sparse, the overall fold was determined. PioC has the conserved fold of all other HiPIP structural models deposited in the PDB. Like other HiPIPs, the cluster in PioC is maintained in a hydrophobic environment, which helps maintain the high reduction potential. PioC has the shortest sequence of all the presented HiPIPs. This results in shorter inter-cysteine loops, which give this protein a more compact structure.

An analysis of previous HiPIP structural models, obtained either by NMR or X-ray crystallography, shows highly conserved structural features (Figure 3.8). Among these are the fold, secluding the cluster from the solvent, and a network of hydrogen bonds shown to be essential to the structural stability of the protein (98) and to be involved in the high reduction potential of HiPIPs (168). The polypeptide contacts with the cluster, be they ligand cysteines or hydrogen bonds, are always present with the following pattern:

$$\mathrm{C_I XX C_{II} X}\mathcal{H}_{\mathrm{II}} \ldots \mathrm{C_{III} X}\mathcal{H}_{\mathrm{III}} \ldots \mathrm{C_{IV} X}\mathcal{H}_{\mathrm{IV}} \mathrm{Ar}\mathcal{H}_{\mathrm{II}}$$

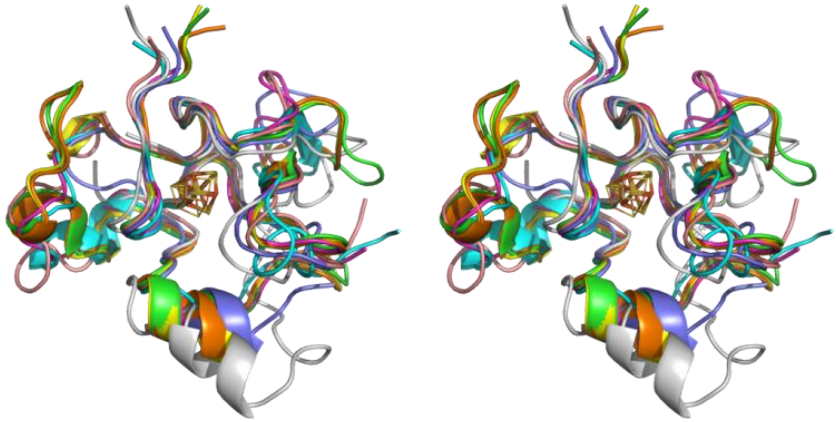

Figure 3.8: superposition of HiPIP structures deposited in PBD.
A. vinosum (1cku), green; *E. halophila* (1pij), cyan; *E. vacuolata* (1hpi), magenta; *M. purpuratum* (3hip), yellow; *R. fermentans* (1hql), pink; *R. marinus* (3h31), grey; *R. tenuis* (1isu), purple; *T. tepidum* (2fla) orange. Stereo cross-eyed view.

where C_i is the i^{th} cysteine ligand, according to the order they appear in the sequence, $\mathcal{H}_i$ is an amino acid whose NH forms a hydrogen bond with the i^{th} ligand cysteine and Ar is an aromatic residue. Of the eight missing NH assignments of PioC four are from the predicted H-bonds (Q30, T39, L52 and A54), two are from neighboring residues (F31 and V40) and two are from ligand cysteines (C25 and C50). On previous NMR studies on other HiPIPs, the assignment of these residues NHs is also missing or tentative (167, 169). The difficulty in assigning these signals could be explained by the proximity to the paramagnetic cluster, as it would originate enhanced relaxation. These missing assignments provide support to the hypothesis that the H-bond network is maintained in PioC.

Other conserved feature is the presence of aromatic or hydrophobic residues that surround the cluster and seclude it from the solvent (Figure 3.10). In PioC, some of these conserved amino acids, like Y15 and Y53, originated no or few NOEs probably due to the proximity to the cluster. This sparse experimental information is translated into high rmsd values.

```
A. vinusom      ---------SAPANAVAADDATAIALKYNQDATKSERVAAARPGLPPEEQHCANCQFMQA
E. vacuolata    ------------MERLSEDDPAAQALEYRHDASSVQHP------AYEEGQTCLNCLLYTD
R. fermentans   -----------AAPLVAETDANAKSLGYVADTTKADKTKY---PKHTKDQSCSTCALYQG
R. tenuis       -----------GTNAA-----MRKAFNYQD------------TA-KNGKKCSGCAQFVP
A. halophila    -------------EPRA---EDGHAHDYVNEAA-----DASGHPRYQEGQLCENCAFWGE
M. purpuratum   ----------VPANAVTESDPAAVALKYHRDAASSERVAAARPGLPPEEQHCENCQFMNP
R. marinus      ELTCTDVSGLTAEEIQ-----MRESLQYTD------------HSPYPDKTCANCQLYVP
T. tepidum      ---------AAPANAVTADDPTAIALKYNQDATKSERVAAARPGLPPEEQHCANCQFMQA
PioC            --------GVAAANAQVTKKASHKDAGYQ-------------ESPNGAKRCGTCRQFRP
                              ^            *                    : *  *

A. vinosum      DAAGATDEWKGCQ--LFPG-KLINVNGWCASWTLKAG
E. vacuolata    A---SAQDWGPCS--VFPG-KLVSANGWCTAWVAR--
R. fermentans   K----TAPQGACP--LFAG-KEVVAKGWCSAWAKKA-
R. tenuis       GA--SPTAAGGCK--VIPGDNQIAPGGYCDAFIVKK-
H. halophila    A---VQDGWGRCTHPDFDE-VLVKAEGWCSVYAPAS-
M. purpuratum   DSA--AADWKGCQ--LFPG-KLINLSGWCASWTLRAG
R. marinus      AE--SPDQCGGCQ--LIKG--PIHPNGYCTSWVQKAT
T. tepidum      NVG--EGDWKGCQ--LFPG-KLINVNGWCASWTLKAG
PioC            PS--SC----------ITVESPISENGWCRLYAGKA-
                              :    :   *:*  :
```

Figure 3.10: sequence alignment of HiPIPs with structures deposited in PDB. Conserved residues are highlighted in grey. Ligand cysteines and residues forming conserved H-bonds with the cluster are in bold. ^ indicates the predicted first amino acid of PioC after processing the Tat signal peptide.

In order to determine if PioC is structurally divergent from the other HiPIPs, the conserved structural features were converted into additional structural restraints (Table 3.2) and a new calculation was performed (Figure 3.9, Table 3.1). The new structural models obtained were more convergent than before (Figure 3.11), and no violations were originated with the additional restraints.

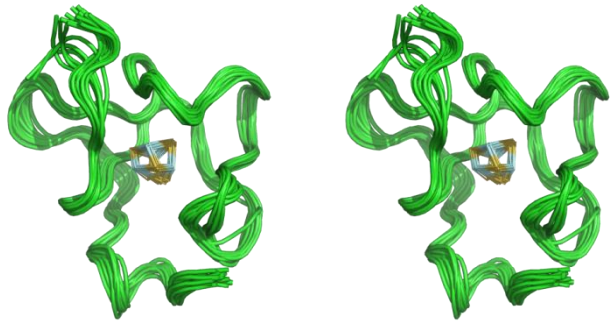

Figure 3.9: superposition of the backbone of the 20 best solutions of the CYANA calculation of the structure of PioC with the additional restraints of Table 3.2. The cluster is represented with blue and yellow lines. Stereo cross-eyed view.

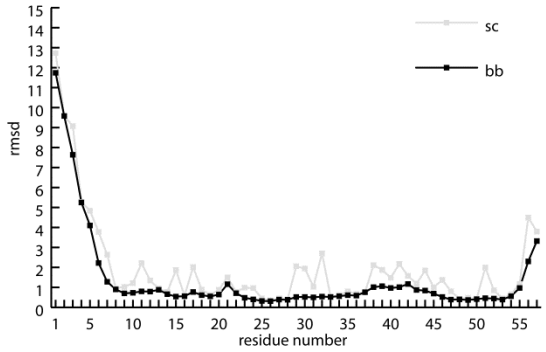

Figure 3.11: rmsd values of the models present in Figure 3.9.
bb, backbone; sc, sidechains.

As such, there are no experimental data suggesting that PioC is structurally divergent from the other HiPIPs.

As expected for a paramagnetic protein, the region surrounding the paramagnetic cluster is less defined due to enhanced relaxation of the signals of close by nuclei. This issue has previously been solved using 1D-NOE measurements of this signals (167, 169). This technique has higher sensitivity and allowed obtaining additional restraints for the cluster region in the proteins. The some approach can be followed to improve the solution structural models of PioC. Alternatively, the paramagnetism of PioC might be used to obtain additional structural information (170). The magnetic moment of PioC might originate a partial alignment of the molecule in solution. If this alignment is confirmed the measurement of residual dipolar couplings can be used to obtain additional structural restraints. Also, the enhancement of relaxation caused by the unpaired electron is itself distance dependent. Further improvements in the structural models can be achieved by studying the relaxation properties of PioC.

Table 3.1: statistics of the CYANA calculations with NOEs and with NOE plus the restraints in Table 3.2

	NOEs	NOEs+Table 3.2
rmsd aa_{7-53} (backbone)	0.93 Å	0.52 Å
rmsd aa_{7-53} (sidechains)	1.49 Å	1.03 Å
average CYANA target function	1.86	1.64

Table 3.2: restraints determined from the conserved structural features of HiPIPs. Values are averages of features found in deposited structural models of HiPIPs and the interval is defined by two or three times the standard deviation.

C28,SG-Q30,H C37,SG-T39,H C50,SG-L52,H C28,SG-A54,H	2.67±0.33 Å
Y15,HD1-cluster	3.07±0.33 Å
C25,PHI	-56±13 °
C25,PSI	-37.5±10.5 °
C25,CHI1	-65.5±14.5 °
C25,CHI2	-62.5±17.5 °
C28,PHI	-96.5±9.5 °
C28,PSI	140±5 °
C28,CHI1	-179.5±5.5 °
C28,CHI2	-175±10 °
C37,PHI	-138±21 °
C37,PSI	131±18.5 °
C37,CHI1	172.5±5.5 °
C37,CHI2	129.5±11.5 °
C50,PHI	-148±9 °
C50,PSI	166.5±7.5 °
C50,CHI1	85±6 °
C50,CHI2	82.5±18.5 °
L52,PHI	-85±13 °
L52,PSI	4±8 °
Y53,PHI	-47±11 °
Y53,PSI	131±9 °
Y53,CHI1	-178±9 °
Y53,CHI2	82.5±18.5 °
A54,PHI	-135.5±28.5 °
A54,PSI	130±24 °

The data presented here agrees with the scheme proposed in Figure 3.12, in which PioC is suggested to transfer electrons between PioA and the cyclic photosynthesis apparatus. To obtain a clearer picture, the other proteins in

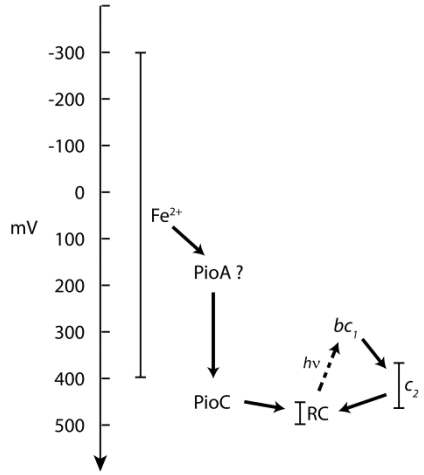

Figure 3.12: electron flow diagram in the periplasm of TIE-1.
The vertical bar represents reduction potential. The solid arrows indicate electron flow. *bc*$_1$, cytochrome *bc*$_1$; *c*$_2$, cytochrome *c*$_2$; RC, photosynthetic reaction center. The dashed arrow indicates the ET through the quinone pool from the light excited RC to the cytochrome *bc*$_1$. The vertical lines indicate the reduction potential range of the associated molecules at circumneutral pH.

Figure 3.12 have to be investigated. Firstly, thermodynamic studies will allow pinpointing them in the reduction potential chart. Secondly, kinetic studies will confirm or disprove the electron flows represented in the figure. Thirdly, structural characterizations will determine the nature of the possible protein-protein interactions. Completion of these tasks will allow a clear understanding of photoferrotrophy in TIE-1.

4

Concluding remarks

4 Concluding remarks

Photoferrotrophy is an ancient metabolism but only recently described. Since its discovery in the 1990s, several studies have focused on the identification and characterization of photoferrotrophs and on iron precipitate formation, but many questions on the biochemical nature of this process and on how it correlates with the geological record remain unanswered. The recent identification of genes involved in this metabolism triggered the present work. This thesis presents the first molecular studies on proteins involved in this form of iron oxidation. The first protein described here, FoxE, is predicted to perform the first step of photoferrotrophy in the bacterium *R. ferrooxidans* SW2, and the second, PioC, is predicted to performed the last step in the bacterium *R. palustris* TIE-1. The studies on these two proteins show that their biophysical characteristics are in agreement with their predicted function.

4.1 Photoferrotrophy in *Rhodobacter ferrooxidans* SW2

FoxE was shown to be thermodynamically and kinetically able to perform oxidation of soluble Fe(II), and this oxidation to be pH dependent, a dependence that can be correlated with the dependence of the solubility of Fe(III) with pH. SW2 has no evident way for FoxE to contact with the exterior of the cell. Considering the data gathered here and also the predicted locations of the different proteins involved, a mechanism might be proposed for iron oxidation (Figure 4.1). Soluble Fe(II) diffuses into the periplasm were it is oxidized to Fe(III) at a rate dependent on pH. Due to a low pH micro environment around the cells of SW2, Fe(III) remains soluble until it diffuses away from the cells where it precipitates. Questions that remain unanswered are concerned with the downstream electron flow. Given the fact that FoxY enhances the rate of iron oxidation of the bacterium *R. capsulatus* SB1003 only

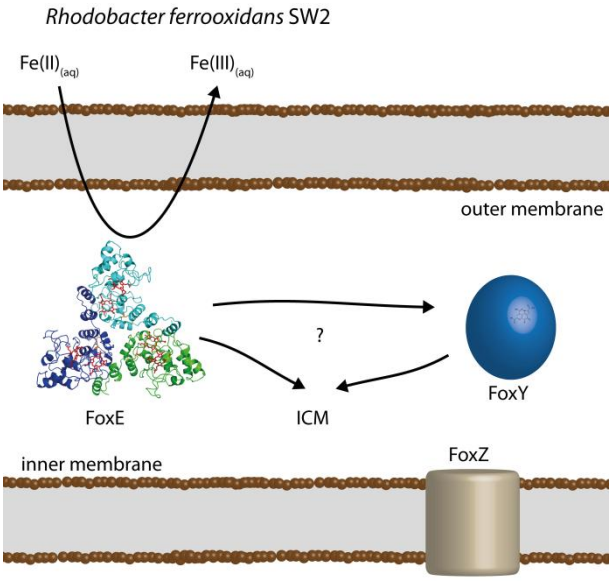

Figure 4.1: proposed mechanism of photoferrotrophy in SW2.
The electron flow between FoxE and the cyclic photosynthetic apparatus in the intra cytoplasmatic membranes (ICM) is unknown.

in the presence of FoxE, it is the probable electron receptor from FoxE. FoxY has homology to quinoproteins, enzymes that bind PQQ as a cofactor and that catalyze the transfer of electrons between sugars, alcohols or amines, to either cytochrome *c* or to ubiquinone (171). The electron donors of these proteins are different from what is proposed for FoxY. However, a PQQ binding protein has been proposed to be involved in Mn(II) oxidation (172), suggesting that this type of enzymes may have undiscovered functions. The electron receptors of known quinoproteins, cytochrome *c* or ubiquinone, also suggest possible entry points of the electrons from Fe(II) in the cyclic photosynthetic apparatus. The path followed to reach this end requires further studies.

In order to continue the characterization of electron flow path in SW2 the same approach used here can be used with FoxY, as a first step. Detailed thermodynamic and kinetic characterization of this electron transfer protein is essential to assess its function and involvement in photoferrotrophy. FoxY is

predicted to bind a single organic cofactor with particular optical features. These characteristics should allow the utilization of standard electrochemistry and UV-visible spectroscopy techniques to achieve this goal. A second and most important step will be the study of the interactions between the proteins involved, in order to link the different partners in the electron flow chain. Having different redox centers with distinctive spectroscopical characteristics, the possible electron transfer between FoxE and FoxY can be evaluated by several spectroscopic techniques, like NMR, EPR or UV-visible. Interactions between electron transfer partners can be transient. NMR has been shown to provide particular insight into these interactions (173), and the native paramagnetic properties of FoxE can be used to probe transient complexes through paramagnetic relaxation enhancement or pseudocontact shifts (174).

FoxZ, contrary to FoxE and FoxY, is not predicted to bind a redox cofactor. According to its sequence, it is predicted to be an inner membrane protein with a transport function. Because there is no precipitation of Fe(III) inside the cells of SW2, it was proposed that SW2 could produce an iron chelator in order to avoid it. In connection with this proposal it was speculated that FoxZ could transport such a chelator to the periplasm. However, production of such a chelator would be energetically unfavorable and no chelator has yet been detected in SW2. Concerning the oligomerization of FoxE, it was proposed in section 2.4 that this cytochrome could have an allosteric inhibitor. FoxZ could be responsible for the transport of such an inhibitor to the periplasm.

4.2 Photoferrotrophy in *Rhodopseudomonas palustris* TIE-1

The second protein studied here, PioC, is a high potential iron-sulfur protein. Thermodynamic and structural characterization is presented. As before, with the collected data and the information on the predicted location of the proteins involved a mechanism might be proposed for iron oxidation of Fe(II) in

TIE-1 (Figure 4.2). Fe(II) diffuses into the pore of the outer membrane β-barrel PioB, where it is oxidized by PioA. This prevents the precipitation of Fe(III) in the periplasm. Although the reduction potentials of PioA are not known, due to its high reduction potential, PioC can probably receive electron from PioA and transfer them further downstream to the cyclic photosynthetic apparatus. Future studies should focus on the characterization of PioA and on the interactions between the proteins involved.

Full characterization of PioA is essential. This decaheme cytochrome was one of the targets of these studies. However, it has been impossible, so far, to design a working expression system for this protein. Other decaheme cytochromes have been successfully produced, including the homolog MtrA from *Shewanella oneidensis* MR-1. PioA, however, has some yet unidentified characteristics that promote its degradation during purification. A similar strategy used for the production of FoxE, was used for PioA. Even though pink

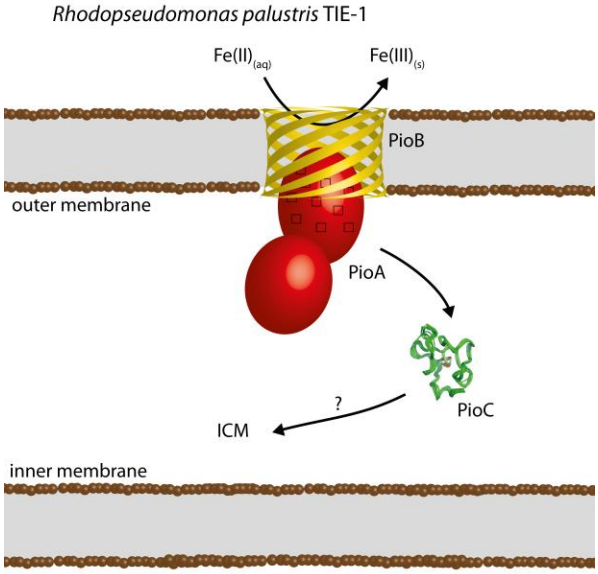

Figure 4.2: proposed mechanism of photoferrotrophy in TIE-1. The electron flow between PioC and the cyclic photosynthetic apparatus in the intra cytoplasmatic membranes (ICM) is unknown.

E. coli cells were obtained as usual for cells expressing cytochromes, no purification protocol was efficient. One possible reason for the instability of PioA, in the used systems, is the lack of PioB. By their homology with other known proteins, PioA and PioB are expected to form a stable complex. The lack of PioB could render PioA too unstable. Another particularity of this decaheme cytochrome is the presence of a non heme binding domain not present in the studied homologs like MtrA. The function of this second domain is unknown and it might be the source of instability of PioA. Several strategies can be followed in order to overcome the difficulties in the production of PioA. If the lack of PioB is the source of instability, the two proteins could be co-expressed and purified together. If possible, the study of the whole PioAB complex would provide an even better characterization of iron oxidation than the study of PioA alone. A second approach would be the production of the decaheme domain without the non heme-biding domain. This might increase the stability of PioA and, by reduction in half of the size of the protein, it could allow a characterization by solution NMR, which is hindered by molecular size. Multi-heme cytochromes tend to be composed by the fusion of smaller multi-heme domains (175). Insight into the mechanism of PioA could be achieved by the study of the separate possible domains of this cytochrome, a strategy that would reduce the size of the molecule under study even further.

NMR is the only spectroscopic method capable of discriminating the ten hemes of a decaheme cytochrome. The 60 kDa size of PioA, however, makes its study by standard solution NMR techniques quite difficult (79). To use this spectroscopy in the characterization of PioA, individual domains would have to be studied separately as stated above, or state of the art NMR techniques would be required to study the whole PioA or the PioAB complex. Solid state NMR is not hindered by the size of the molecule under study and has been used before in the study of paramagnetic proteins (176, 177). This approach

could allow the molecular detail that solution NMR has provided for other smaller cytochromes. Besides NMR, which should provide discrimination between cofactors, the methods used in the thermodynamic and kinetic characterization of FoxE can be used for PioA.

Again, a complete picture of the process of iron oxidation in TIE-1 requires the study of the interactions between the proteins involved. As with FoxE and FoxY, PioA and PioC have different spectral properties that should allow achieving this objective. The study on how PioC interacts with the cyclic photosynthetic apparatus should close the electron transfer chain between Fe(II) and the RC. Important to this issue is the localization of the different proteins in the cell of TIE-1. The RC is known to be exclusively located in the ICM. The location of PioA and PioC still requires determination. Tagging of these proteins by fusion with green fluorescent protein and its derivatives can be used to achieve this objective through fluorescence microscopy (178). This approach would not be trivial as GFP requires oxygen for proper folding and photoferrotrophy is an anaerobic process. Alternatively, cryo electron microscopy can be used to localize these proteins by tagging with antibodies.

Even though the information on each of the photoferrotrophic strategies described here is still limited, it is possible to conclude that the two bacteria, TIE-1 and SW2, used different strategies for the same objective. Despite the fact that both bacteria use *c*-type cytochrome to oxidize iron, there is no homology between the two systems described here. Even the way both bacteria seem to handle Fe(III) precipitation is different. These differences suggest that the marks ancient photoferrotrophs may have left on the geological record might be different depending on the strategy followed. Considering this hypothesis, it may be possible to identified different photoferrotrophic strategies as the origin of specific geological formations. At

the same time, the interpretation of the geological record, concerning photoferrotrophy, is more complex and must be performed with care.

4.3 Comments on biotechnological applications

Several biotechnological applications, from bioremediation to MFCs, use live cells in order to achieve their objective. This approach presents several variables that are hard to control. Using axenic cultures has the advantage of allowing a higher control of the many variables involved. In the case of the genetically tractable TIE-1, molecular biology tools can be used in order to tune the system for the different objectives targeted. For instance, overexpression of the *pio* operon could be used in order to increase iron oxidation in the cathode of an MFC. An even tighter control of a biotechnological system can be achieved if the detailed molecular characterization of proteins involved in a particular pathway is known. The studies presented here lead to the understanding of the role each cofactor or even each amino acid in a specific reaction. This level of detail should lead to a better optimization of the biotechnological system being developed. This is true not only for genetically tractable organisms like TIE-1. The proteins of SW2 can be used in heterologous systems, extending this capacity to other organisms.

5

Appendices

Appendix A: Expression and production of *c*-type cytochromes

The characterization and spectroscopical study of a protein requires substantial amounts of native protein that demand a reliable and efficient production system. The production of *c*-type cytochromes is limited by the covalent attachment of the heme cofactors. In *E. coli*, this attachment is performed by the enzymes coded by the *ccm* operon. This operon is only expressed in anaerobic conditions in the presence of nitrate, nitrite or TMAO as terminal electron acceptor. In order to produce *c*-type cytochromes in aerobic conditions, the plasmid pEC86 (134), constitutively expressing the *ccm* operon, was used. This plasmid allows the expression of the *ccm* machinery, even in aerobic conditions, and its use is now standard in the production of *c*-type cytochromes in *E. coli*.

Cytochrome production depends on several factors like the *E.* coli strain, the expression vector, periplasmatic signal peptide, and growth conditions and all these where considered in the production of FoxE:

a) The used strain was *E. coli* strain JCB7123. This strain has unknown mutations that have been shown to confer an increased capacity to produce cytochromes (179) (180).
b) An important aspect to consider is the control of protein expression levels as, in some cases (181), maturation of holo-cytochrome is probably limited by the ccm enzymes that work at a lower rate than polypeptide synthesis. In these cases, overexpression results in production of a mixture of forms with different number of hemes attached. To avoid production of incompletely matured forms of FoxE,

the plasmid pUX19 was used. This plasmid provided expression levels that allowed full maturation of FoxE.

c) Because of possible differences in the recognition of signal peptides in different species, the native signal peptide of FoxE was replaced with pelB, which is native to *E. coli*.

d) Different growth conditions were tested in the production of FoxE. These were culture medium (Lysogenic Broth (LB) or Terrific Broth (TB)), temperature (37°C or 30°C), culture medium oxygenation (aerobic or micro aerobic), induction and incubation time. To test each set of growth conditions 1 mL of culture of each set was pelleted and resuspended in 50 μL of SDS-PAGE loading buffer. The suspensions were incubated 5 min in boiling water and loaded into an SDS-PAGE gel. After run the gel was stained with *c*-type cytochrome specific stain and FoxE production was evaluated by the intensity of the FoxE band. The best conditions determined were LB culture medium at 30°C in micro aerobic condition (3.5 L of culture medium per 5 L flask and 140 rpm agitation) with cells collected 24 h after inoculum. Induction resulted in no FoxE production and the best conditions determined relied only on leaky expression of the pUX19 plasmid.

Appendix B: Paramagnetic NMR spectroscopy

NMR spectroscopy is a powerful technique that can provide information on molecular structure, thermodynamics, kinetics, dynamics or molecular interactions, and it does all this in an individual atom basis. This is achieved through the magnetic properties of the nucleus of some atoms. These interact not only with an applied magnetic field but also with the fields generated by the molecule's moving electrons. These local fields are molecule specific and give origin to the chemical shift.

The fact that electrons are the source of the chemical shift makes NMR spectroscopy particularly suitable to study electron transfer proteins. The two types of protein studied in this work, cytochromes and HiPIPs, can have unpaired electrons, depending on redox state. These electrons give origin to distinctive spectroscopic characteristics. The chemical shift of a nucleus in a paramagnetic molecule is given by:

$$\delta = \delta_{dia} + \delta_{pc} + \delta_{Fc} \qquad \text{B-1}$$

in which δ_{dia} is the diamagnetic chemical shift, δ_{pc} is the paramagnetic pseudo-contact shift and δ_{Fc} is the paramagnetic Fermi contact shift. The pseudo-contact shift is originated by a through-space interaction between the paramagnetic center and a nucleus according to the following equation (182):

$$\delta_{pc} = \frac{1}{12\pi r^2}\left[\Delta\chi_{ax}(3\cos^2\theta - 1) + \frac{3}{2}\Delta\chi_{rh}\sin^2\theta\cos 2\varphi\right] \qquad \text{B-2}$$

where $\Delta\chi$ is the magnetic susceptibility of the center (that describes how its magnetic effects propagate in space) and r, θ and φ are the polar coordinates of the nucleus in the magnetic axis of the center. As a through-space interaction, pseudo-contact shifts can and have been used in refinement of solution structures of proteins, particularly in the regions around paramagnetic centers that tend to lack other structural information due to increased relaxation (183). The Fermi contact shift is proportional to the unpaired

electron density on the nucleus (ρ) and for a single electron on a singly populated energy level can be given by (182):

$$\delta_{Fc} = \frac{2\pi g\beta S(S+1)A}{3\gamma kT}\rho \qquad \text{B-3}$$

where A is the hyperfine coupling constant, g is the electron g-factor, β is the Bohr-magneton, S is the electron spin state, γ is the nuclear gyromagnetic ratio, k is the Boltzmann constant and T is the temperature. Because the Fermi contact shift is proportional to the unpaired electron density, it only affects the atoms covalently attached to the paramagnetic center. Although it has a short range it is the dominating contribution in the chemical shift of the affected nuclei.

NMR is particularly suitable to study multi-heme cytochromes. First, NMR provides spectral resolution. In order to study the mechanistic details of these proteins, spectral resolution of each individual heme is required. As the number of hemes in a cytochrome increases, NMR is the only spectroscopic technique that can discriminate between different cofactors. The unpaired electrons in a heme are delocalized in the porphyrin ring π orbitals originating a specific pattern of Fermi contact shifts (184). These shifts place the signals of the porphyrin ring outside the spectral region crowded with peptide signals, allowing their observation (Figure 2.4). Second, changing the redox state of the heme always results in a change of spin state, which affects the paramagnetic shifts of the heme. Therefore, NMR allows the observation of each individual heme in a redox state sensitive manner. Because of this, every microstate described in 1.3.1 has a distinctive spectral signature. At any given pH and reduction fraction of a multi-heme cytochrome, the observed NMR spectrum will have the weighted contributions of all of these signatures, and thus allow determining the relative populations of their associated microstates. The contribution of each microstate depends on the rate of conversion between

microstates in relation to the NMR time scale. In the case of FoxE, because the conversion rate between the four possible microstates is slow, the spectra in Figure 2.4 are the weighted sums of the spectra of each individual microstate.

Appendix C: Bioelectrochemistry

In the study of electron transfer proteins bioelectrochemistry techniques are invaluable. In the case of multi-heme cytochromes NMR provides the spectral resolution required to follow the redox behavior of individual hemes, which allows the determination of the relative populations of the different possible microstates. However, in order to determine absolute reduction potentials of each individual heme, the data from the NMR must be conjugated with redox titrations, where the poised potential is known (185). For the thermodynamic characterization of FoxE, a redox titration protocol was devised. Having a distinctive redox dependent UV-visible spectrum, the overall reduction fraction of cytochromes is easily followed with this spectroscopy. Therefore, an optically transparent thin layer electrochemical cell (OTTLE) was used (Figure C.1). An OTTLE is a spectrophotometer cell that, in this case, is UV and visible radiation transparent and has a thin rectangular reservoir. The poised potential was controlled by a potentiostat through a three electrode system. The potential is imposed through a working electrode relative to a reference electrode. The system is completed with an auxiliary electrode that minimizes the current through the reference electrode, preventing its potential to change during the experiment. The working electrodes used were platinum rectangular meshes that fit the OTTLE reservoir, intercepting the light path without blocking the light. The OTTLE allows the fitting of a metallic wire as the auxiliary electrode and of a reference electrode that touches the sample above the rectangular reservoir. In this work these were a platinum wire and a saturated calomel electrode, respectively. This design allows a large ratio of electrode-area to sample-volume, which minimizes the time required to reach equilibrium between electrode and analyte, and minimizes the amount of protein required. Because the electron transfer between the working electrode and the cytochrome is usually slow, a mixture of redox mediators was added to

the protein sample. These are small redox active molecules that mediate this electron transfer in a fast manner.

HiPIPs are one electron transfer proteins with a single redox center. As such, determining this single center reduction potential is less complex than for the multi-heme cytochromes. A successful approach to characterize these proteins is cyclic voltammetry. In this technique, a cyclic potential sweep in the reduction potential range of the studied protein is performed and the resulting current is measured. This allows the determination of the reduction potential of the molecule under study. Figure C.1B shows the cyclic voltammetry assembly used.

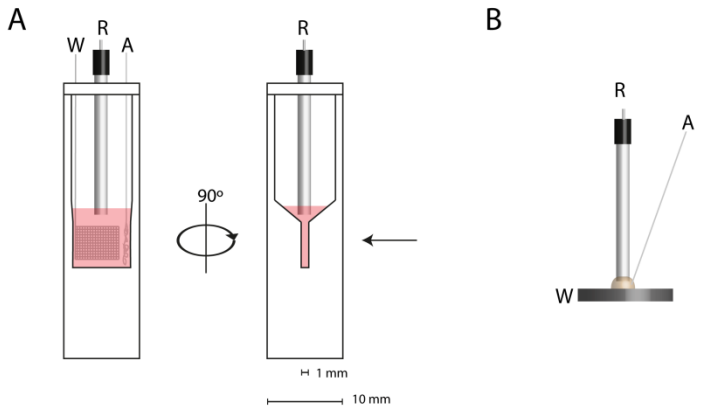

Figure C.1: schematic representations of the OTTLE used in the redox titration of FoxE (A) and of the cyclic voltammetry assembly for the study of PioC (B).
The working electrodes (W) are a platinum mesh in A and a graphite disc in B. The reference electrodes (R) are a saturated calomel electrode in A and a silver/silver chloride electrode in B. The auxiliary electrode (A) is a platinum wire in both cases.

Appendix D: Matlab routine

Matlab routine for the calculation of the reduction pseudo-first order rate constants for a protein with two independent redox centers:

- Input: kinetic traces, protein concentration and initial oxidation fraction of the two centers.
- Output: one pseudo-first order rate constant for each center, the contribution of each center for the kinetic traces and the respective standard errors.

File FoxE_kin.m:

```
clear
data = dlmread('FoxE_7_300.txt', '\t');          % input kinetic traces
FoxE = [1e-6 1e-6];                              % protein concentration
fA = [1 .77];           % initial oxidation fractions of redox center A
fB = [1 .23];           % initial oxidation fractions of redox center B

%-------------------------------------------
A0 = FoxE .* fA;    % initial concentrations of oxidized redox center A
B0 = FoxE .* fB     % initial concentrations of oxidized redox center B
t= data(1:size(data,1),1:2:size(data,2)); % time domain from input data
trace = data(1:size(data,1),2:2:size(data,2));   % kinetic traces from
input data

k0 = [10 10 .5];                                   % initial estimation
[k, MQ] = fminsearch(@(k) FoxE_fun(k, t, trace, A0, B0, FoxE), k0);


KI = k(1);
KII = k(2);
r = k(3);

tp = t;
for n = 1:size(t,2)
    clear A B
    A = r*A0(n)*exp(-KI*tp(:,n));
    B = (1-r)*B0(n)*exp(-KII*tp(:,n));
    rf(:,n) = 1 - (A+B)/FoxE(n);
end


plot(tp,rf)
hold on
```

```
plot(t,trace, '.', 'MarkerSize',0.5)


% derivation

tp = t;

drf = zeros(size(t,1),3);
for n = 1:size(t,2)
    clear dA dB
    dA(:,1) = - r.*A0(n).*t(:,n).*exp(-KI.*t(:,n));
    dB(:,1) = 0*t(:,n);
    dA(:,2) = 0*t(:,n);
    dB(:,2) = - (1-r).*B0(n).*t(:,n).*exp(-KII.*t(:,n));
    dA(:,3) = A0(n)*exp(-KI*t(:,n));
    dB(:,3) = B0(n)*exp(-KII*t(:,n));
    drf = drf -( dA + dB ) / FoxE(n);
end

alfa = drf'/.3 * drf/.3;

stderr = (diag(inv(alfa))).^.5;                          % standard error

format short
[k;stderr']
MQ                                                        % least squares

clear A B A0 B0 FoxE alfa ans dA dB data fA fB k0 n rf t tp trace drf
```

File FoxE_fun.m:

```
function MQ = FoxE_fun(k, t, trace, A0, B0, FoxE)


KI = k(1);

KII = k(2);

r = k(3);


for n = 1:size(t,2)

    clear A B

    A = r*A0(n)*exp(-KI*t(:,n));

    B = (1-r)*B0(n)*exp(-KII*t(:,n));
```

```
    rf(:,n) = 1 - (A+B)/FoxE(n);
end


MQ = sum( sum( (rf-trace).^2 ) )
```

Appendix E: PioC NMR signals assignment

Table E.1: assignment of PioC ^{13}C signals.
Tentative assignments are in italic.

Resonance			chemical shift /ppm
1	Asn	C	175.05
1	Asn	Ca	53.14
1	Asn	Cb	38.91
2	Ala	C	177.29
2	Ala	Ca	52.63
2	Ala	Cb	19.15
3	Gln	C	175.91
3	Gln	Ca	55.81
3	Gln	Cb	29.39
3	Gln	Cg	33.80
4	Val	C	176.20
4	Val	Ca	62.18
4	Val	Cb	32.86
4	Val	Cga	20.97
4	Val	Cga	20.47
5	Thr	C	173.94
5	Thr	Ca	61.85
5	Thr	Cb	69.81
5	Thr	Cg2	21.62
6	Lys	C	176.13
6	Lys	Ca	55.82
6	Lys	Cb	33.30
6	Lys	Cd	29.02
6	Lys	Ce	42.12
6	Lys	Cg	24.40
7	Lys	C	175.88
7	Lys	Ca	56.62
7	Lys	Cb	34.74
7	Lys	Cd	30.12
7	Lys	Ce	42.52
7	Lys	Cg	26.35
8	Ala	C	177.50
8	Ala	Ca	51.46
8	Ala	Cb	19.63
9	Ser	C	174.92
9	Ser	Ca	56.95
9	Ser	Cb	64.89
10	His	C	177.61
10	His	Ca	58.76
10	His	Cb	28.33
10	His	Cd2	117.47
10	His	Ce1	137.18
11	Lys	C	179.57
11	Lys	Ca	59.31
11	Lys	Cb	32.39
11	Lys	Cd	29.25
11	Lys	Ce	42.10
11	Lys	Cg	24.62
12	Asp	C	178.19
12	Asp	Ca	57.23
12	Asp	Cb	40.17
13	Ala	C	176.14
13	Ala	Ca	52.90
13	Ala	Cb	24.44
14	Gly	C	175.10
14	Gly	Ca	46.80
15	Tyr	C	174.73
15	Tyr	Ca	59.18
15	Tyr	Cb	39.40

16	Gln	C	172.90	26	Gly	Ca	46.24
16	Gln	Ca	52.72	27	Thr	C	173.48
16	Gln	Cb	32.67	27	Thr	Ca	60.85
16	Gln	Cd	181.42	27	Thr	Cb	69.17
16	Gln	Cg	32.85	27	Thr	Cg2	21.00
17	Glu	C	174.61	28	Cys	C	176.41
17	Glu	Ca	56.38	28	Cys	Ca	80.38
17	Glu	Cb	29.32	29	Arg	Ca	58.88
17	Glu	Cg	36.85	29	Arg	Cb	31.08
18	Ser	Ca	56.15	29	Arg	Cd	43.63
18	Ser	Cb	63.96	29	Arg	Cg	27.33
19	Pro	C	176.05	30	Gln	Ca	55.26
19	Pro	Ca	63.03	30	Gln	Cb	29.73
19	Pro	Cb	33.40	30	Gln	Cg	33.64
19	Pro	Cd	51.25	31	Phe	C	177.99
19	Pro	Cg	27.58	*31*	*Phe*	*Ca*	*58.67*
20	Asn	C	175.66	*31*	*Phe*	*Cb*	*38.82*
20	Asn	Ca	50.00	31	Phe	Cd*	134.18
20	Asn	Cb	36.21	31	Phe	Ce*	128.97
21	Gly	C	174.05	31	Phe	Cz	130.44
21	Gly	Ca	46.75	32	Arg	Ca	50.11
22	Ala	C	177.90	32	Arg	Cb	29.98
22	Ala	Ca	52.20	32	Arg	Cd	42.81
22	Ala	Cb	19.17	32	Arg	Cg	25.42
23	Lys	C	173.01	33	Pro	Ca	61.21
23	Lys	Ca	56.73	33	Pro	Cb	30.32
23	Lys	Cb	32.18	33	Pro	Cd	50.40
23	Lys	Cd	29.19	33	Pro	Cg	26.24
23	Lys	Ce	42.00	34	Pro	C	177.96
23	Lys	Cg	24.52	34	Pro	Ca	64.35
24	Arg	Ca	53.44	34	Pro	Cb	35.00
24	Arg	Cb	33.30	34	Pro	Cd	50.25
24	Arg	Cd	43.65	34	Pro	Cg	24.49
24	Arg	Cg	26.39	35	Ser	C	174.33
25	Cys	C	177.55	35	Ser	Ca	57.39
25	*Cys*	*Ca*	*90.15* *88.30*	35	Ser	Cb	64.39
26	Gly	C	175.99	36	Ser	C	169.40

36	Ser	Ca	57.31
36	Ser	Cb	66.00
37	Cys	C	173.76
37	Cys	Ca	90.28
38	Ile	Ca	64.05
38	Ile	Cb	38.48
38	Ile	Cd1	13.21
38	Ile	Cg1	26.86
38	Ile	Cg2	18.72
39	Thr	Ca	63.30
39	Thr	Cb	73.97
39	Thr	Cg2	25.03
40	Val	C	173.84
40	Val	Ca	62.89
40	Val	Cb	36.93
40	Val	Cga	23.87
40	Val	Cgb	26.28
41	Glu	C	174.65
41	Glu	Ca	56.95
41	Glu	Cb	31.03
41	Glu	Cg	36.24
42	Ser	Ca	58.98
42	Ser	Cb	62.67
43	Pro	C	174.23
43	Pro	Ca	62.61
43	Pro	Cb	34.68
43	Pro	Cd	50.53
43	Pro	Cg	24.33
44	Ile	C	175.41
44	Ile	Ca	58.13
44	Ile	Cb	39.23
44	Ile	Cd1	20.98
44	Ile	Cg1	26.87
44	Ile	Cg2	22.13
45	Ser	C	175.49
45	Ser	Ca	55.32
45	Ser	Ca	55.19
45	Ser	Cb	65.01
46	Glu	C	175.93
46	Glu	Ca	58.61
46	Glu	Cb	29.21
46	Glu	Cg	35.03
47	Asn	C	172.15
47	Asn	Ca	52.89
47	Asn	Cb	39.98
48	Gly	C	172.90
48	Gly	Ca	45.53
49	Trp	Ca	65.74
49	Trp	Cb	31.26
49	Trp	Cd1	127.14
49	Trp	Ce3	119.89
49	Trp	Ch2	124.32
49	Trp	Cz2	114.69
49	Trp	Cz3	122.18
50	Cys	C	170.57
50	*Cys*	*Ca*	*90.15* *88.30*
51	Arg	Ca	57.34
51	Arg	Ca	57.47
51	Arg	Cb	30.09
51	Arg	Cd	43.44
51	Arg	Cg	28.20
52	*Leu*	*C*	*173.24*
52	Leu	Ca	53.45
52	Leu	Cb	43.18
52	Leu	Cda	22.19
52	Leu	Cdb	25.59
52	Leu	Cg	27.84
54	Ala	C	175.02
54	Ala	Ca	50.85
54	Ala	Cb	20.73
55	Gly	C	174.45
55	Gly	Ca	45.80
56	Lys	C	175.49
56	Lys	Ca	57.15

56	Lys	Cb	33.54	56	Lys	Cg	25.16
56	Lys	Cd	29.83	57	Ala	Ca	53.74
56	Lys	Ce	42.24	57	Ala	Cb	20.11

Table E.2: assignment of PioC ^{15}N signals.
Tentative assignments are in italic.

Resonance			chemical shift/.ppm
1	Asn	N	118.93
1	Asn	Nd2	112.64
2	Ala	N	124.12
3	Gln	N	120.04
3	Gln	Ne2	112.45
4	Val	N	121.62
5	Thr	N	119.34
6	Lys	N	124.93
7	Lys	N	123.80
8	Ala	N	124.33
9	Ser	N	117.19
10	His	N	118.39
11	Lys	N	118.45
12	Asp	N	121.51
13	Ala	N	120.19
14	Gly	N	107.02
15	Tyr	N	118.36
16	Gln	N	126.54
16	Gln	Ne2	114.37
17	Glu	N	117.20
18	Ser	N	114.86
20	Asn	N	118.41
20	Asn	Nd2	108.02
21	Gly	N	113.60
22	Ala	N	128.80
23	Lys	N	120.41
24	Arg	N	117.91
26	Gly	N	99.58
27	Thr	N	111.87
28	Cfs	N	132.03
29	Arg	N	133.48
29	Arg	Ne	83.92
30	Gln	Ne2	112.33
32	Arg	N	130.19
35	Ser	N	113.80
36	Ser	N	116.89
37	Cys	N	131.04
38	Ile	N	127.95
41	Glu	N	124.84
42	Ser	N	117.50
44	Ile	N	120.18
45	Ser	N	118.35
46	Glu	N	123.13
47	Asn	N	118.89
47	Asn	Nd2	113.76
48	Gly	N	104.63
49	Trp	N	115.70
49	Trp	Ne1	129.49
51	Arg	N	117.13
51	Arg	Ne	84.13
53	*Tyr*	*N*	*126.04*
55	Gly	N	111.71
56	Lys	N	122.15
57	Ala	N	130.41

Table E.3: assignment of PioC ^{1}H signals.
Tentative assignments are in italic

Resonance			chemical shift/ ppm
1	Asn	H	8.24
1	Asn	Ha	4.64
1	Asn	Hba	2.69
1	Asn	Hbb	2.77
1	Asn	Hd2a	6.84
1	Asn	Hd2b	7.51
2	Ala	H	8.20
2	Ala	Ha	4.30
2	Ala	Hb	1.34
3	Gln	H	8.34
3	Gln	Ha	4.26
3	Gln	Hba	1.93
3	Gln	Hbb	2.02
3	Gln	He2a	6.80
3	Gln	He2b	7.45
3	Gln	Hga	2.30
4	Val	H	8.10
4	Val	Ha	4.11
4	Val	Hb	2.02
4	Val	Hga	0.88
4	Val	Hgb	0.88
5	Thr	H	8.25
5	Thr	Ha	4.25
5	Thr	Hb	4.08
5	Thr	Hg2	1.14
6	Lys	H	8.26
6	Lys	Ha	4.31
6	Lys	Hba	1.69
6	Lys	Hbb	1.78
6	Lys	Hda	1.64
6	Lys	Heb	2.96
6	Lys	Hga	1.38
7	Lys	H	8.42
7	Lys	Ha	4.13
7	Lys	Hba	1.39
7	Lys	Hbb	1.45
7	Lys	Hda	1.30
7	Lys	Hea	2.74
7	Lys	Heb	2.90
7	Lys	Hga	0.96
7	Lys	Hgb	1.32
8	Ala	H	8.75
8	Ala	Ha	4.49
8	Ala	Hb	1.58
9	Ser	H	9.07
9	Ser	Ha	4.40
9	Ser	Hba	4.07
9	Ser	Hbb	4.32
10	His	H	9.63
10	His	Ha	4.23
10	His	Hba	3.30
10	His	Hbb	3.38
10	His	Hd2	6.68
10	His	He1	8.21
11	Lys	H	8.48
11	Lys	Ha	4.19
11	Lys	Hba	1.76
11	Lys	Hbb	1.91
11	Lys	Hda	1.60
11	Lys	Hdb	1.70
11	Lys	Hea	2.97
11	Lys	Heb	3.00
11	Lys	Hga	1.43
11	Lys	Hgb	1.50
12	Asp	H	8.12
12	Asp	Ha	4.35

12	Asp	Ha	4.36	20	Asn	H	7.91
12	Asp	Hba	2.72	20	Asn	Ha	4.40
12	Asp	Hbb	2.86	20	Asn	Hba	0.70
13	Ala	H	8.23	20	Asn	Hbb	1.05
13	Ala	Ha	4.28	20	Asn	Hd2a	3.98
13	Ala	Hb	1.91	20	Asn	Hd2b	6.15
14	Gly	H	7.67	21	Gly	H	8.16
14	Gly	Haa	3.72	21	Gly	Haa	3.37
14	Gly	Hab	3.89	21	Gly	Hab	3.69
15	Tyr	H	8.19	22	Ala	H	8.77
15	Tyr	Ha	4.50	22	Ala	Ha	4.20
15	Tyr	Hba	2.37	22	Ala	Hb	1.34
15	Tyr	Hbb	2.57	23	Lys	H	7.61
16	Gln	H	8.65	23	Lys	Ha	3.85
16	Gln	Ha	4.65	23	Lys	Hba	0.27
16	Gln	Hba	1.93	23	Lys	Hbb	1.55
16	Gln	Hbb	2.12	23	Lys	Hdb	1.40
16	Gln	He2a	6.57	23	Lys	Hea	2.90
16	Gln	He2b	7.34	23	Lys	Hga	1.15
16	Gln	Hga	2.49	23	Lys	Hgb	1.30
16	Gln	Hgb	2.77	24	Arg	H	7.45
17	Glu	H	8.21	24	Arg	Ha	6.13
17	Glu	Ha	4.07	24	Arg	Hba	1.81
17	Glu	Hba	1.82	24	Arg	Hbb	2.45
17	Glu	Hbb	2.28	24	Arg	Hda	3.01
17	Glu	Hgb	2.35	24	Arg	Hdb	3.50
18	Ser	H	7.28	24	Arg	Hga	1.45
18	Ser	Ha	4.98	24	Arg	Hgb	1.71
18	Ser	Hba	3.68	*25*	*Cys*	*Ha*	*8.19* *8.94*
18	Ser	Hbb	3.73				
19	Pro	Ha	4.16	26	Gly	H	8.61
19	Pro	Hba	1.70	26	Gly	Haa	3.81
19	Pro	Hbb	1.95	26	Gly	Hab	3.92
19	Pro	Hda	3.41	27	Thr	H	8.61
19	Pro	Hdb	4.03	27	Thr	Ha	4.70
19	Pro	Hga	1.70	27	Thr	Hb	4.96
19	Pro	Hgb	1.87	27	Thr	Hg2	1.19
				28	Cys	H	8.35

28	Cys	Ha	3.86	34	Pro	Hba	2.14
29	Arg	H	9.26	34	Pro	Hbb	2.40
29	Arg	Ha	4.46	34	Pro	Hda	3.34
29	Arg	Hba	1.86	34	Pro	Hdb	3.59
29	Arg	Hbb	1.95	34	Pro	Hga	1.86
29	Arg	Hda	3.10	34	Pro	Hgb	1.93
29	Arg	Hdb	3.16	35	Ser	H	8.14
29	Arg	He	6.94	35	Ser	Ha	5.42
29	Arg	Hga	1.66	35	Ser	Hba	3.83
29	Arg	Hgb	1.73	35	Ser	Hbb	4.05
30	Gln	Ha	4.21	36	Ser	H	7.54
30	Gln	Hba	1.82	36	Ser	Ha	4.67
30	Gln	He2a	6.75	36	Ser	Hba	3.48
30	Gln	He2b	7.40	36	Ser	Hbb	3.57
30	Gln	Hga	2.19	37	Cys	H	8.53
31	*Phe*	*Ha*	*4.98*	37	Cys	Ha	3.84
31	*Phe*	*Hba*	*2.75*	38	Ile	H	8.35
31	*Phe*	*Hbb*	*2.46*	38	Ile	Ha	4.16
31	Phe	Hd	7.26	38	Ile	Hb	2.04
31	Phe	He	7.11	38	Ile	Hd1	0.92
31	Phe	Hz	7.06	38	Ile	Hg1a	1.47
32	Arg	H	8.18	38	Ile	Hg1b	1.68
32	Arg	Ha	4.59	38	Ile	Hg2	1.01
32	Arg	Hba	1.14	39	Thr	Ha	4.64
32	Arg	Hbb	1.28	39	Thr	Hb	4.05
32	Arg	Hda	2.92	39	Thr	Hg2	1.27
32	Arg	Hdb	3.34	40	Val	Ha	5.02
32	Arg	Hga	1.40	40	Val	Hga	1.24
32	Arg	Hgb	1.50	40	Val	Hgb	3.22
33	Pro	Ha	3.39	41	Glu	H	8.59
33	Pro	Hba	1.71	41	Glu	Ha	3.77
33	Pro	Hbb	2.24	41	Glu	Hba	1.73
33	Pro	Hda	2.79	41	Glu	Hbb	1.83
33	Pro	Hdb	3.52	41	Glu	Hga	2.15
33	Pro	Hga	1.79	41	Glu	Hgb	2.19
33	Pro	Hgb	1.89	42	Ser	H	8.41
34	Pro	Ha	4.40	42	Ser	Ha	4.05

42	Ser	Hba	3.54
42	Ser	Hbb	4.07
43	Pro	Ha	4.59
43	Pro	Hba	2.03
43	Pro	Hbb	2.34
43	Pro	Hda	3.29
43	Pro	Hdb	3.41
43	Pro	Hga	1.91
43	Pro	Hgb	1.93
44	Ile	H	7.27
44	Ile	Ha	4.12
44	Ile	Hb	1.35
44	Ile	Hd1	0.10
44	Ile	Hg1a	0.29
44	Ile	Hg1b	1.03
44	Ile	Hg2	0.83
45	Ser	H	7.84
45	Ser	Ha	4.86
45	Ser	Hba	3.64
45	Ser	Hbb	3.96
46	Glu	H	9.11
46	Glu	Ha	3.33
46	Glu	Ha	3.34
46	Glu	Hba	1.97
46	Glu	Hbb	2.12
46	Glu	Hga	2.04
46	Glu	Hgb	2.24
47	Asn	H	7.97
47	Asn	Ha	4.98
47	Asn	Ha	5.00
47	Asn	Hba	2.42
47	Asn	Hbb	3.00
47	Asn	Hd2a	6.86
47	Asn	Hd2b	7.56
48	Gly	H	7.19
48	Gly	Haa	4.12
48	Gly	Hab	3.77
49	Trp	H	7.85
49	Trp	Hba	2.85
49	Trp	Hbb	3.88
49	Trp	He1	10.06
49	Trp	He3	6.85
49	Trp	Hh2	7.01
49	Trp	Hz2	7.37
49	Trp	Hz3	6.91
50	*Cys*	*Ha*	*8.19* *8.94*
51	Arg	H	6.77
51	Arg	Ha	3.59
51	Arg	Hba	1.63
51	Arg	Hbb	1.65
51	Arg	Hda	3.11
51	Arg	Hdb	3.18
51	Arg	He	7.25
51	Arg	Hga	1.54
51	Arg	Hgb	1.68
52	Leu	Ha	4.09
52	Leu	Hba	1.01
52	Leu	Hda	0.66
52	Leu	Hdb	0.98
52	Leu	Hg	1.67
53	*Tyr*	*H*	*8.52*
53	*Tyr*	*Ha*	*6.63*
54	Ala	Ha	4.27
54	Ala	Hb	1.01
55	Gly	H	8.32
55	Gly	Haa	3.68
55	Gly	Hab	3.98
56	Lys	H	8.42
56	Lys	Ha	4.13
56	Lys	Hba	1.66
56	Lys	Hbb	1.80
56	Lys	Hdb	1.66
56	Lys	Heb	2.97
56	Lys	Hga	1.38

57	Ala	H	8.02
57	Ala	Ha	4.08
57	Ala	Hb	1.30

Appendix F: CCPNMR CFS definition

Here is presented the definition of the CFS (161) chemComp file for the CCPNMR Analysis software. The file was based on the file for cys. CFS cannot be placed in an N or a C-terminal.

protein+Cfs+msd_ccpnRef_2012-06-21-10-20-13_00005.xml

```
<?xml version="1.0" encoding="UTF-8"?>
<_StorageUnit release="2.0.5" originator="CCPN Python XmlIO"
packageGuid="www.ccpn.ac.uk_Fogh_2006-08-16-14:22:51_00046" time="Tue Jun 26 09:34:09 2012">
<CHEM.NonStdChemComp _ID="_1" ccpCode="Cfs" code3Letter="CFS" createdBy="isaraiva"
guid="msd_ccpnRef_2012-06-21-10-20-13_00005" hasStdChirality="true"molType="protein"
stdChemCompCode="Cys">
<CHEM.ChemComp.commonNames>
<IMPL.Text>cys-Fe-S</IMPL.Text>
</CHEM.ChemComp.commonNames>
<CHEM.ChemComp.name>
<IMPL.Text>Cys-Fe-S</IMPL.Text>
</CHEM.ChemComp.name>
<IMPL.DataObject.applicationData>
<IMPL.AppDataString>
<IMPL.ApplicationData.application>
<IMPL.Line>ccpNmr</IMPL.Line>
</IMPL.ApplicationData.application>
<IMPL.ApplicationData.keyword>
<IMPL.Line>commonNameMapping</IMPL.Line>
</IMPL.ApplicationData.keyword>
<IMPL.AppDataString.value>
<IMPL.String>['HA*', 'HA']</IMPL.String>
</IMPL.AppDataString.value>
</IMPL.AppDataString>
<IMPL.AppDataString>
<IMPL.ApplicationData.application>
<IMPL.Line>ccpNmr</IMPL.Line>
</IMPL.ApplicationData.application>
<IMPL.ApplicationData.keyword>
<IMPL.Line>commonNameMapping</IMPL.Line>
</IMPL.ApplicationData.keyword>
<IMPL.AppDataString.value>
<IMPL.String>['HA#', 'HA']</IMPL.String>
</IMPL.AppDataString.value>
</IMPL.AppDataString>
<IMPL.AppDataString>
<IMPL.ApplicationData.application>
<IMPL.Line>ccpNmr</IMPL.Line>
</IMPL.ApplicationData.application>
<IMPL.ApplicationData.keyword>
<IMPL.Line>commonNameMapping</IMPL.Line>
</IMPL.ApplicationData.keyword>
<IMPL.AppDataString.value>
<IMPL.String>['HA%', 'HA']</IMPL.String>
</IMPL.AppDataString.value>
</IMPL.AppDataString>
<IMPL.AppDataString>
<IMPL.ApplicationData.application>
<IMPL.Line>ccpNmr</IMPL.Line>
```

```
</IMPL.ApplicationData.application>
<IMPL.ApplicationData.keyword>
<IMPL.Line>commonNameMapping</IMPL.Line>
</IMPL.ApplicationData.keyword>
<IMPL.AppDataString.value>
<IMPL.String>['HA+', 'HA']</IMPL.String>
</IMPL.AppDataString.value>
</IMPL.AppDataString>
</IMPL.DataObject.applicationData>
<CHEM.ChemComp.chemAtomSets>
<CHEM.ChemAtomSet _ID="_2" distCorr="1.8" isEquivalent="false" isProchiral="true"
name="HB*">
<CHEM.ChemAtomSet.chemAtoms>_3 _4</CHEM.ChemAtomSet.chemAtoms>
</CHEM.ChemAtomSet>
</CHEM.ChemComp.chemAtomSets>
<CHEM.ChemComp.chemAtoms>
<CHEM.ChemAtom _ID="_5" elementSymbol="C" name="C">
<CHEM.ChemAtom.boundLinkEnds>_6</CHEM.ChemAtom.boundLinkEnds>
<CHEM.AbstractChemAtom.chemBonds>_7 _8 _9 _10</CHEM.AbstractChemAtom.chemBonds>
<CHEM.AbstractChemAtom.chemCompVars>_11</CHEM.AbstractChemAtom.chemCompVars>
<CHEM.AbstractChemAtom.chemTorsions>_12 _13</CHEM.AbstractChemAtom.chemTorsions>
</CHEM.ChemAtom>
<CHEM.ChemAtom _ID="_14" chirality="R" elementSymbol="C" name="CA">
<CHEM.AbstractChemAtom.chemBonds>_15 _16 _17 _9</CHEM.AbstractChemAtom.chemBonds>
<CHEM.AbstractChemAtom.chemCompVars>_11</CHEM.AbstractChemAtom.chemCompVars>
<CHEM.AbstractChemAtom.chemTorsions>_18 _19 _12 _13 _20</CHEM.AbstractChemAtom.chemTorsions>
<CHEM.ChemAtom.remoteLinkEnds>_6 _21</CHEM.ChemAtom.remoteLinkEnds>
</CHEM.ChemAtom>
<CHEM.ChemAtom _ID="_22" elementSymbol="C" name="CB">
<CHEM.AbstractChemAtom.chemBonds>_23 _24 _16 _25</CHEM.AbstractChemAtom.chemBonds>
<CHEM.AbstractChemAtom.chemCompVars>_11</CHEM.AbstractChemAtom.chemCompVars>
<CHEM.AbstractChemAtom.chemTorsions>_19 _26 _20</CHEM.AbstractChemAtom.chemTorsions>
</CHEM.ChemAtom>
<CHEM.ChemAtom _ID="_27" elementSymbol="Fe" name="FE">
<CHEM.ChemAtom.boundLinkEnds>_28 _29</CHEM.ChemAtom.boundLinkEnds>
<CHEM.AbstractChemAtom.chemBonds>_30 _31 _32 _33</CHEM.AbstractChemAtom.chemBonds>
<CHEM.AbstractChemAtom.chemCompVars>_11</CHEM.AbstractChemAtom.chemCompVars>
<CHEM.AbstractChemAtom.chemTorsions>_20 _26</CHEM.AbstractChemAtom.chemTorsions>
<CHEM.ChemAtom.remoteLinkEnds>_34 _35</CHEM.ChemAtom.remoteLinkEnds>
</CHEM.ChemAtom>
<CHEM.LinkAtom _ID="_36" name="FE_1_1">
<CHEM.LinkAtom.boundLinkEnd>_28</CHEM.LinkAtom.boundLinkEnd>
<CHEM.AbstractChemAtom.chemBonds>_30</CHEM.AbstractChemAtom.chemBonds>
<CHEM.AbstractChemAtom.chemCompVars>_11</CHEM.AbstractChemAtom.chemCompVars>
</CHEM.LinkAtom>
<CHEM.LinkAtom _ID="_37" name="FE_2_1">
<CHEM.LinkAtom.boundLinkEnd>_29</CHEM.LinkAtom.boundLinkEnd>
<CHEM.AbstractChemAtom.chemBonds>_31</CHEM.AbstractChemAtom.chemBonds>
<CHEM.AbstractChemAtom.chemCompVars>_11</CHEM.AbstractChemAtom.chemCompVars>
</CHEM.LinkAtom>
<CHEM.ChemAtom _ID="_38" elementSymbol="H" name="H">
<CHEM.AbstractChemAtom.chemBonds>_39</CHEM.AbstractChemAtom.chemBonds>
<CHEM.AbstractChemAtom.chemCompVars>_11</CHEM.AbstractChemAtom.chemCompVars>
</CHEM.ChemAtom>
<CHEM.ChemAtom _ID="_40" elementSymbol="H" name="HA">
<CHEM.AbstractChemAtom.chemBonds>_15</CHEM.AbstractChemAtom.chemBonds>
<CHEM.AbstractChemAtom.chemCompVars>_11</CHEM.AbstractChemAtom.chemCompVars>
</CHEM.ChemAtom>
<CHEM.ChemAtom _ID="_3" elementSymbol="H" name="HB2">
<CHEM.AbstractChemAtom.chemBonds>_25</CHEM.AbstractChemAtom.chemBonds>
<CHEM.AbstractChemAtom.chemCompVars>_11</CHEM.AbstractChemAtom.chemCompVars>
</CHEM.ChemAtom>
<CHEM.ChemAtom _ID="_4" elementSymbol="H" name="HB3">
<CHEM.AbstractChemAtom.chemBonds>_24</CHEM.AbstractChemAtom.chemBonds>
<CHEM.AbstractChemAtom.chemCompVars>_11</CHEM.AbstractChemAtom.chemCompVars>
</CHEM.ChemAtom>
<CHEM.ChemAtom _ID="_41" elementSymbol="N" name="N">
<CHEM.ChemAtom.boundLinkEnds>_21</CHEM.ChemAtom.boundLinkEnds>
```

```
<CHEM.AbstractChemAtom.chemBonds>_42 _39 _17</CHEM.AbstractChemAtom.chemBonds>
<CHEM.AbstractChemAtom.chemCompVars>_11</CHEM.AbstractChemAtom.chemCompVars>
<CHEM.AbstractChemAtom.chemTorsions>_18 _19 _12 _13</CHEM.AbstractChemAtom.chemTorsions>
</CHEM.ChemAtom>
<CHEM.ChemAtom _ID="_43" elementSymbol="O" name="O">
<CHEM.AbstractChemAtom.chemBonds>_8</CHEM.AbstractChemAtom.chemBonds>
<CHEM.AbstractChemAtom.chemCompVars>_11</CHEM.AbstractChemAtom.chemCompVars>
</CHEM.ChemAtom>
<CHEM.ChemAtom _ID="_44" elementSymbol="O" name="O'">
<CHEM.AbstractChemAtom.chemBonds>_7</CHEM.AbstractChemAtom.chemBonds>
<CHEM.AbstractChemAtom.chemCompVars>_11</CHEM.AbstractChemAtom.chemCompVars>
</CHEM.ChemAtom>
<CHEM.ChemAtom _ID="_45" elementSymbol="S" name="SE">
<CHEM.ChemAtom.boundLinkEnds>_34 _35</CHEM.ChemAtom.boundLinkEnds>
<CHEM.AbstractChemAtom.chemBonds>_46 _47 _33</CHEM.AbstractChemAtom.chemBonds>
<CHEM.AbstractChemAtom.chemCompVars>_11</CHEM.AbstractChemAtom.chemCompVars>
<CHEM.AbstractChemAtom.chemTorsions>_26</CHEM.AbstractChemAtom.chemTorsions>
</CHEM.ChemAtom>
<CHEM.LinkAtom _ID="_48" name="SE_1_1">
<CHEM.LinkAtom.boundLinkEnd>_34</CHEM.LinkAtom.boundLinkEnd>
<CHEM.AbstractChemAtom.chemBonds>_46</CHEM.AbstractChemAtom.chemBonds>
<CHEM.AbstractChemAtom.chemCompVars>_11</CHEM.AbstractChemAtom.chemCompVars>
</CHEM.LinkAtom>
<CHEM.LinkAtom _ID="_49" name="SE_2_1">
<CHEM.LinkAtom.boundLinkEnd>_35</CHEM.LinkAtom.boundLinkEnd>
<CHEM.AbstractChemAtom.chemBonds>_47</CHEM.AbstractChemAtom.chemBonds>
<CHEM.AbstractChemAtom.chemCompVars>_11</CHEM.AbstractChemAtom.chemCompVars>
</CHEM.LinkAtom>
<CHEM.ChemAtom _ID="_50" elementSymbol="S" name="SG">
<CHEM.AbstractChemAtom.chemBonds>_23 _32</CHEM.AbstractChemAtom.chemBonds>
<CHEM.AbstractChemAtom.chemCompVars>_11</CHEM.AbstractChemAtom.chemCompVars>
<CHEM.AbstractChemAtom.chemTorsions>_19 _26 _20</CHEM.AbstractChemAtom.chemTorsions>
<CHEM.ChemAtom.remoteLinkEnds>_28 _29</CHEM.ChemAtom.remoteLinkEnds>
</CHEM.ChemAtom>
<CHEM.LinkAtom _ID="_51" name="next_1">
<CHEM.LinkAtom.boundLinkEnd>_6</CHEM.LinkAtom.boundLinkEnd>
<CHEM.AbstractChemAtom.chemBonds>_10</CHEM.AbstractChemAtom.chemBonds>
<CHEM.AbstractChemAtom.chemCompVars>_11</CHEM.AbstractChemAtom.chemCompVars>
<CHEM.AbstractChemAtom.chemTorsions>_12</CHEM.AbstractChemAtom.chemTorsions>
</CHEM.LinkAtom>
<CHEM.LinkAtom _ID="_52" name="prev_1">
<CHEM.LinkAtom.boundLinkEnd>_21</CHEM.LinkAtom.boundLinkEnd>
<CHEM.AbstractChemAtom.chemBonds>_53 _42</CHEM.AbstractChemAtom.chemBonds>
<CHEM.AbstractChemAtom.chemCompVars>_11</CHEM.AbstractChemAtom.chemCompVars>
<CHEM.AbstractChemAtom.chemTorsions>_18 _13</CHEM.AbstractChemAtom.chemTorsions>
</CHEM.LinkAtom>
<CHEM.LinkAtom _ID="_54" name="prev_2">
<CHEM.AbstractChemAtom.chemBonds>_53</CHEM.AbstractChemAtom.chemBonds>
<CHEM.AbstractChemAtom.chemCompVars>_11</CHEM.AbstractChemAtom.chemCompVars>
<CHEM.AbstractChemAtom.chemTorsions>_18</CHEM.AbstractChemAtom.chemTorsions>
<CHEM.LinkAtom.remoteLinkEnd>_21</CHEM.LinkAtom.remoteLinkEnd>
</CHEM.LinkAtom>
</CHEM.ChemComp.chemAtoms>
<CHEM.ChemComp.chemBonds>
<CHEM.ChemBond _ID="_25">
<CHEM.ChemBond.chemAtoms>_22 _3</CHEM.ChemBond.chemAtoms>
</CHEM.ChemBond>
<CHEM.ChemBond _ID="_24">
<CHEM.ChemBond.chemAtoms>_22 _4</CHEM.ChemBond.chemAtoms>
</CHEM.ChemBond>
<CHEM.ChemBond _ID="_32">
<CHEM.ChemBond.chemAtoms>_50 _27</CHEM.ChemBond.chemAtoms>
</CHEM.ChemBond>
<CHEM.ChemBond _ID="_15">
<CHEM.ChemBond.chemAtoms>_14 _40</CHEM.ChemBond.chemAtoms>
</CHEM.ChemBond>
<CHEM.ChemBond _ID="_10" bondType="singleplanar" stereochem="unknown">
<CHEM.ChemBond.chemAtoms>_51 _5</CHEM.ChemBond.chemAtoms>
```

```
</CHEM.ChemBond>
<CHEM.ChemBond _ID="_53">
<CHEM.ChemBond.chemAtoms>_52 _54</CHEM.ChemBond.chemAtoms>
</CHEM.ChemBond>
<CHEM.ChemBond _ID="_39">
<CHEM.ChemBond.chemAtoms>_38 _41</CHEM.ChemBond.chemAtoms>
</CHEM.ChemBond>
<CHEM.ChemBond _ID="_46">
<CHEM.ChemBond.chemAtoms>_48 _45</CHEM.ChemBond.chemAtoms>
</CHEM.ChemBond>
<CHEM.ChemBond _ID="_9">
<CHEM.ChemBond.chemAtoms>_14 _5</CHEM.ChemBond.chemAtoms>
</CHEM.ChemBond>
<CHEM.ChemBond _ID="_42" bondType="singleplanar" stereochem="unknown">
<CHEM.ChemBond.chemAtoms>_41 _52</CHEM.ChemBond.chemAtoms>
</CHEM.ChemBond>
<CHEM.ChemBond _ID="_7" bondType="double">
<CHEM.ChemBond.chemAtoms>_5 _44</CHEM.ChemBond.chemAtoms>
</CHEM.ChemBond>
<CHEM.ChemBond _ID="_30">
<CHEM.ChemBond.chemAtoms>_36 _27</CHEM.ChemBond.chemAtoms>
</CHEM.ChemBond>
<CHEM.ChemBond _ID="_8" bondType="double">
<CHEM.ChemBond.chemAtoms>_43 _5</CHEM.ChemBond.chemAtoms>
</CHEM.ChemBond>
<CHEM.ChemBond _ID="_17">
<CHEM.ChemBond.chemAtoms>_41 _14</CHEM.ChemBond.chemAtoms>
</CHEM.ChemBond>
<CHEM.ChemBond _ID="_23">
<CHEM.ChemBond.chemAtoms>_22 _50</CHEM.ChemBond.chemAtoms>
</CHEM.ChemBond>
<CHEM.ChemBond _ID="_16">
<CHEM.ChemBond.chemAtoms>_22 _14</CHEM.ChemBond.chemAtoms>
</CHEM.ChemBond>
<CHEM.ChemBond _ID="_31">
<CHEM.ChemBond.chemAtoms>_37 _27</CHEM.ChemBond.chemAtoms>
</CHEM.ChemBond>
<CHEM.ChemBond _ID="_47">
<CHEM.ChemBond.chemAtoms>_49 _45</CHEM.ChemBond.chemAtoms>
</CHEM.ChemBond>
<CHEM.ChemBond _ID="_33">
<CHEM.ChemBond.chemAtoms>_45 _27</CHEM.ChemBond.chemAtoms>
</CHEM.ChemBond>
</CHEM.ChemComp.chemBonds>
<CHEM.ChemComp.chemCompVars>
<CHEM.ChemCompVar _ID="_11" formalCharge="0" isAromatic="false" isParamagnetic="false"
linking="middle">
<CHEM.ChemCompVar.descriptor>
<IMPL.Line>link:FE_1,FE_2,SE_1,SE_2</IMPL.Line>
</CHEM.ChemCompVar.descriptor>
<CHEM.ChemCompVar.stereoSmiles>
<IMPL.String>N[C@@H](CS)C=O</IMPL.String>
</CHEM.ChemCompVar.stereoSmiles>
<CHEM.ChemCompVar.chemAtoms>
_43 _48 _41 _50 _22 _5 _52 _38 _14 _40 _3 _54 _4 _51 _27 _44 _45 _37 _36 _49
</CHEM.ChemCompVar.chemAtoms>
<CHEM.ChemCompVar.specificSysNames>_55 _56 _57</CHEM.ChemCompVar.specificSysNames>
</CHEM.ChemCompVar>
</CHEM.ChemComp.chemCompVars>
<CHEM.ChemComp.chemTorsions>
<CHEM.ChemTorsion _ID="_19" name="CHI1">
<CHEM.ChemTorsion.chemAtoms>_41 _14 _22 _50</CHEM.ChemTorsion.chemAtoms>
<CHEM.ChemTorsion.sysNames>_58 _59</CHEM.ChemTorsion.sysNames>
</CHEM.ChemTorsion>
<CHEM.ChemTorsion _ID="_12" name="PSI">
<CHEM.ChemTorsion.chemAtoms>_41 _14 _5 _51</CHEM.ChemTorsion.chemAtoms>
<CHEM.ChemTorsion.sysNames>_60 _61</CHEM.ChemTorsion.sysNames>
</CHEM.ChemTorsion>
```

```
<CHEM.ChemTorsion _ID="_26" name="CHI3">
<CHEM.ChemTorsion.chemAtoms>_22 _50 _27 _45</CHEM.ChemTorsion.chemAtoms>
<CHEM.ChemTorsion.sysNames>_62</CHEM.ChemTorsion.sysNames>
</CHEM.ChemTorsion>
<CHEM.ChemTorsion _ID="_20" name="CHI2">
<CHEM.ChemTorsion.chemAtoms>_14 _22 _50 _27</CHEM.ChemTorsion.chemAtoms>
<CHEM.ChemTorsion.sysNames>_63 _64</CHEM.ChemTorsion.sysNames>
</CHEM.ChemTorsion>
<CHEM.ChemTorsion _ID="_18" name="OMEGA">
<CHEM.ChemTorsion.chemAtoms>_54 _52 _41 _14</CHEM.ChemTorsion.chemAtoms>
<CHEM.ChemTorsion.sysNames>_65 _66</CHEM.ChemTorsion.sysNames>
</CHEM.ChemTorsion>
<CHEM.ChemTorsion _ID="_13" name="PHI">
<CHEM.ChemTorsion.chemAtoms>_52 _41 _14 _5</CHEM.ChemTorsion.chemAtoms>
<CHEM.ChemTorsion.sysNames>_67 _68</CHEM.ChemTorsion.sysNames>
</CHEM.ChemTorsion>
</CHEM.ChemComp.chemTorsions>
<CHEM.ChemComp.linkEnds>
<CHEM.LinkEnd _ID="_28" linkCode="FE_1">
<CHEM.LinkEnd.boundLinkAtom>_36</CHEM.LinkEnd.boundLinkAtom>
</CHEM.LinkEnd>
<CHEM.LinkEnd _ID="_29" linkCode="FE_2">
<CHEM.LinkEnd.boundLinkAtom>_37</CHEM.LinkEnd.boundLinkAtom>
</CHEM.LinkEnd>
<CHEM.LinkEnd _ID="_34" linkCode="SE_1">
<CHEM.LinkEnd.boundLinkAtom>_48</CHEM.LinkEnd.boundLinkAtom>
</CHEM.LinkEnd>
<CHEM.LinkEnd _ID="_35" linkCode="SE_2">
<CHEM.LinkEnd.boundLinkAtom>_49</CHEM.LinkEnd.boundLinkAtom>
</CHEM.LinkEnd>
<CHEM.LinkEnd _ID="_6" linkCode="next">
<CHEM.LinkEnd.boundLinkAtom>_51</CHEM.LinkEnd.boundLinkAtom>
</CHEM.LinkEnd>
<CHEM.LinkEnd _ID="_21" linkCode="prev">
<CHEM.LinkEnd.boundLinkAtom>_52</CHEM.LinkEnd.boundLinkAtom>
<CHEM.LinkEnd.remoteLinkAtom>_54</CHEM.LinkEnd.remoteLinkAtom>
</CHEM.LinkEnd>
</CHEM.ChemComp.linkEnds>
<CHEM.ChemComp.namingSystems>
<CHEM.NamingSystem _ID="_69" name="AQUA">
<CHEM.NamingSystem.atomSetVariantSystems>_70 _71
_72</CHEM.NamingSystem.atomSetVariantSystems>
<CHEM.NamingSystem.atomSysNames>
<CHEM.AtomSysName _ID="_73" atomName="HB*">
<CHEM.AtomSysName.sysName>
<IMPL.Line>QB</IMPL.Line>
</CHEM.AtomSysName.sysName>
</CHEM.AtomSysName>
</CHEM.NamingSystem.atomSysNames>
</CHEM.NamingSystem>
<CHEM.NamingSystem _ID="_71" name="BMRB">
<CHEM.NamingSystem.atomSysNames>
<CHEM.AtomSysName _ID="_74" atomName="H*">
<CHEM.AtomSysName.sysName>
<IMPL.Line>H</IMPL.Line>
</CHEM.AtomSysName.sysName>
</CHEM.AtomSysName>
<CHEM.AtomSysName _ID="_75" atomName="H*" atomSubType="2">
<CHEM.AtomSysName.sysName>
<IMPL.Line>H</IMPL.Line>
</CHEM.AtomSysName.sysName>
</CHEM.AtomSysName>
<CHEM.AtomSysName _ID="_76" atomName="O'">
<CHEM.AtomSysName.sysName>
<IMPL.Line>O1</IMPL.Line>
</CHEM.AtomSysName.sysName>
</CHEM.AtomSysName>
<CHEM.AtomSysName _ID="_77" atomName="O''">
```

```
<CHEM.AtomSysName.sysName>
<IMPL.Line>O2</IMPL.Line>
</CHEM.AtomSysName.sysName>
</CHEM.AtomSysName>
</CHEM.NamingSystem.atomSysNames>
</CHEM.NamingSystem>
<CHEM.NamingSystem _ID="_78" name="CIF">
<CHEM.NamingSystem.chemCompSysNames>
<CHEM.ChemCompSysName _ID="_79" sysName="CFS"></CHEM.ChemCompSysName>
</CHEM.NamingSystem.chemCompSysNames>
</CHEM.NamingSystem>
<CHEM.NamingSystem _ID="_80" name="CING">
<CHEM.NamingSystem.chemCompSysNames>
<CHEM.ChemCompSysName _ID="_55" sysName="CFS">
<CHEM.ChemCompSysName.specificChemCompVars>_11</CHEM.ChemCompSysName.specificChemCompVars>
</CHEM.ChemCompSysName>
</CHEM.NamingSystem.chemCompSysNames>
</CHEM.NamingSystem>
<CHEM.NamingSystem _ID="_81" name="CYANA2.1">
<CHEM.NamingSystem.atomSetVariantSystems>_82</CHEM.NamingSystem.atomSetVariantSystems>
<CHEM.NamingSystem.atomVariantSystems>_82</CHEM.NamingSystem.atomVariantSystems>
<IMPL.DataObject.applicationData>
<IMPL.AppDataInt value="12">
<IMPL.ApplicationData.application>
<IMPL.Line>xeasy</IMPL.Line>
</IMPL.ApplicationData.application>
<IMPL.ApplicationData.keyword>
<IMPL.Line>atomSerial_C.1</IMPL.Line>
</IMPL.ApplicationData.keyword>
</IMPL.AppDataInt>
<IMPL.AppDataInt value="3">
<IMPL.ApplicationData.application>
<IMPL.Line>xeasy</IMPL.Line>
</IMPL.ApplicationData.application>
<IMPL.ApplicationData.keyword>
<IMPL.Line>atomSerial_CA.1</IMPL.Line>
</IMPL.ApplicationData.keyword>
</IMPL.AppDataInt>
<IMPL.AppDataInt value="5">
<IMPL.ApplicationData.application>
<IMPL.Line>xeasy</IMPL.Line>
</IMPL.ApplicationData.application>
<IMPL.ApplicationData.keyword>
<IMPL.Line>atomSerial_CB.1</IMPL.Line>
</IMPL.ApplicationData.keyword>
</IMPL.AppDataInt>
<IMPL.AppDataInt value="2">
<IMPL.ApplicationData.application>
<IMPL.Line>xeasy</IMPL.Line>
</IMPL.ApplicationData.application>
<IMPL.ApplicationData.keyword>
<IMPL.Line>atomSerial_H.1</IMPL.Line>
</IMPL.ApplicationData.keyword>
</IMPL.AppDataInt>
<IMPL.AppDataInt value="4">
<IMPL.ApplicationData.application>
<IMPL.Line>xeasy</IMPL.Line>
</IMPL.ApplicationData.application>
<IMPL.ApplicationData.keyword>
<IMPL.Line>atomSerial_HA.1</IMPL.Line>
</IMPL.ApplicationData.keyword>
</IMPL.AppDataInt>
<IMPL.AppDataInt value="6">
<IMPL.ApplicationData.application>
<IMPL.Line>xeasy</IMPL.Line>
</IMPL.ApplicationData.application>
<IMPL.ApplicationData.keyword>
<IMPL.Line>atomSerial_HB2.1</IMPL.Line>
```

```
</IMPL.ApplicationData.keyword>
</IMPL.AppDataInt>
<IMPL.AppDataInt value="7">
<IMPL.ApplicationData.application>
<IMPL.Line>xeasy</IMPL.Line>
</IMPL.ApplicationData.application>
<IMPL.ApplicationData.keyword>
<IMPL.Line>atomSerial_HB3.1</IMPL.Line>
</IMPL.ApplicationData.keyword>
</IMPL.AppDataInt>
<IMPL.AppDataInt value="10">
<IMPL.ApplicationData.application>
<IMPL.Line>xeasy</IMPL.Line>
</IMPL.ApplicationData.application>
<IMPL.ApplicationData.keyword>
<IMPL.Line>atomSerial_FE.1</IMPL.Line>
</IMPL.ApplicationData.keyword>
</IMPL.AppDataInt>
<IMPL.AppDataInt value="11">
<IMPL.ApplicationData.application>
<IMPL.Line>xeasy</IMPL.Line>
</IMPL.ApplicationData.application>
<IMPL.ApplicationData.keyword>
<IMPL.Line>atomSerial_SE.1</IMPL.Line>
</IMPL.ApplicationData.keyword>
</IMPL.AppDataInt>
<IMPL.AppDataInt value="1">
<IMPL.ApplicationData.application>
<IMPL.Line>xeasy</IMPL.Line>
</IMPL.ApplicationData.application>
<IMPL.ApplicationData.keyword>
<IMPL.Line>atomSerial_N.1</IMPL.Line>
</IMPL.ApplicationData.keyword>
</IMPL.AppDataInt>
<IMPL.AppDataInt value="9">
<IMPL.ApplicationData.application>
<IMPL.Line>xeasy</IMPL.Line>
</IMPL.ApplicationData.application>
<IMPL.ApplicationData.keyword>
<IMPL.Line>atomSerial_SG.1</IMPL.Line>
</IMPL.ApplicationData.keyword>
</IMPL.AppDataInt>
<IMPL.AppDataInt value="8">
<IMPL.ApplicationData.application>
<IMPL.Line>xeasy</IMPL.Line>
</IMPL.ApplicationData.application>
<IMPL.ApplicationData.keyword>
<IMPL.Line>atomSerial_HB*.1</IMPL.Line>
</IMPL.ApplicationData.keyword>
</IMPL.AppDataInt>
</IMPL.DataObject.applicationData>
<CHEM.NamingSystem.atomSysNames>
<CHEM.AtomSysName _ID="_83" atomName="H*">
<CHEM.AtomSysName.sysName>
<IMPL.Line>H</IMPL.Line>
</CHEM.AtomSysName.sysName>
</CHEM.AtomSysName>
<CHEM.AtomSysName _ID="_84" atomName="H*" atomSubType="2">
<CHEM.AtomSysName.sysName>
<IMPL.Line>H</IMPL.Line>
</CHEM.AtomSysName.sysName>
</CHEM.AtomSysName>
<CHEM.AtomSysName _ID="_85" atomName="HB*">
<CHEM.AtomSysName.sysName>
<IMPL.Line>QB</IMPL.Line>
</CHEM.AtomSysName.sysName>
</CHEM.AtomSysName>
</CHEM.NamingSystem.atomSysNames>
```

```
<CHEM.NamingSystem.chemCompSysNames>
<CHEM.ChemCompSysName _ID="_56" sysName="CFS">
<CHEM.ChemCompSysName.specificChemCompVars>_11</CHEM.ChemCompSysName.specificChemCompVars>
</CHEM.ChemCompSysName>
</CHEM.NamingSystem.chemCompSysNames>
<CHEM.NamingSystem.chemTorsionSysNames>
<CHEM.ChemTorsionSysName _ID="_62" sysName="CHI3"></CHEM.ChemTorsionSysName>
<CHEM.ChemTorsionSysName _ID="_67" sysName="PHI"></CHEM.ChemTorsionSysName>
<CHEM.ChemTorsionSysName _ID="_65" sysName="OMEGA"></CHEM.ChemTorsionSysName>
<CHEM.ChemTorsionSysName _ID="_60" sysName="PSI"></CHEM.ChemTorsionSysName>
<CHEM.ChemTorsionSysName _ID="_58" sysName="CHI1"></CHEM.ChemTorsionSysName>
<CHEM.ChemTorsionSysName _ID="_63" sysName="CHI2"></CHEM.ChemTorsionSysName>
</CHEM.NamingSystem.chemTorsionSysNames>
</CHEM.NamingSystem>
<CHEM.NamingSystem _ID="_82" name="DIANA">
<CHEM.NamingSystem.atomSetVariantSystems>_86</CHEM.NamingSystem.atomSetVariantSystems>
<CHEM.NamingSystem.atomVariantSystems>_86</CHEM.NamingSystem.atomVariantSystems>
<IMPL.DataObject.applicationData>
<IMPL.AppDataInt value="11">
<IMPL.ApplicationData.application>
<IMPL.Line>xeasy</IMPL.Line>
</IMPL.ApplicationData.application>
<IMPL.ApplicationData.keyword>
<IMPL.Line>atomSerial_C.1</IMPL.Line>
</IMPL.ApplicationData.keyword>
</IMPL.AppDataInt>
<IMPL.AppDataInt value="3">
<IMPL.ApplicationData.application>
<IMPL.Line>xeasy</IMPL.Line>
</IMPL.ApplicationData.application>
<IMPL.ApplicationData.keyword>
<IMPL.Line>atomSerial_CA.1</IMPL.Line>
</IMPL.ApplicationData.keyword>
</IMPL.AppDataInt>
<IMPL.AppDataInt value="5">
<IMPL.ApplicationData.application>
<IMPL.Line>xeasy</IMPL.Line>
</IMPL.ApplicationData.application>
<IMPL.ApplicationData.keyword>
<IMPL.Line>atomSerial_CB.1</IMPL.Line>
</IMPL.ApplicationData.keyword>
</IMPL.AppDataInt>
<IMPL.AppDataInt value="2">
<IMPL.ApplicationData.application>
<IMPL.Line>xeasy</IMPL.Line>
</IMPL.ApplicationData.application>
<IMPL.ApplicationData.keyword>
<IMPL.Line>atomSerial_H.1</IMPL.Line>
</IMPL.ApplicationData.keyword>
</IMPL.AppDataInt>
<IMPL.AppDataInt value="4">
<IMPL.ApplicationData.application>
<IMPL.Line>xeasy</IMPL.Line>
</IMPL.ApplicationData.application>
<IMPL.ApplicationData.keyword>
<IMPL.Line>atomSerial_HA.1</IMPL.Line>
</IMPL.ApplicationData.keyword>
</IMPL.AppDataInt>
<IMPL.AppDataInt value="6">
<IMPL.ApplicationData.application>
<IMPL.Line>xeasy</IMPL.Line>
</IMPL.ApplicationData.application>
<IMPL.ApplicationData.keyword>
<IMPL.Line>atomSerial_HB2.1</IMPL.Line>
</IMPL.ApplicationData.keyword>
</IMPL.AppDataInt>
<IMPL.AppDataInt value="7">
<IMPL.ApplicationData.application>
```

```
<IMPL.Line>xeasy</IMPL.Line>
</IMPL.ApplicationData.application>
<IMPL.ApplicationData.keyword>
<IMPL.Line>atomSerial_HB3.1</IMPL.Line>
</IMPL.ApplicationData.keyword>
</IMPL.AppDataInt>
<IMPL.AppDataInt value="10">
<IMPL.ApplicationData.application>
<IMPL.Line>xeasy</IMPL.Line>
</IMPL.ApplicationData.application>
<IMPL.ApplicationData.keyword>
<IMPL.Line>atomSerial_HG.1</IMPL.Line>
</IMPL.ApplicationData.keyword>
</IMPL.AppDataInt>
<IMPL.AppDataInt value="1">
<IMPL.ApplicationData.application>
<IMPL.Line>xeasy</IMPL.Line>
</IMPL.ApplicationData.application>
<IMPL.ApplicationData.keyword>
<IMPL.Line>atomSerial_N.1</IMPL.Line>
</IMPL.ApplicationData.keyword>
</IMPL.AppDataInt>
<IMPL.AppDataInt value="9">
<IMPL.ApplicationData.application>
<IMPL.Line>xeasy</IMPL.Line>
</IMPL.ApplicationData.application>
<IMPL.ApplicationData.keyword>
<IMPL.Line>atomSerial_SG.1</IMPL.Line>
</IMPL.ApplicationData.keyword>
</IMPL.AppDataInt>
<IMPL.AppDataInt value="8">
<IMPL.ApplicationData.application>
<IMPL.Line>xeasy</IMPL.Line>
</IMPL.ApplicationData.application>
<IMPL.ApplicationData.keyword>
<IMPL.Line>atomSerial_HB*.1</IMPL.Line>
</IMPL.ApplicationData.keyword>
</IMPL.AppDataInt>
</IMPL.DataObject.applicationData>
<CHEM.NamingSystem.atomSysNames>
<CHEM.AtomSysName _ID="_87" atomName="H">
<CHEM.AtomSysName.sysName>
<IMPL.Line>HN</IMPL.Line>
</CHEM.AtomSysName.sysName>
</CHEM.AtomSysName>
<CHEM.AtomSysName _ID="_88" atomName="H*">
<CHEM.AtomSysName.sysName>
<IMPL.Line>HN</IMPL.Line>
</CHEM.AtomSysName.sysName>
</CHEM.AtomSysName>
<CHEM.AtomSysName _ID="_89" atomName="H*" atomSubType="2">
<CHEM.AtomSysName.sysName>
<IMPL.Line>HN</IMPL.Line>
</CHEM.AtomSysName.sysName>
</CHEM.AtomSysName>
</CHEM.NamingSystem.atomSysNames>
<CHEM.NamingSystem.chemCompSysNames>
<CHEM.ChemCompSysName _ID="_57" sysName="CFS">
<CHEM.ChemCompSysName.specificChemCompVars>_11</CHEM.ChemCompSysName.specificChemCompVars>
</CHEM.ChemCompSysName>
</CHEM.NamingSystem.chemCompSysNames>
<CHEM.NamingSystem.chemTorsionSysNames>
<CHEM.ChemTorsionSysName _ID="_68" sysName="PHI"></CHEM.ChemTorsionSysName>
<CHEM.ChemTorsionSysName _ID="_66" sysName="OMEGA"></CHEM.ChemTorsionSysName>
<CHEM.ChemTorsionSysName _ID="_61" sysName="PSI"></CHEM.ChemTorsionSysName>
<CHEM.ChemTorsionSysName _ID="_59" sysName="CHI1"></CHEM.ChemTorsionSysName>
<CHEM.ChemTorsionSysName _ID="_64" sysName="CHI2"></CHEM.ChemTorsionSysName>
</CHEM.NamingSystem.chemTorsionSysNames>
```

```
</CHEM.NamingSystem>
<CHEM.NamingSystem _ID="_90" name="DISGEO">
<CHEM.NamingSystem.atomSetVariantSystems>_91</CHEM.NamingSystem.atomSetVariantSystems>
<CHEM.NamingSystem.atomVariantSystems>_91</CHEM.NamingSystem.atomVariantSystems>
<CHEM.NamingSystem.atomSysNames>
<CHEM.AtomSysName _ID="_92" atomName="HB2">
<CHEM.AtomSysName.sysName>
<IMPL.Line>HB1</IMPL.Line>
</CHEM.AtomSysName.sysName>
</CHEM.AtomSysName>
<CHEM.AtomSysName _ID="_93" atomName="HB3">
<CHEM.AtomSysName.sysName>
<IMPL.Line>HB2</IMPL.Line>
</CHEM.AtomSysName.sysName>
</CHEM.AtomSysName>
</CHEM.NamingSystem.atomSysNames>
</CHEM.NamingSystem>
<CHEM.NamingSystem _ID="_91" name="DISMAN"></CHEM.NamingSystem>
<CHEM.NamingSystem _ID="_94" name="GROMOS">
<CHEM.NamingSystem.atomSysNames>
<CHEM.AtomSysName _ID="_95" atomName="C">
<CHEM.AtomSysName.sysName>
<IMPL.Line>C</IMPL.Line>
</CHEM.AtomSysName.sysName>
</CHEM.AtomSysName>
<CHEM.AtomSysName _ID="_96" atomName="CA">
<CHEM.AtomSysName.sysName>
<IMPL.Line>CA</IMPL.Line>
</CHEM.AtomSysName.sysName>
</CHEM.AtomSysName>
<CHEM.AtomSysName _ID="_97" atomName="CB">
<CHEM.AtomSysName.sysName>
<IMPL.Line>CB</IMPL.Line>
</CHEM.AtomSysName.sysName>
</CHEM.AtomSysName>
<CHEM.AtomSysName _ID="_98" atomName="H">
<CHEM.AtomSysName.sysName>
<IMPL.Line>H</IMPL.Line>
</CHEM.AtomSysName.sysName>
</CHEM.AtomSysName>
<CHEM.AtomSysName _ID="_99" atomName="HA">
<CHEM.AtomSysName.sysName>
<IMPL.Line>HCA1</IMPL.Line>
</CHEM.AtomSysName.sysName>
</CHEM.AtomSysName>
<CHEM.AtomSysName _ID="_100" atomName="HB*">
<CHEM.AtomSysName.sysName>
<IMPL.Line>Q2B</IMPL.Line>
</CHEM.AtomSysName.sysName>
</CHEM.AtomSysName>
<CHEM.AtomSysName _ID="_101" atomName="HB2">
<CHEM.AtomSysName.sysName>
<IMPL.Line>HCB1</IMPL.Line>
</CHEM.AtomSysName.sysName>
</CHEM.AtomSysName>
<CHEM.AtomSysName _ID="_102" atomName="HB3">
<CHEM.AtomSysName.sysName>
<IMPL.Line>HCB2</IMPL.Line>
</CHEM.AtomSysName.sysName>
</CHEM.AtomSysName>
<CHEM.AtomSysName _ID="_103" atomName="N">
<CHEM.AtomSysName.sysName>
<IMPL.Line>N</IMPL.Line>
</CHEM.AtomSysName.sysName>
</CHEM.AtomSysName>
<CHEM.AtomSysName _ID="_104" atomName="O">
<CHEM.AtomSysName.sysName>
<IMPL.Line>O</IMPL.Line>
```

```
</CHEM.AtomSysName.sysName>
</CHEM.AtomSysName>
<CHEM.AtomSysName _ID="_105" atomName="SG">
<CHEM.AtomSysName.sysName>
<IMPL.Line>SG</IMPL.Line>
</CHEM.AtomSysName.sysName>
</CHEM.AtomSysName>
</CHEM.NamingSystem.atomSysNames>
</CHEM.NamingSystem>
<CHEM.NamingSystem _ID="_106" name="IUPAC">
<CHEM.NamingSystem.atomSetVariantSystems>_107</CHEM.NamingSystem.atomSetVariantSystems>
<CHEM.NamingSystem.atomVariantSystems>_108 _71 _109 _90 _70 _81 _69
_110</CHEM.NamingSystem.atomVariantSystems>
<CHEM.NamingSystem.atomSysNames>
<CHEM.AtomSysName _ID="_111" atomName="C">
<CHEM.AtomSysName.sysName>
<IMPL.Line>C</IMPL.Line>
</CHEM.AtomSysName.sysName>
</CHEM.AtomSysName>
<CHEM.AtomSysName _ID="_112" atomName="CA">
<CHEM.AtomSysName.sysName>
<IMPL.Line>CA</IMPL.Line>
</CHEM.AtomSysName.sysName>
</CHEM.AtomSysName>
<CHEM.AtomSysName _ID="_113" atomName="CB">
<CHEM.AtomSysName.sysName>
<IMPL.Line>CB</IMPL.Line>
</CHEM.AtomSysName.sysName>
</CHEM.AtomSysName>
<CHEM.AtomSysName _ID="_114" atomName="FE">
<CHEM.AtomSysName.sysName>
<IMPL.Line>FE</IMPL.Line>
</CHEM.AtomSysName.sysName>
</CHEM.AtomSysName>
<CHEM.AtomSysName _ID="_115" atomName="H">
<CHEM.AtomSysName.sysName>
<IMPL.Line>H</IMPL.Line>
</CHEM.AtomSysName.sysName>
</CHEM.AtomSysName>
<CHEM.AtomSysName _ID="_116" atomName="HA">
<CHEM.AtomSysName.sysName>
<IMPL.Line>HA</IMPL.Line>
</CHEM.AtomSysName.sysName>
</CHEM.AtomSysName>
<CHEM.AtomSysName _ID="_117" atomName="HB2">
<CHEM.AtomSysName.sysName>
<IMPL.Line>HB2</IMPL.Line>
</CHEM.AtomSysName.sysName>
</CHEM.AtomSysName>
<CHEM.AtomSysName _ID="_118" atomName="HB3">
<CHEM.AtomSysName.sysName>
<IMPL.Line>HB3</IMPL.Line>
</CHEM.AtomSysName.sysName>
</CHEM.AtomSysName>
<CHEM.AtomSysName _ID="_119" atomName="N">
<CHEM.AtomSysName.sysName>
<IMPL.Line>N</IMPL.Line>
</CHEM.AtomSysName.sysName>
</CHEM.AtomSysName>
<CHEM.AtomSysName _ID="_120" atomName="O">
<CHEM.AtomSysName.sysName>
<IMPL.Line>O</IMPL.Line>
</CHEM.AtomSysName.sysName>
</CHEM.AtomSysName>
<CHEM.AtomSysName _ID="_121" atomName="O'">
<CHEM.AtomSysName.sysName>
<IMPL.Line>O'</IMPL.Line>
</CHEM.AtomSysName.sysName>
```

```
</CHEM.AtomSysName>
<CHEM.AtomSysName _ID="_122" atomName="SE">
<CHEM.AtomSysName.sysName>
<IMPL.Line>SE</IMPL.Line>
</CHEM.AtomSysName.sysName>
</CHEM.AtomSysName>
<CHEM.AtomSysName _ID="_123" atomName="SG">
<CHEM.AtomSysName.sysName>
<IMPL.Line>SG</IMPL.Line>
</CHEM.AtomSysName.sysName>
</CHEM.AtomSysName>
</CHEM.NamingSystem.atomSysNames>
</CHEM.NamingSystem>
<CHEM.NamingSystem _ID="_86" name="MOLMOL">
<CHEM.NamingSystem.atomSetVariantSystems>_90</CHEM.NamingSystem.atomSetVariantSystems>
<CHEM.NamingSystem.atomSysNames>
<CHEM.AtomSysName _ID="_124" atomName="H">
<CHEM.AtomSysName.altSysNames>
<IMPL.Line>H</IMPL.Line>
</CHEM.AtomSysName.altSysNames>
<CHEM.AtomSysName.sysName>
<IMPL.Line>HN</IMPL.Line>
</CHEM.AtomSysName.sysName>
</CHEM.AtomSysName>
<CHEM.AtomSysName _ID="_125" atomName="HB2">
<CHEM.AtomSysName.altSysNames>
<IMPL.Line>1HB</IMPL.Line>
</CHEM.AtomSysName.altSysNames>
<CHEM.AtomSysName.sysName>
<IMPL.Line>HB1</IMPL.Line>
</CHEM.AtomSysName.sysName>
</CHEM.AtomSysName>
<CHEM.AtomSysName _ID="_126" atomName="HB3">
<CHEM.AtomSysName.altSysNames>
<IMPL.Line>2HB</IMPL.Line>
</CHEM.AtomSysName.altSysNames>
<CHEM.AtomSysName.sysName>
<IMPL.Line>HB2</IMPL.Line>
</CHEM.AtomSysName.sysName>
</CHEM.AtomSysName>
</CHEM.NamingSystem.atomSysNames>
</CHEM.NamingSystem>
<CHEM.NamingSystem _ID="_110" name="MSD">
<CHEM.NamingSystem.chemCompSysNames>
<CHEM.ChemCompSysName _ID="_127" sysName="CYS_LFOH"></CHEM.ChemCompSysName>
</CHEM.NamingSystem.chemCompSysNames>
</CHEM.NamingSystem>
<CHEM.NamingSystem _ID="_107" name="MSI">
<CHEM.NamingSystem.atomVariantSystems>_72</CHEM.NamingSystem.atomVariantSystems>
<CHEM.NamingSystem.atomSysNames>
<CHEM.AtomSysName _ID="_128" atomName="H">
<CHEM.AtomSysName.sysName>
<IMPL.Line>HN</IMPL.Line>
</CHEM.AtomSysName.sysName>
</CHEM.AtomSysName>
<CHEM.AtomSysName _ID="_129" atomName="H1">
<CHEM.AtomSysName.sysName>
<IMPL.Line>HN1</IMPL.Line>
</CHEM.AtomSysName.sysName>
</CHEM.AtomSysName>
<CHEM.AtomSysName _ID="_130" atomName="H1" atomSubType="2">
<CHEM.AtomSysName.sysName>
<IMPL.Line>HN1</IMPL.Line>
</CHEM.AtomSysName.sysName>
</CHEM.AtomSysName>
<CHEM.AtomSysName _ID="_131" atomName="H2">
<CHEM.AtomSysName.sysName>
<IMPL.Line>HN2</IMPL.Line>
```

```
</CHEM.AtomSysName.sysName>
</CHEM.AtomSysName>
<CHEM.AtomSysName _ID="_132" atomName="H2" atomSubType="2">
<CHEM.AtomSysName.sysName>
<IMPL.Line>HN2</IMPL.Line>
</CHEM.AtomSysName.sysName>
</CHEM.AtomSysName>
<CHEM.AtomSysName _ID="_133" atomName="H3">
<CHEM.AtomSysName.sysName>
<IMPL.Line>HN3</IMPL.Line>
</CHEM.AtomSysName.sysName>
</CHEM.AtomSysName>
<CHEM.AtomSysName _ID="_134" atomName="HB*">
<CHEM.AtomSysName.altSysNames>
<IMPL.Line>HBX</IMPL.Line>
</CHEM.AtomSysName.altSysNames>
<CHEM.AtomSysName.sysName>
<IMPL.Line>HB*</IMPL.Line>
</CHEM.AtomSysName.sysName>
</CHEM.AtomSysName>
<CHEM.AtomSysName _ID="_135" atomName="HB2">
<CHEM.AtomSysName.altSysNames>
<IMPL.Line>HBS</IMPL.Line>
</CHEM.AtomSysName.altSysNames>
<CHEM.AtomSysName.sysName>
<IMPL.Line>HB1</IMPL.Line>
</CHEM.AtomSysName.sysName>
</CHEM.AtomSysName>
<CHEM.AtomSysName _ID="_136" atomName="HB3">
<CHEM.AtomSysName.altSysNames>
<IMPL.Line>HBR</IMPL.Line>
</CHEM.AtomSysName.altSysNames>
<CHEM.AtomSysName.sysName>
<IMPL.Line>HB2</IMPL.Line>
</CHEM.AtomSysName.sysName>
</CHEM.AtomSysName>
</CHEM.NamingSystem.atomSysNames>
</CHEM.NamingSystem>
<CHEM.NamingSystem _ID="_137" name="PDB">
<CHEM.NamingSystem.atomSysNames>
<CHEM.AtomSysName _ID="_138" atomName="C">
<CHEM.AtomSysName.sysName>
<IMPL.Line>C</IMPL.Line>
</CHEM.AtomSysName.sysName>
</CHEM.AtomSysName>
<CHEM.AtomSysName _ID="_139" atomName="CA">
<CHEM.AtomSysName.sysName>
<IMPL.Line>CA</IMPL.Line>
</CHEM.AtomSysName.sysName>
</CHEM.AtomSysName>
<CHEM.AtomSysName _ID="_140" atomName="CB">
<CHEM.AtomSysName.sysName>
<IMPL.Line>CB</IMPL.Line>
</CHEM.AtomSysName.sysName>
</CHEM.AtomSysName>
<CHEM.AtomSysName _ID="_141" atomName="H">
<CHEM.AtomSysName.altSysNames>
<IMPL.Line>1HN</IMPL.Line>
<IMPL.Line>HN</IMPL.Line>
</CHEM.AtomSysName.altSysNames>
<CHEM.AtomSysName.sysName>
<IMPL.Line>H</IMPL.Line>
</CHEM.AtomSysName.sysName>
</CHEM.AtomSysName>
<CHEM.AtomSysName _ID="_142" atomName="H''">
<CHEM.AtomSysName.altSysNames>
<IMPL.Line>H''</IMPL.Line>
</CHEM.AtomSysName.altSysNames>
```

```
<CHEM.AtomSysName.sysName>
<IMPL.Line>HXT</IMPL.Line>
</CHEM.AtomSysName.sysName>
</CHEM.AtomSysName>
<CHEM.AtomSysName _ID="_143" atomName="H1">
<CHEM.AtomSysName.altSysNames>
<IMPL.Line>1HN</IMPL.Line>
<IMPL.Line>H</IMPL.Line>
<IMPL.Line>H1</IMPL.Line>
<IMPL.Line>HN1</IMPL.Line>
</CHEM.AtomSysName.altSysNames>
<CHEM.AtomSysName.sysName>
<IMPL.Line>1H</IMPL.Line>
</CHEM.AtomSysName.sysName>
</CHEM.AtomSysName>
<CHEM.AtomSysName _ID="_144" atomName="H1" atomSubType="2">
<CHEM.AtomSysName.altSysNames>
<IMPL.Line>1HN</IMPL.Line>
<IMPL.Line>H</IMPL.Line>
<IMPL.Line>H1</IMPL.Line>
<IMPL.Line>HN1</IMPL.Line>
</CHEM.AtomSysName.altSysNames>
<CHEM.AtomSysName.sysName>
<IMPL.Line>1H</IMPL.Line>
</CHEM.AtomSysName.sysName>
</CHEM.AtomSysName>
<CHEM.AtomSysName _ID="_145" atomName="H2">
<CHEM.AtomSysName.altSysNames>
<IMPL.Line>2HN</IMPL.Line>
<IMPL.Line>H2</IMPL.Line>
<IMPL.Line>HN2</IMPL.Line>
</CHEM.AtomSysName.altSysNames>
<CHEM.AtomSysName.sysName>
<IMPL.Line>2H</IMPL.Line>
</CHEM.AtomSysName.sysName>
</CHEM.AtomSysName>
<CHEM.AtomSysName _ID="_146" atomName="H2" atomSubType="2">
<CHEM.AtomSysName.altSysNames>
<IMPL.Line>2HN</IMPL.Line>
<IMPL.Line>H2</IMPL.Line>
<IMPL.Line>HN2</IMPL.Line>
</CHEM.AtomSysName.altSysNames>
<CHEM.AtomSysName.sysName>
<IMPL.Line>2H</IMPL.Line>
</CHEM.AtomSysName.sysName>
</CHEM.AtomSysName>
<CHEM.AtomSysName _ID="_147" atomName="H3">
<CHEM.AtomSysName.altSysNames>
<IMPL.Line>3HN</IMPL.Line>
<IMPL.Line>H3</IMPL.Line>
<IMPL.Line>HN3</IMPL.Line>
</CHEM.AtomSysName.altSysNames>
<CHEM.AtomSysName.sysName>
<IMPL.Line>3H</IMPL.Line>
</CHEM.AtomSysName.sysName>
</CHEM.AtomSysName>
<CHEM.AtomSysName _ID="_148" atomName="HA">
<CHEM.AtomSysName.sysName>
<IMPL.Line>HA</IMPL.Line>
</CHEM.AtomSysName.sysName>
</CHEM.AtomSysName>
<CHEM.AtomSysName _ID="_149" atomName="HB*">
<CHEM.AtomSysName.sysName>
<IMPL.Line>QB</IMPL.Line>
</CHEM.AtomSysName.sysName>
</CHEM.AtomSysName>
<CHEM.AtomSysName _ID="_150" atomName="HB2">
<CHEM.AtomSysName.altSysNames>
```

```
<IMPL.Line>HB1</IMPL.Line>
</CHEM.AtomSysName.altSysNames>
<CHEM.AtomSysName.sysName>
<IMPL.Line>1HB</IMPL.Line>
</CHEM.AtomSysName.sysName>
</CHEM.AtomSysName>
<CHEM.AtomSysName _ID="_151" atomName="HB3">
<CHEM.AtomSysName.altSysNames>
<IMPL.Line>HB2</IMPL.Line>
</CHEM.AtomSysName.altSysNames>
<CHEM.AtomSysName.sysName>
<IMPL.Line>2HB</IMPL.Line>
</CHEM.AtomSysName.sysName>
</CHEM.AtomSysName>
<CHEM.AtomSysName _ID="_152" atomName="HG">
<CHEM.AtomSysName.sysName>
<IMPL.Line>HG</IMPL.Line>
</CHEM.AtomSysName.sysName>
</CHEM.AtomSysName>
<CHEM.AtomSysName _ID="_153" atomName="N">
<CHEM.AtomSysName.sysName>
<IMPL.Line>N</IMPL.Line>
</CHEM.AtomSysName.sysName>
</CHEM.AtomSysName>
<CHEM.AtomSysName _ID="_154" atomName="O">
<CHEM.AtomSysName.sysName>
<IMPL.Line>O</IMPL.Line>
</CHEM.AtomSysName.sysName>
</CHEM.AtomSysName>
<CHEM.AtomSysName _ID="_155" atomName="O'">
<CHEM.AtomSysName.altSysNames>
<IMPL.Line>O'</IMPL.Line>
</CHEM.AtomSysName.altSysNames>
<CHEM.AtomSysName.sysName>
<IMPL.Line>O</IMPL.Line>
</CHEM.AtomSysName.sysName>
</CHEM.AtomSysName>
<CHEM.AtomSysName _ID="_156" atomName="O''">
<CHEM.AtomSysName.altSysNames>
<IMPL.Line>O''</IMPL.Line>
</CHEM.AtomSysName.altSysNames>
<CHEM.AtomSysName.sysName>
<IMPL.Line>OXT</IMPL.Line>
</CHEM.AtomSysName.sysName>
</CHEM.AtomSysName>
<CHEM.AtomSysName _ID="_157" atomName="SG">
<CHEM.AtomSysName.sysName>
<IMPL.Line>SG</IMPL.Line>
</CHEM.AtomSysName.sysName>
</CHEM.AtomSysName>
</CHEM.NamingSystem.atomSysNames>
</CHEM.NamingSystem>
<CHEM.NamingSystem _ID="_70" name="PDB_REMED">
<CHEM.NamingSystem.atomSysNames>
<CHEM.AtomSysName _ID="_158" atomName="H''">
<CHEM.AtomSysName.sysName>
<IMPL.Line>HXT</IMPL.Line>
</CHEM.AtomSysName.sysName>
</CHEM.AtomSysName>
<CHEM.AtomSysName _ID="_159" atomName="O'">
<CHEM.AtomSysName.sysName>
<IMPL.Line>O</IMPL.Line>
</CHEM.AtomSysName.sysName>
</CHEM.AtomSysName>
<CHEM.AtomSysName _ID="_160" atomName="O''">
<CHEM.AtomSysName.sysName>
<IMPL.Line>OXT</IMPL.Line>
</CHEM.AtomSysName.sysName>
```

```
</CHEM.AtomSysName>
</CHEM.NamingSystem.atomSysNames>
</CHEM.NamingSystem>
<CHEM.NamingSystem _ID="_108" name="SYBYL">
<CHEM.NamingSystem.atomVariantSystems>_107</CHEM.NamingSystem.atomVariantSystems>
<CHEM.NamingSystem.atomSysNames>
<CHEM.AtomSysName _ID="_161" atomName="H''">
<CHEM.AtomSysName.sysName>
<IMPL.Line>HOCAP</IMPL.Line>
</CHEM.AtomSysName.sysName>
</CHEM.AtomSysName>
<CHEM.AtomSysName _ID="_162" atomName="H1">
<CHEM.AtomSysName.sysName>
<IMPL.Line>HNCAP</IMPL.Line>
</CHEM.AtomSysName.sysName>
</CHEM.AtomSysName>
<CHEM.AtomSysName _ID="_163" atomName="H1" atomSubType="2">
<CHEM.AtomSysName.sysName>
<IMPL.Line>HNCAP</IMPL.Line>
</CHEM.AtomSysName.sysName>
</CHEM.AtomSysName>
<CHEM.AtomSysName _ID="_164" atomName="HB3">
<CHEM.AtomSysName.sysName>
<IMPL.Line>HB1</IMPL.Line>
</CHEM.AtomSysName.sysName>
</CHEM.AtomSysName>
<CHEM.AtomSysName _ID="_165" atomName="O'">
<CHEM.AtomSysName.sysName>
<IMPL.Line>O</IMPL.Line>
</CHEM.AtomSysName.sysName>
</CHEM.AtomSysName>
<CHEM.AtomSysName _ID="_166" atomName="O''">
<CHEM.AtomSysName.sysName>
<IMPL.Line>OXT</IMPL.Line>
</CHEM.AtomSysName.sysName>
</CHEM.AtomSysName>
</CHEM.NamingSystem.atomSysNames>
</CHEM.NamingSystem>
<CHEM.NamingSystem _ID="_72" name="UCSF">
<CHEM.NamingSystem.atomSysNames>
<CHEM.AtomSysName _ID="_167" atomName="HB2">
<CHEM.AtomSysName.sysName>
<IMPL.Line>HB1</IMPL.Line>
</CHEM.AtomSysName.sysName>
</CHEM.AtomSysName>
<CHEM.AtomSysName _ID="_168" atomName="HB3">
<CHEM.AtomSysName.sysName>
<IMPL.Line>HB2</IMPL.Line>
</CHEM.AtomSysName.sysName>
</CHEM.AtomSysName>
<CHEM.AtomSysName _ID="_169" atomName="HG">
<CHEM.AtomSysName.sysName>
<IMPL.Line>HSG</IMPL.Line>
</CHEM.AtomSysName.sysName>
</CHEM.AtomSysName>
</CHEM.NamingSystem.atomSysNames>
</CHEM.NamingSystem>
<CHEM.NamingSystem _ID="_109" name="XPLOR">
<CHEM.NamingSystem.atomSysNames>
<CHEM.AtomSysName _ID="_170" atomName="H">
<CHEM.AtomSysName.sysName>
<IMPL.Line>HN</IMPL.Line>
</CHEM.AtomSysName.sysName>
</CHEM.AtomSysName>
<CHEM.AtomSysName _ID="_171" atomName="H*">
<CHEM.AtomSysName.altSysNames>
<IMPL.Line>HT%</IMPL.Line>
<IMPL.Line>HT*</IMPL.Line>
```

```
<IMPL.Line>HT+</IMPL.Line>
</CHEM.AtomSysName.altSysNames>
<CHEM.AtomSysName.sysName>
<IMPL.Line>HT#</IMPL.Line>
</CHEM.AtomSysName.sysName>
</CHEM.AtomSysName>
<CHEM.AtomSysName _ID="_172" atomName="H*" atomSubType="2">
<CHEM.AtomSysName.altSysNames>
<IMPL.Line>HT%</IMPL.Line>
<IMPL.Line>HT*</IMPL.Line>
<IMPL.Line>HT+</IMPL.Line>
</CHEM.AtomSysName.altSysNames>
<CHEM.AtomSysName.sysName>
<IMPL.Line>HT#</IMPL.Line>
</CHEM.AtomSysName.sysName>
</CHEM.AtomSysName>
<CHEM.AtomSysName _ID="_173" atomName="H1">
<CHEM.AtomSysName.sysName>
<IMPL.Line>HT1</IMPL.Line>
</CHEM.AtomSysName.sysName>
</CHEM.AtomSysName>
<CHEM.AtomSysName _ID="_174" atomName="H1" atomSubType="2">
<CHEM.AtomSysName.sysName>
<IMPL.Line>HT1</IMPL.Line>
</CHEM.AtomSysName.sysName>
</CHEM.AtomSysName>
<CHEM.AtomSysName _ID="_175" atomName="H2">
<CHEM.AtomSysName.sysName>
<IMPL.Line>HT2</IMPL.Line>
</CHEM.AtomSysName.sysName>
</CHEM.AtomSysName>
<CHEM.AtomSysName _ID="_176" atomName="H2" atomSubType="2">
<CHEM.AtomSysName.sysName>
<IMPL.Line>HT2</IMPL.Line>
</CHEM.AtomSysName.sysName>
</CHEM.AtomSysName>
<CHEM.AtomSysName _ID="_177" atomName="H3">
<CHEM.AtomSysName.sysName>
<IMPL.Line>HT3</IMPL.Line>
</CHEM.AtomSysName.sysName>
</CHEM.AtomSysName>
<CHEM.AtomSysName _ID="_178" atomName="HA">
<CHEM.AtomSysName.altSysNames>
<IMPL.Line>HA*</IMPL.Line>
</CHEM.AtomSysName.altSysNames>
<CHEM.AtomSysName.sysName>
<IMPL.Line>HA</IMPL.Line>
</CHEM.AtomSysName.sysName>
</CHEM.AtomSysName>
<CHEM.AtomSysName _ID="_179" atomName="HB*">
<CHEM.AtomSysName.altSysNames>
<IMPL.Line>HB%</IMPL.Line>
<IMPL.Line>HB*</IMPL.Line>
<IMPL.Line>HB+</IMPL.Line>
</CHEM.AtomSysName.altSysNames>
<CHEM.AtomSysName.sysName>
<IMPL.Line>HB#</IMPL.Line>
</CHEM.AtomSysName.sysName>
</CHEM.AtomSysName>
<CHEM.AtomSysName _ID="_180" atomName="HB3">
<CHEM.AtomSysName.sysName>
<IMPL.Line>HB1</IMPL.Line>
</CHEM.AtomSysName.sysName>
</CHEM.AtomSysName>
<CHEM.AtomSysName _ID="_181" atomName="O'">
<CHEM.AtomSysName.sysName>
<IMPL.Line>OT1</IMPL.Line>
</CHEM.AtomSysName.sysName>
```

```
</CHEM.AtomSysName>
<CHEM.AtomSysName _ID="_182" atomName="O''">
<CHEM.AtomSysName.sysName>
<IMPL.Line>OT2</IMPL.Line>
</CHEM.AtomSysName.sysName>
</CHEM.AtomSysName>
</CHEM.NamingSystem.atomSysNames>
</CHEM.NamingSystem>
</CHEM.ChemComp.namingSystems>
</CHEM.NonStdChemComp>
</_StorageUnit>
<!-- End of Memops Data -->
```

6

References

References

1. Sessions, A. L., Doughty, D. M., Welander, P. V, Summons, R. E., and Newman, D. K. (2009) The continuing puzzle of the great oxidation event. *Curr. Biol.* **19**, R567–74

2. Kappler, A., Pasquero, C., Konhauser, K. O., and Newman, D. K. (2005) Deposition of banded iron formations by anoxygenic phototrophic Fe(II)-oxidizing bacteria. *Geology* **33**, 865–868

3. Newman, D. K., and Banfield, J. F. (2002) Geomicrobiology: how molecular-scale interactions underpin biogeochemical systems. *Science* **296**, 1071–7

4. Widdel, F., Schnell, S., Heising, S., Ehrenreich, A., Assmus, B., and Schink, B. (1993) Ferrous iron oxidation by anoxygenic phototrophic bacteria. *Nature* **362**, 834–836

5. Ehrenreich, A., and Widdel, F. (1994) Anaerobic oxidation of ferrous iron by purple bacteria, a new type of phototrophic metabolism. *Appl. Environ. Microbiol.* **60**, 4517–26

6. Xiong, J. (2000) Molecular Evidence for the Early Evolution of Photosynthesis. *Science* **289**, 1724–1730

7. Stumm, W., and Morgan, J. J. (1996) *Aquatic chemistry : chemical equilibria and rates in natural waters*, 3rd Ed. Wiley, New York

8. Weber, K. a, Achenbach, L. a, and Coates, J. D. (2006) Microorganisms pumping iron: anaerobic microbial iron oxidation and reduction. *Nat. Rev. Microbiol.* **4**, 752–64

9. Kasting, J. (1993) Earth's early atmosphere. *Science* **259**, 920–926

10. Walker, J. C. G., and Brimblecombe, P. (1985) Iron and sulfur in the pre-biologic ocean. *Precambrian Res.* **28**, 205–222

11. Vargas, M., Kashefi, K., Blunt-harris, E. L., and Lovley, D. R. (1998) Microbiological evidence for Fe (III) reduction on early Earth. *Nature* **395**, 65–67

12. Kostka, J. E., and Nealson, K. H. (1995) Dissolution and Reduction of Magnetite by Bacteria. *Environ. Sci. Technol.* **29**, 2535–2540

13. Fredrickson, J. K., Zachara, J. M., Kennedy, D. W., Dong, H., Onstott, T. C., Hinman, N. W., and Li, S. (1998) Biogenic iron mineralization accompanying the dissimilatory reduction of hydrous ferric oxide by a groundwater bacterium. *Geochim. Cosmochim. Acta* **62**, 3239–3257

14. Shi, L., Richardson, D. J., Wang, Z., Kerisit, S. N., Rosso, K. M., Zachara, J. M., and Fredrickson, J. K. (2009) The roles of outer membrane cytochromes of Shewanella and Geobacter in extracellular electron transfer. *Environ. Microbiol. Rep.* **1**, 220–227

15. Shi, L., Squier, T. C., Zachara, J. M., and Fredrickson, J. K. (2007) Respiration of metal (hydr)oxides by Shewanella and Geobacter: a key role for multihaem c-type cytochromes. *Mol. Microbiol.* **65**, 12–20

16. Pronk, J. T., and Johnson, D. B. (1992) Oxidation and Reduction of Iron by Acidophilic Bacteria. *Geomicrobiol. J.* **10**, 153–171

17. Emerson, D., Fleming, E. J., and McBeth, J. M. (2010) Iron-oxidizing bacteria: an environmental and genomic perspective. *Annu. Rev. Microbiol.* **64**, 561–83

18. Valdés, J., Pedroso, I., Quatrini, R., Dodson, R. J., Tettelin, H., Blake, R., Eisen, J. a, and Holmes, D. S. (2008) Acidithiobacillus ferrooxidans metabolism: from genome sequence to industrial applications. *BMC genomics* **9**, 597

19. Gonzalez-Toril, E., Llobet-Brossa, E., Casamayor, E. O., Amann, R., and Amils, R. (2003) Microbial Ecology of an Extreme Acidic Environment, the Tinto River. *Appl. Environ. Microbiol.* **69**, 4853–4865

20. Amouric, A., Brochier-Armanet, C., Johnson, D. B., Bonnefoy, V., and Hallberg, K. B. (2011) Phylogenetic and genetic variation among Fe(II)-oxidizing acidithiobacilli supports the view that these comprise multiple

species with different ferrous iron oxidation pathways. *Microbiology* **157**, 111–22

21. Appia-Ayme, C., Guiliani, N., Ratouchniak, J., and Bonnefoy, V. (1999) Characterization of an operon encoding two c-type cytochromes, an aa3-type cytochrome oxidase, and rusticyanin in Thiobacillus ferrooxidans ATCC 33020. *Appl. Environ. Microbiol.* **65**, 4781–4787

22. Castelle, C., Guiral, M., Malarte, G., Ledgham, F., Leroy, G., Brugna, M., and Giudici-Orticoni, M.-T. (2008) A new iron-oxidizing/O2-reducing supercomplex spanning both inner and outer membranes, isolated from the extreme acidophile Acidithiobacillus ferrooxidans. *J. Biol. Chem.* **283**, 25803–11

23. Quatrini, R., Appia-Ayme, C., Denis, Y., Jedlicki, E., Holmes, D. S., and Bonnefoy, V. (2009) Extending the models for iron and sulfur oxidation in the extreme acidophile Acidithiobacillus ferrooxidans. *BMC genomics* **10**, 394

24. Hedrich, S., Schlömann, M., and Johnson, D. B. (2011) The iron-oxidizing proteobacteria. *Microbiology* **157**, 1551–64

25. Hallberg, K. B., González-Toril, E., and Johnson, D. B. (2010) Acidithiobacillus ferrivorans, sp. nov.; facultatively anaerobic, psychrotolerant iron-, and sulfur-oxidizing acidophiles isolated from metal mine-impacted environments. *Extremophiles* **14**, 9–19

26. Huber, H., and Stetter, K. O. (1989) Thiobacillus prosperus sp. nov., represents a new group of halotolerant metal-mobilizing bacteria isolated from a marine geothermal field. *Arch. Microbiol.* **151**, 479–485

27. Hallberg, K. B., Hedrich, S., and Johnson, D. B. (2011) Acidiferrobacter thiooxydans, gen. nov. sp. nov.; an acidophilic, thermo-tolerant, facultatively anaerobic iron- and sulfur-oxidizer of the family Ectothiorhodospiraceae. *Extremophiles* **15**, 271–9

28. Bruun, A.-M., Finster, K., Gunnlaugsson, H. P., N⊘rnberg, P., and Friedrich, M. W. (2010) A Comprehensive Investigation on Iron Cycling in a Freshwater Seep Including Microscopy, Cultivation and Molecular Community Analysis. *Geomicrobiol. J.* **27**, 15–34

29. Emerson, D., and Revsbech, N. P. (1994) Investigation of an Iron-Oxidizing Microbial Mat Community Located near Aarhus, Denmark: Field Studies. *Appl. Environ. Microbiol.* **60**, 4022–31

30. Emerson, D., and Weiss, J. V (2004) Bacterial Iron Oxidation in Circumneutral Freshwater Habitats: Findings from the Field and the Laboratory. *Geomicrobiol. J.* **21**, 405–414

31. Haaijer, S. C. M., Harhangi, H. R., Meijerink, B. B., Strous, M., Pol, A., Smolders, A. J. P., Verwegen, K., Jetten, M. S. M., and Op den Camp, H. J. M. (2008) Bacteria associated with iron seeps in a sulfur-rich, neutral pH, freshwater ecosystem. *ISME J.* **2**, 1231–42

32. James, R., and Ferris, F. (2004) Evidence for microbial-mediated iron oxidation at a neutrophilic groundwater spring. *Chem. Geol.* **212**, 301–311

33. Bogdanov, Y. A., Lisitzin, A. P., Binns, R. a., Gorshkov, A. I., Gurvich, E. G., Dritz, V. a., Dubinina, G. a., Bogdanova, O. Y., Sivkov, A. V., and Kuptsov, V. M. (1997) Low-temperature hydrothermal deposits of Franklin Seamount, Woodlark Basin, Papua New Guinea. *Mar. Geol.* **142**, 99–117

34. Emerson, D., and Moyer, C. (2010) Microbiology of Seamounts: Common Patterns Observed in Community Structure. *Oceanography* **23**, 148–163

35. Kennedy, C. B., Martinez, R. E., Scott, S. D., and Ferris, F. G. (2003) Surface chemistry and reactivity of bacteriogenic iron oxides from Axial Volcano, Juan de Fuca Ridge, north-east Pacific Ocean. *Geobiology* **1**, 59–69

36. Emerson, D., Weiss, J. V, and Megonigal, J. P. (1999) Iron-oxidizing bacteria are associated with ferric hydroxide precipitates (Fe-plaque) on the roots of wetland plants. *Appl. Environ. Microbiol.* **65**, 2758–2761

37. Weiss, J. V, Emerson, D., Backer, S. M., and Megonigal, J. P. (2003) Enumeration of Fe (II)-oxidizing and Fe (III)-reducing bacteria in the root zone of wetland plants: implications for a rhizosphere iron cycle. *Biogeochemistry* **64**, 77–96

38. Weiss, J. V, Rentz, J. A., Plaia, T., Neubauer, S. C., Merrill-Floyd, M., Lilburn, T., Bradburne, C., Megonigal, J. P., and Emerson, D. (2007) Characterization of Neutrophilic Fe(II)-Oxidizing Bacteria Isolated from the Rhizosphere of Wetland Plants and Description of Ferritrophicum radicicola gen. nov. sp. nov., and Sideroxydans paludicola sp. nov. *Geomicrobiol. J.* **24**, 559–570

39. Emerson, D., and Floyd, M. M. (2005) Enrichment and isolation of iron-oxidizing bacteria at neutral pH. *Methods. Enzymol.* **397**, 112–123

40. Ehrenberg, G. C. (1837) Remarks on the real occurrence of fossil infusoria, and their extensive diffusion. *Scientific memoirs, selected from the transactions of foreign Academies of Science and Learned Societies and from foreign journals*, 400–413

41. Liu, J., Wang, Z., Belchik, S. M., Edwards, M. J., Liu, C., Kennedy, D. W., Merkley, E. D., Lipton, M. S., Butt, J. N., Richardson, D. J., Zachara, J. M., Fredrickson, J. K., Rosso, K. M., and Shi, L. (2012) Identification and Characterization of MtoA: A Decaheme c-Type Cytochrome of the Neutrophilic Fe(II)-Oxidizing Bacterium Sideroxydans lithotrophicus ES-1. *Front. Microbiol.* **3**, 1–11

42. Hartshorne, R. S., Reardon, C. L., Ross, D. E., Nuester, J., Clarke, T. a, Gates, A. J., Mills, P. C., Fredrickson, J. K., Zachara, J. M., Shi, L., Beliaev, A. S., Marshall, M. J., Tien, M., Brantley, S., Butt, J. N., and Richardson, D. J. (2009) Characterization of an electron conduit between bacteria and the extracellular environment. *Proc. Natl. Acad. Sci. U. S. A.* **106**, 22169–74

43. Emerson, D., Rentz, J. A., Lilburn, T. G., Davis, R. E., Aldrich, H., Chan, C., and Moyer, C. L. (2007) A novel lineage of proteobacteria involved in formation of marine Fe-oxidizing microbial mat communities. *PloS one* **2**, e667

44. Singer, E., Emerson, D., Webb, E. A., Barco, R. A., Kuenen, J. G., Nelson, W. C., Chan, C. S., Comolli, L. R., Ferriera, S., Johnson, J., Heidelberg, J. F., and Edwards, K. J. (2011) Mariprofundus ferrooxydans PV-1 the first genome of a marine Fe(II) oxidizing Zetaproteobacterium. *PloS one* **6**, e25386

45. Straub, K. L., Benz, M., Schink, B., and Widdel, F. (1996) Anaerobic, nitrate-dependent microbial oxidation of ferrous iron. *Appl. Environ. Microbiol.* **62**, 1458–60

46. Benz, M., Brune, A., and Schink, B. (1998) Anaerobic and aerobic oxidation of ferrous iron at neutral pH by chemoheterotrophic nitrate-reducing bacteria. *Arch. Microbiol.* **169**, 159–65

47. Straub, K. L., and Buchholz-Cleven, B. E. (1998) Enumeration and detection of anaerobic ferrous iron-oxidizing, nitrate-reducing bacteria from diverse European sediments. *Appl. Environ. Microbiol.* **64**, 4846–56

48. Edwards, K. J., Rogers, D. R., Wirsen, C. O., and McCollom, T. M. (2003) Isolation and Characterization of Novel Psychrophilic, Neutrophilic, Fe-Oxidizing, Chemolithoautotrophic - and -Proteobacteria from the Deep Sea. *Appl. Environ. Microbiol.* **69**, 2906–2913

49. Kappler, A., Schink, B., and Newman, D. K. (2005) Fe (III) mineral formation and cell encrustation by the nitrate-dependent Fe (II)-oxidizer strain BoFeN1. *Geobiology* **3**, 235–245

50. Muehe, E. M., Gerhardt, S., Schink, B., and Kappler, A. (2009) Ecophysiology and the energetic benefit of mixotrophic Fe(II) oxidation by various strains of nitrate-reducing bacteria. *FEMS Microbiol. Ecol.* **70**, 335–43

51. Garrels, R. M., Perry, E. A., and Mackenzie, F. T. (1973) Genesis of Precambrian Iron-Formations and the Development of Atmospheric Oxygen. *Econ. Geol.* **68**, 1173–1179

52. Jiao, Y., and Newman, D. K. (2007) The pio operon is essential for phototrophic Fe(II) oxidation in Rhodopseudomonas palustris TIE-1. *J. Bacteriol.* **189**, 1765–73

53. Croal, L. R., Jiao, Y., and Newman, D. K. (2007) The fox operon from Rhodobacter strain SW2 promotes phototrophic Fe(II) oxidation in Rhodobacter capsulatus SB1003. *J. Bacteriol.* **189**, 1774–82

54. Heising, S., and Schink, B. (1998) Phototrophic oxidation of ferrous iron by a Rhodomicrobium vannielii strain. *Microbiology* **144**, 2263–9

55. Heising, S., Richter, L., Ludwig, W., and Schink, B. (1999) Chlorobium ferrooxidans sp. nov., a phototrophic green sulfur bacterium that oxidizes ferrous iron in coculture with a " Geospirillum " sp . strain. *Arch. Microbiol.* **172**, 116–124

56. Straub, K. L., Rainey, F. A., and Widdel, F. (1999) Rhodovulum iodosum sp. nov. and Rhodovulum robiginosum sp. nov., two new marine phototrophic ferrous-iron-oxidizing purple bacteria. *Int. J. Syst. Bacteriol.* **49**, 729–735

57. Croal, L. R., Johnson, C. M., Beard, B. L., and Newman, D. K. (2004) Iron isotope fractionation by Fe(II)-oxidizing photoautotrophic bacteria 1. *Geochim. Cosmochim. Acta* **68**, 1227–1242

58. Hegler, F., Posth, N. R., Jiang, J., and Kappler, A. (2008) Physiology of phototrophic iron(II)-oxidizing bacteria: implications for modern and ancient environments. *FEMS Microbiol. Ecol.* **66**, 250–60

59. Jiao, Y., Croal, L. R., Kappler, A., and Newman, D. K. (2005) Isolation and characterization of a genetically tractable photoautotrophic Fe(II)-oxidizing bacterium, Rhodopseudomonas palustris strain TIE-1. *Appl. Environ. Microbiol.* **71**, 4487–96

60. Thöny-Meyer, L., Fischer, F., Kunzler, P., Ritz, D., and Hennecke, H. (1995) Escherichia coli genes required for cytochrome c maturation. *J. Bacteriol.* **177**

61. Coursolle, D., and Gralnick, J. a (2010) Modularity of the Mtr respiratory pathway of Shewanella oneidensis strain MR-1. *Mol. Microbiol.* **77**, 995–1008

62. Messerschmidt, A., Huber, R., Poulas, T., Wieghardt, K., Cygler, M., and Bode, W. (eds.) (2006) *Handbook of Metalloproteins*. John Wiley & Sons, Ltd, Chichester , 31–192

63. Reedy, C. J., Elvekrog, M. M., and Gibney, B. R. (2008) Development of a heme protein structure-electrochemical function database. *Nucleic Acids Res.* **36**, D307–13

64. Matias, P. M., Coelho, A. V, Valente, F. M. a, Plácido, D., LeGall, J., Xavier, A. V, Pereira, I. a C., and Carrondo, M. A. (2002) Sulfate

respiration in Desulfovibrio vulgaris Hildenborough. Structure of the 16-heme cytochrome c HmcA AT 2.5-A resolution and a view of its role in transmembrane electron transfer. *J. Biol. Chem.* **277**, 47907–16

65. Carlson, H. K., Iavarone, a. T., Gorur, A., Yeo, B. S., Tran, R., Melnyk, R. a., Mathies, R. a., Auer, M., and Coates, J. D. (2012) Surface multiheme c-type cytochromes from Thermincola potens and implications for respiratory metal reduction by Gram-positive bacteria. *Proc. Natl. Acad. Sci. U. S. A.* **109**, 1702–1707

66. Myers, C. R., and Myers, J. M. (1997) Cloning and sequence of cymA, a gene encoding a tetraheme cytochrome c required for reduction of iron (III), fumarate, and nitrate by Shewanella putrefaciens MR-1. *J. Bacteriol.* **179**, 1143

67. Beliaev, A. S., and Saffarini, D. A. (1998) Shewanella putrefaciens mtrB encodes an outer membrane protein required for Fe (III) and Mn (IV) reduction. *J. Bacteriol.* **180**, 6292

68. Beliaev, A. S., Saffarini, D. A., McLaughlin, J. L., and Hunnicutt, D. (2001) MtrC, an outer membrane decahaem c cytochrome required for metal reduction in Shewanella putrefaciens MR-1. *Mol. Microbiol.* **39**, 722–30

69. Myers, J. M., and Myers, C. R. (2001) Role for outer membrane cytochromes OmcA and OmcB of Shewanella putrefaciens MR-1 in reduction of manganese dioxide. *Appl. Environ. Microbiol.* **67**, 260–9

70. Conrad, L. S., Karlsson, J. J., and Ulstrup, J. (1995) Electron transfer and spectral alpha-band properties of the di-heme protein cytochrome c4 from Pseudomonas stutzeri. *Eur. J. Biochem.* **231**, 133–41

71. Correia, I. J., Paquete, C. M., Louro, R. O., Catarino, T., Turner, D. L., and Xavier, A. V (2002) Thermodynamic and kinetic characterization of trihaem cytochrome c3 from Desulfuromonas acetoxidans. *Eur. J. Biochem.* **269**, 5722–5730

72. Morgado, L., Bruix, M., Pessanha, M., Londer, Y. Y., and Salgueiro, C. a (2010) Thermodynamic characterization of a triheme cytochrome family from Geobacter sulfurreducens reveals mechanistic and functional diversity. *Biophys. J.* **99**, 293–301

73. Paquete, C. M., Pereira, P. M., Catarino, T., Turner, D. L., Louro, R. O., and Xavier, A. V (2007) Functional properties of type I and type II cytochromes c3 from Desulfovibrio africanus. *Biochim. Biophys. Acta* **1767**, 178–88

74. Paquete, C. M., Turner, D. L., Louro, R. O., Xavier, A. V, and Catarino, T. (2007) Thermodynamic and kinetic characterisation of individual haems in multicentre cytochromes c3. *Biochim. Biophys. Acta* **1767**, 1169–79

75. Louro, R. O., Catarino, T., LeGall, J., Turner, D. L., and Xavier, A. V (2001) Cooperativity between electrons and protons in a monomeric cytochrome c(3): the importance of mechano-chemical coupling for energy transduction. *ChemBioChem* **2**, 831–7

76. Fonseca, B. M., Saraiva, I. H., Paquete, C. M., Soares, C. M., Pacheco, I., Salgueiro, C. A., and Louro, R. O. (2009) The tetraheme cytochrome from Shewanella oneidensis MR-1 shows thermodynamic bias for functional specificity of the hemes. *J. Biol. Inorg. Chem.* **14**, 375–85

77. Pessanha, M., Rothery, E. L., Louro, R. O., Turner, D. L., Miles, C. S., Reid, G. a, Chapman, S. K., Xavier, A. V, and Salgueiro, C. a (2004) Redox behaviour of the haem domain of flavocytochrome c3 from Shewanella frigidimarina probed by NMR. *FEBS Lett.* **578**, 185–90

78. Pessanha, M., Louro, R. O., Correia, I. J., Rothery, E. L., Pankhurst, K. L., Reid, G. a, Chapman, S. K., Turner, D. L., and Salgueiro, C. a (2003) Thermodynamic characterization of a tetrahaem cytochrome isolated from a facultative aerobic bacterium, Shewanella frigidimarina: a putative redox model for flavocytochrome c3. *Biochem. J.* **370**, 489–95

79. Pessanha, M., Rothery, E. L., Miles, C. S., Reid, G. a, Chapman, S. K., Louro, R. O., Turner, D. L., Salgueiro, C. a, and Xavier, A. V (2009) Tuning of functional heme reduction potentials in Shewanella fumarate reductases. *Biochim. Biophys. Acta* **1787**, 113–20

80. Correia, I. J., Paquete, C. M., Coelho, A., Almeida, C. C., Catarino, T., Louro, R. O., Frazão, C., Saraiva, L. M., Carrondo, M. A., Turner, D. L., and Xavier, A. V (2004) Proton-assisted two-electron transfer in natural variants of tetraheme cytochromes from Desulfomicrobium Sp. *J. Biol. Chem.* **279**, 52227–37

81. Catarino, T., Coletta, M., LeGall, J., and Xavier, A. V (1991) Kinetic study of the reduction mechanism for Desulfovibrio gigas cytochrome c3. *Eur. J. Biochem.* **202**, 1107–1113

82. Paquete, C. M., Saraiva, I. H., Calçada, E., and Louro, R. O. (2010) Molecular basis for directional electron transfer. *J. Biol. Chem.* **285**, 10370–5

83. Santos, H., Moura, J. J., Moura, I., LeGall, J., and Xavier, A. V (1984) NMR studies of electron transfer mechanisms in a protein with interacting redox centres: Desulfovibrio gigas cytochrome c3. *Eur. J. Biochem.* **141**, 283–96

84. Fonseca, B. M., Paquete, C. M., Salgueiro, C. A., and Louro, R. O. (2012) The role of intramolecular interactions in the functional control of multiheme cytochromes c. *FEBS Lett.* **586**, 504–509

85. Turner, D. L., Salgueiro, C. a, Catarino, T., LeGall, J., and Xavier, A. V (1994) Homotropic and heterotropic cooperativity in the tetrahaem cytochrome c3 from Desulfovibrio vulgaris. *Biochim. Biophys. Acta* **1187**, 232–235

86. Morgado, L., Bruix, M., Orshonsky, V., Londer, Y. Y., Duke, N. E. C., Yang, X., Pokkuluri, P. R., Schiffer, M., and Salgueiro, C. A. (2008) Structural insights into the modulation of the redox properties of two Geobacter sulfurreducens homologous triheme cytochromes. *Biochim. Biophys. Acta* **1777**, 1157–65

87. Louro, R. O. (2007) Proton thrusters: overview of the structural and functional features of soluble tetrahaem cytochromes c3. *J. Biol. Inorg. Chem.* **12**, 1–10

88. Catarino, T., and Turner, D. L. (2001) Thermodynamic control of electron transfer rates in multicentre redox proteins. *ChemBioChem* **2**, 416–424

89. Carter Jr., C. W., Kraut, J., Freer, S. T., Alden, R. A., Sieker, L. C., Adman, E., and Jensen, L. H. (1972) A Comparison of Fe4S4 * Clusters in High-Potential Iron Protein and in Ferredoxin. *Proc. Natl. Acad. Sci. U. S. A.* **69**, 3526–3529

90. Heering, H. a, Bulsink, Y. B. M., Hagen, W. R., and Meyer, T. E. (1995) Influence of Charge and Polarity on the Redox Potentials of High-Potential Iron-Sulfur Proteins: Evidence for the Existence of Two Groups. *Biochemistry* **34**, 14675–14686

91. Dey, A., Jenney, F. E., Adams, M. W. W., Babini, E., Takahashi, Y., Fukuyama, K., Hodgson, K. O., Hedman, B., and Solomon, E. I. (2007) Solvent tuning of electrochemical potentials in the active sites of HiPIP versus ferredoxin. *Science* **318**, 1464–8

92. Van Driessche, G., Vandenberghe, I., Devreese, B., Samyn, B., Meyer, T. E., Leigh, R., Cusanovich, M. A., Bartsch, R. G., Fischer, U., and Van Beeumen, J. J. (2003) Amino acid sequences and distribution of high-potential iron-sulfur proteins that donate electrons to the photosynthetic reaction center in phototropic proteobacteria. *J. Mol. Evol.* **57**, 181–99

93. Menin, L., Gaillard, J., Parot, P., Schoepp, B., Nitschke, W., and Verméglio, A. (1998) Role of HiPIP as electron donor to the RC-bound cytochrome in photosynthetic purple bacteria. *Photosynth. Res.* **55**, 343–348

94. Pereira, M. M., Antunes, A. M., Nunes, O. C., Da Costa, M. S., and Teixeira, M. (1994) A membrane-bound HIPIP type center in the thermohalophile Rhodothermus marinus. *FEBS Lett.* **352**, 327–330

95. Pereira, M. M., Carita, J. N., and Teixeira, M. (1999) Membrane-bound electron transfer chain of the thermohalophilic bacterium Rhodothermus marinus: a novel multihemic cytochrome bc, a new complex III. *Biochemistry* **38**, 1268–75

96. Brasseur, G., Bruscella, P., Bonnefoy, V., and Lemesle-Meunier, D. (2002) The bc(1) complex of the iron-grown acidophilic chemolithotrophic bacterium Acidithiobacillus ferrooxidans functions in the reverse but not in the forward direction. Is there a second bc(1) complex? *Biochim. Biophys. Acta* **1555**, 37–43

97. Bruscella, P., Cassagnaud, L., Ratouchniak, J., Brasseur, G., Lojou, E., Amils, R., and Bonnefoy, V. (2005) The HiPIP from the acidophilic Acidithiobacillus ferrooxidans is correctly processed and translocated in

Escherichia coli, in spite of the periplasm pH difference between these two micro-organisms. *Microbiology* **151**, 1421–31

98. Agarwal, A., Li, D., and Cowan, J. A. (1995) Role of aromatic residues in stabilization of the [Fe4S4] cluster in high-potential iron proteins (HiPIPs): physical characterization and stability studies of Tyr-19 mutants of Chromatium vinosum HiPIP. *Proc. Natl. Acad. Sci. U. S. A.* **92**, 9440–4

99. Zeng, J., Liu, Q., Zhang, X., Mo, H., Wang, Y., Chen, Q., and Liu, Y. (2010) Functional Roles of the Aromatic Residues in the Stabilization of the [Fe4S4] Cluster in the Iro Protein from Acidithiobacillus ferrooxidans. *J. Microbiol. Biotechnol.* **20**, 294–300

100. Winter, C.-J. (2005) Into the hydrogen energy economy - milestones. *Int. J. Hydrogen Energy* **30**, 681–685

101. Turner, J., Sverdrup, G., Mann, M. K., Maness, P., Kroposki, B., Ghirardi, M., Evans, R. J., and Blake, D. (2008) Renewable hydrogen production. *Int. J. Energ. Res.* **32**, 379–407

102. McKinlay, J. B., and Harwood, C. S. (2010) Photobiological production of hydrogen gas as a biofuel. *Curr. Opin. Biotechnol.* **21**, 244–51

103. Hemschemeier, A., Melis, A., and Happe, T. (2009) Analytical approaches to photobiological hydrogen production in unicellular green algae. *Photosynth. Res.* **102**, 523–40

104. Sakurai, H., and Masukawa, H. (2007) Promoting R & D in photobiological hydrogen production utilizing mariculture-raised cyanobacteria. *Mar. Biotechnol.* **9**, 128–45

105. Gosse, J. L., Engel, B. J., Rey, F. E., Harwood, C. S., Scriven, L. E., and Flickinger, M. C. (2007) Hydrogen production by photoreactive nanoporous latex coatings of nongrowing Rhodopseudomonas palustris CGA009. *Biotechnol. Prog.* **23**, 124–30

106. Suwansaard, M., Choorit, W., Zeilstra-Ryalls, J. H., and Prasertsan, P. (2010) Phototropic H(2) production by a newly isolated strain of Rhodopseudomonas palustris. *Biotechnol. Lett.*

107. Rey, F. E., Heiniger, E. K., and Harwood, C. S. (2007) Redirection of metabolism for biological hydrogen production. *Appl. Environ. Microbiol.* **73**, 1665–71

108. Zabut, B., Elkahlout, K., Yucel, M., Gunduz, U., Turker, L., and Eroglu, I. (2006) Hydrogen gas production by combined systems of Rhodobacter sphaeroides O.U.001 and Halobacterium salinarum in a photobioreactor. *Int. J. Hydrogen Energy* **31**, 1553–1562

109. Kim, E.-J., Kim, M.-S., and Lee, J. K. (2008) Hydrogen evolution under photoheterotrophic and dark fermentative conditions by recombinant Rhodobacter sphaeroides containing the genes for fermentative pyruvate metabolism of Rhodospirillum rubrum. *Int. J. Hydrogen Energy* **33**, 5131–5136

110. Laurinavichene, T., Tekucheva, D., Laurinavichius, K., Ghirardi, M., Seibert, M., and Tsygankov, A. (2008) Towards the integration of dark and photo fermentative waste treatment. 1. Hydrogen photoproduction by purple bacterium Rhodobacter capsulatus using potential products of starch fermentation. *Int. J. Hydrogen Energy* **33**, 7020–7026

111. Egland, P. G., Pelletier, D. a, Dispensa, M., Gibson, J., and Harwood, C. S. (1997) A cluster of bacterial genes for anaerobic benzene ring biodegradation. *Proc. Natl. Acad. Sci. U. S. A.* **94**, 6484–9

112. Noh, U., Heck, S., Giffhorn, F., and Kohring, G.-W. (2002) Phototrophic transformation of phenol to 4-hydroxyphenylacetate by Rhodopseudomonas palustris. *Appl. Microbiol. Biotechnol.* **58**, 830–5

113. Urlacher, V. B., and Eiben, S. (2006) Cytochrome P450 monooxygenases: perspectives for synthetic application. *Trends Biotechnol.* **24**, 324–30

114. Allocati, N., Federici, L., Masulli, M., and Di Ilio, C. (2009) Glutathione transferases in bacteria. *FEBS J.* **276**, 58–75

115. Logan, B. E., Hamelers, B., Rozendal, R., Schröder, U., Keller, J., Freguia, S., Aelterman, P., Verstraete, W., and Rabaey, K. (2006) Microbial Fuel Cells: Methodology and Technology. *Environ. Sci. Technol.* **40**, 5181–5192

116. Logan, B. E. (2009) Exoelectrogenic bacteria that power microbial fuel cells. *Nat Rev Micro* **7**, 375–381

117. Kiely, P. D., Regan, J. M., and Logan, B. E. (2011) The electric picnic: synergistic requirements for exoelectrogenic microbial communities. *Curr. Opin. Biotechnol.* **22**, 378–85

118. Von Canstein, H., Ogawa, J., Shimizu, S., and Lloyd, J. R. (2008) Secretion of flavins by Shewanella species and their role in extracellular electron transfer. *Appl. Environ. Microbiol.* **74**, 615–23

119. Rabaey, K., Boon, N., Siciliano, S. D., Verhaege, M., and Verstraete, W. (2004) Biofuel cells select for microbial consortia that self-mediate electron transfer. *Appl. Environ. Microbiol.* **70**, 5373–82

120. Rabaey, K., Boon, N., Höfte, M., and Verstraete, W. (2005) Microbial phenazine production enhances electron transfer in biofuel cells. *Environ. Sci. Technol.* **39**, 3401–8

121. Gorby, Y. a, Yanina, S., McLean, J. S., Rosso, K. M., Moyles, D., Dohnalkova, A., Beveridge, T. J., Chang, I. S., Kim, B. H., Kim, K. S., Culley, D. E., Reed, S. B., Romine, M. F., Saffarini, D. A., Hill, E. a, Shi, L., Elias, D. a, Kennedy, D. W., Pinchuk, G., Watanabe, K., Ishii, S., Logan, B. E., Nealson, K. H., and Fredrickson, J. K. (2006) Electrically conductive bacterial nanowires produced by Shewanella oneidensis strain MR-1 and other microorganisms. *Proc. Natl. Acad. Sci. U. S. A.* **103**, 11358–63

122. Reguera, G., McCarthy, K. D., Mehta, T., Nicoll, J. S., Tuominen, M. T., and Lovley, D. R. (2005) Extracellular electron transfer via microbial nanowires. *Nature* **435**, 1098–101

123. Bond, D. R., and Lovley, D. R. (2003) Electricity Production by Geobacter sulfurreducens Attached to Electrodes. *Appl. Environ. Microbiol.* **69**, 1548–1555

124. Rozendal, R., Hamelers, H., Euverink, G., Metz, S., and Buisman, C. (2006) Principle and perspectives of hydrogen production through biocatalyzed electrolysis. *Int. J. Hydrogen Energy* **31**, 1632–1640

125. Liu, H., Grot, S., and Logan, B. E. (2005) Electrochemically assisted microbial production of hydrogen from acetate. *Environ. Sci. Technol.* **39**, 4317–20

126. Kim, Y., and Logan, B. E. (2011) Hydrogen production from inexhaustible supplies of fresh and salt water using microbial reverse-electrodialysis electrolysis cells. *Proc. Natl. Acad. Sci. U. S. A.*

127. He, Z., and Angenent, L. T. (2006) Application of Bacterial Biocathodes in Microbial Fuel Cells. *Electroanalysis* **18**, 2009–2015

128. Rhoads, A., Beyenal, H., and Lewandowski, Z. (2005) Microbial fuel cell using anaerobic respiration as an anodic reaction and biomineralized manganese as a cathodic reactant. *Environ. Sci. Technol.* **39**, 4666–71

129. Ter Heijne, A., Hamelers, H. V. M., and Buisman, C. J. N. (2007) Microbial fuel cell operation with continuous biological ferrous iron oxidation of the catholyte. *Environ. Sci. Technol.* **41**, 4130–4

130. Miot, J., Benzerara, K., Obst, M., Kappler, A., Hegler, F., Schädler, S., Bouchez, C., Guyot, F., and Morin, G. (2009) Extracellular iron biomineralization by photoautotrophic iron-oxidizing bacteria. *Appl. Environ. Microbiol.* **75**, 5586–91

131. Schadler, S., Burkhardt, C., Hegler, F., Straub, K. L., Miot, J., Benzerara, K., and Kappler, A. (2009) Formation of Cell-Iron-Mineral Aggregates by Phototrophic and Nitrate-Reducing Anaerobic Fe(II)-Oxidizing Bacteria. *Geomicrobiol. J.* **26**, 93–103

132. Kappler, A., and Newman, D. K. (2004) Formation of Fe(III)-minerals by Fe(II)-oxidizing photoautotrophic bacteria. *Geochim. Cosmochim. Acta* **68**, 1217–1226

133. Jeffrey, V., and Joachim, M. (1991) New pUC-derived cloning vectors with different selectable markers and DNA replication origins. *Gene* **100**, 189–194

134. Arslan, E., Schulz, H., Zufferey, R., Künzler, P., and Thöny-Meyer, L. (1998) Overproduction of the Bradyrhizobium japonicum c-type cytochrome subunits of the cbb3 oxidase in Escherichia coli. *Biochem. Biophys. Res. Commun.* **251**, 744–7

135. Francis, R. T., and Becker, R. R. (1984) Specific indication of hemoproteins in polyacrylamide gels using a double-staining process. *Anal. Biochem.* **136**, 509–514

136. Inubushi, T., and Becker, E. D. (1983) Efficient detection of paramagnetically shifted NMR resonances by optimizing the WEFT pulse sequence. *J. Magn. Reson.* **51**, 128–133

137. Parkhurst, D. L., and Appelo, C. A. J. (1999) Users's guide to PHREEQC (version 2) - A computer program for speciation, batch-reaction, one-dimensional transport, and inverse geochemical calculations. *U.S. Geological Survey Water-Resources Investigations Report*, 99–4259

138. Lagarias, J. C., Reeds, J. a., Wright, M. H., and Wright, P. E. (1998) Convergence Properties of the Nelder--Mead Simplex Method in Low Dimensions. *SIAM J. Optim.* **9**, 112–147

139. Press, W. H., Flannery, B. P., Teukolshy, S. A., and Vetterling, W. T. (1989) *Numerical recipes - The art of Scientific Computing (FORTRAN Version)*. Cambridge University Press, Cambridge

140. Pereira, L., Saraiva, I. H., Coelho, R., Newman, D. K., Louro, R. O., and Frazão, C. (2012) Crystallization and preliminary crystallographic studies of FoxE from Rhodobacter ferrooxidans SW2, an FeII oxidoreductase involved in photoferrotrophy. *Acta Crystallogr., Sect. F: Struct. Biol. Cryst. Commun.* **68**, 1106–1108

141. Zoppellaro, G., Bren, K. L., Ensign, A. a, Harbitz, E., Kaur, R., Hersleth, H.-P., Ryde, U., Hederstedt, L., and Andersson, K. K. (2009) Studies of ferric heme proteins with highly anisotropic/highly axial low spin (S = 1/2) electron paramagnetic resonance signals with bis-histidine and histidine-methionine axial iron coordination. *Biopolymers* **91**, 1064–82

142. Dantas, J. M., Saraiva, I. H., Morgado, L., Silva, M. a, Schiffer, M., Salgueiro, C. a, and Louro, R. O. (2011) Orientation of the axial ligands and magnetic properties of the hemes in the cytochrome c(7) family from Geobacter sulfurreducens determined by paramagnetic NMR. *Dalton Trans.* **40**, 12713–8

143. Xavier, A. V, Czerwinski, E. W., Bethge, P. H., and Mathews, F. S. (1978) Identification of the haem ligands of cytochrome b562 by X-ray and NMR methods. *Nature* **275**, 245–247

144. Louro, R. O., Correia, I. J., Brennan, L., Coutinho, I. B., Xavier, A. V, and Turner, D. L. (1998) Electronic Structure of Low-Spin Ferric Porphyrins: 13 C NMR Studies of the Influence of Axial Ligand Orientation. *J. Am. Chem. Soc.* **120**, 13240–13247

145. Louro, R. O., Catarino, T., Paquete, C. M., and Turner, D. L. (2004) Distance dependence of interactions between charged centres in proteins with common structural features. *FEBS Lett.* **576**, 77–80

146. Moser, C. C., and Dutton, P. L. (1992) Engineering protein structure for electron transfer function in photosynthetic reaction centers. *Biochim. Biophys. Acta* **1101**, 171–176

147. Bird, L. J., Bonnefoy, V., and Newman, D. K. (2011) Bioenergetic challenges of microbial iron metabolisms. *Trends Microbiol.* **19**, 330–40

148. Straub, K. L., Benz, M., and Schink, B. (2001) Iron metabolism in anoxic environments at near neutral pH. *FEMS Microbiol. Ecol.* **34**, 181–186

149. Wang, Z., Liu, C., Wang, X., Marshall, M. J., Zachara, J. M., Rosso, K. M., Dupuis, M., Fredrickson, J. K., Heald, S., and Shi, L. (2008) Kinetics of reduction of Fe(III) complexes by outer membrane cytochromes MtrC and OmcA of Shewanella oneidensis MR-1. *Appl. Environ. Microbiol.* **74**, 6746–55

150. Hegler, F., Schmidt, C., Schwarz, H., and Kappler, A. (2010) Does a low-pH microenvironment around phototrophic Fe(II) -oxidizing bacteria prevent cell encrustation by Fe(III) minerals? *FEMS Microbiol. Ecol.* **74**, 592–600

151. Lieutaud, C., Alric, J., Bauzan, M., Nitschke, W., and Schoepp-Cothenet, B. (2005) Study of the high-potential iron sulfur protein in Halorhodospira halophila confirms that it is distinct from cytochrome c as electron carrier. *Proc. Natl. Acad. Sci. U. S. A.* **102**, 3260–5

152. Schoepp, B., Parot, P., Menin, L., Gaillard, J., Richaud, P., and Verméglio, A. (1995) In vivo participation of a high potential iron-sulfur protein as

electron donor to the photochemical reaction center of Rubrivivax gelatinosus. *Biochemistry* **34**, 11736–42

153. Menin, L., Schoepp, B., Parot, P., and Verméglio, A. (1997) Photoinduced cyclic electron transfer in Rhodocyclus tenuis cells: participation of HiPIP or cyt c8 depending on the ambient redox potential. *Biochemistry* **36**, 12183–8

154. Hochkoeppler, a, Zannoni, D., Ciurli, S., Meyer, T. E., Cusanovich, M. A., and Tollin, G. (1996) Kinetics of photo-induced electron transfer from high-potential iron-sulfur protein to the photosynthetic reaction center of the purple phototroph Rhodoferax fermentans. *Proc. Natl. Acad. Sci. U. S. A.* **93**, 6998–7002

155. Bendtsen, J. D., Nielsen, H., Widdick, D., Palmer, T., and Brunak, S. (2005) Prediction of twin-arginine signal peptides. *BMC Bioinformatics* **6**, 167

156. Fourmond, V., Hoke, K., Heering, H. a, Baffert, C., Leroux, F., Bertrand, P., and Léger, C. (2009) SOAS: a free program to analyze electrochemical data and other one-dimensional signals. *Bioelectrochemistry* **76**, 141–7

157. Schleucher, J., Schwendinger, M., Sattler, M., Schmidt, P., Schedletzky, O., Glaser, S. J., Sørensen, O. W., and Griesinger, C. (1994) A general enhancement scheme in heteronuclear multidimensional NMR employing pulsed field gradients. *J. Biomol. NMR* **4**, 301–6

158. Lescop, E., Schanda, P., and Brutscher, B. (2007) A set of BEST triple-resonance experiments for time-optimized protein resonance assignment. *J. Magn. Reson.* **187**, 163–9

159. Vranken, W. F., Boucher, W., Stevens, T. J., Fogh, R. H., Pajon, A., Llinas, M., Ulrich, E. L., Markley, J. L., Ionides, J., and Laue, E. D. (2005) The CCPN data model for NMR spectroscopy: development of a software pipeline. *Proteins* **59**, 687–96

160. Herrmann, T., Güntert, P., and Wüthrich, K. (2002) Protein NMR Structure Determination with Automated NOE Assignment Using the New Software CANDID and the Torsion Angle Dynamics Algorithm DYANA. *J. Mol. Biol.* **319**, 209–227

161. Banci, L., Bertini, I., Eltis, L. D., Felli, I. C., Kastrau, D. H., Luchinat, C., Piccioli, M., Pierattelli, R., and Smith, M. (1994) The three-dimensional structure in solution of the paramagnetic high-potential iron-sulfur protein I from Ectothiorhodospira halophila through nuclear magnetic resonance. *Eur. J. Biochem.* **225**, 715–25

162. Priem, A. H., Klaassen, A. a K., Reijerse, E. J., Meyer, T. E., Luchinat, C., Capozzi, F., Dunham, W. R., and Hagen, W. R. (2005) EPR analysis of multiple forms of [4Fe-4S](3+) clusters in HiPIPs. *J. Biol. Inorg. Chem.* **10**, 417–24

163. Moss, D. A., Leonhard, M., Bauscher, M., and Mäntele, W. (1991) Electrochemical redox titration of cofactors in the reaction center from Rhodobacter sphaeroids. *FEBS* **283**, 33–36

164. Battistuzzi, G., Borsari, M., and Ferretti, S. (1995) Cyclic Voltammetry and 1H-NMR of Rhodopseudomonas Palustris Cytochrome c2 pH-Dependent Conformational States. *Eur. J. Biochem.* **232**, 206–213

165. Pettigrew, G. W., Bartsch, R. G., Meyer, T. E., and Kamen, M. D. (1978) Redox potentials of the photosynthetic bacterial cytochromes c2 and the structural bases for variability. *Biochim. Biophys. Acta* **503**, 509–523

166. Bertini, I., Dikiy, A., Kastrau, D. H. W., Luchinat, C., and Sompornpisut, P. (1995) Three-dimensional solution structure of the oxidized high potential iron-sulfur protein from Chromatium vinosum through NMR. Comparative analysis with the solution structure of the reduced species. *Biochemistry* **34**, 9851–9858

167. Banci, L., Bertini, I., Dikiy, A., Kastrau, D. H., Luchinat, C., and Sompornpisut, P. (1995) The three-dimensional solution structure of the reduced high-potential iron-sulfur protein from Chromatium vinosum through NMR. *Biochemistry* **34**, 206–19

168. Low, D. W., and Hill, M. G. (2000) Backbone-Engineered High-Potential Iron Proteins: Effects of Active-Site Hydrogen Bonding on Reduction Potential. *J. Am. Chem. Soc.* **122**, 11039–11040

169. Bertini, I., Felli, I. C., Kastrau, D. H., Luchinat, C., Piccioli, M., and Viezzoli, M. S. (1994) Sequence-specific assignment of the 1H and 15N nuclear magnetic resonance spectra of the reduced recombinant high-

potential iron-sulfur protein I from Ectothiorhodospira halophila. *Eur. J. Biochem.* **225**, 703–14

170. Bertini, I., Luchinat, C., Parigi, G., and Pierattelli, R. (2005) NMR spectroscopy of paramagnetic metalloproteins. *Chembiochem* **6**, 1536–1549

171. Matsushita, K., Toyama, H., Yamada, M., and Adachi, O. (2002) Quinoproteins: structure, function, and biotechnological applications. *Appl. Microbiol. Biotechnol.* **58**, 13–22

172. Johnson, H. A., and Tebo, B. M. (2008) In vitro studies indicate a quinone is involved in bacterial Mn(II) oxidation. *Arch. Microbiol.* **189**, 59–69

173. Ubbink, M. (2009) The courtship of proteins: understanding the encounter complex. *FEBS Lett.* **583**, 1060–1066

174. Keizers, P. H. J., and Ubbink, M. (2011) Paramagnetic tagging for protein structure and dynamics analysis. *Prog. Nucl. Magn. Reson. Spectrosc.* **58**, 88–96

175. Sharma, S., Cavallaro, G., and Rosato, A. (2010) A systematic investigation of multiheme c-type cytochromes in prokaryotes. *J. Biol. Inorg. Chem.* **15**, 559–71

176. Wickramasinghe, N. P., Shaibat, M. a, Jones, C. R., Casabianca, L. B., De Dios, A. C., Harwood, J. S., and Ishii, Y. (2008) Progress in 13C and 1H solid-state nuclear magnetic resonance for paramagnetic systems under very fast magic angle spinning. *J. Chem. Phys.* **128**, 052210

177. Balayssac, S., Bertini, I., Bhaumik, A., Lelli, M., and Luchinat, C. (2008) Paramagnetic shifts in solid-state NMR of proteins to elicit structural information. *Proc. Natl. Acad. Sci. U. S. A.* **105**, 17284–9

178. Lippincott-Schwartz, J., and Patterson, G. H. (2003) Development and Use of Fluorescent Protein Markers in Living Cells. *Science* **300**, 87

179. Iobbi-Nivol, C., Crooke, H., Griffiths, L., Grove, J., Hussain, H., Pommier, J., Mejean, V., and Cole, J. A. (1994) A reassessment of the range of c -

type cytochromes synthesized by Escherichia coli K-12. *FEMS Microbiol. Lett.* **119**, 89–94

180. Gordon, E. H., Steensma, E., and Ferguson, S. J. (2001) The cytochrome c domain of dimeric cytochrome cd(1) of Paracoccus pantotrophus can be produced at high levels as a monomeric holoprotein using an improved c-type cytochrome expression system in Escherichia coli. *Biochem. Biophys. Res. Commun.* **281**, 788–94

181. Londer, Y. Y., Pokkuluri, P. R., Tiede, D. M., and Schiffer, M. (2002) Production and preliminary characterization of a recombinant triheme cytochrome c7 from Geobacter sulfurreducens in Escherichia coli• 1. *Biochim. Biophys. Acta* **1554**, 202–211

182. Luchinat, C., Bertini, I., and Parigi, G. (2002) Magnetic susceptibility in paramagnetic NMR. *Prog. Nucl. Magn. Reson. Spectrosc.* **40**, 249–273

183. Barry, C. D., North, A. C. T., Glasel, J. A., Williams, R. J. P., and Xavier, A. V (1971) Quantitative Determination of Mononucleotide Conformations in Solution using Lanthanide Ion Shift and Broadening NMR Probes. *Nature* **232**, 236–245

184. Turner, D. L. (1993) Evaluation of 13C and 1H Fermi contact shifts in horse cytochrome c The origin of the anti-Curie effect. *Eur. J. Biochem.* **211**, 563–568

185. Dutton, P. L. (1978) Redox potentiometry: determination of midpoint potentials of oxidation-reduction components of biological electron-transfer systems. *Methods. Enzymol.* **54**, 411–435